Novel Adsorbents for Acid Gas Treatment in Process Streams

by

Sabereh Rezaei

A thesis submitted in partial fulfillment of the requirements for the degree of

Doctor of Philosophy

in

Chemical Engineering

Department of Chemical and Materials Engineering

University of Alberta

Abstract

The objective of this dissertation was to find novel adsorbents addressing problems associated with acid gases. They are the most common contaminants in multiple aspects of petroleum processing and combustion gas clean up, which reduce the efficiency of petroleum refining and product quality. This refers to any gas stream containing significant amount of acidic gases such as hydrogen sulfide (H_2S) or carbon dioxide (CO_2).

Engelhard Titanosilicate-2 (ETS-2) has shown to be a promising substrate to load active metal sites for deep H_2S removal (to sub-ppm levels) for gas purification applications at room temperature. Because of the high external surface area and the cation exchange capacity of ETS-2, active sites can be highly dispersed and very accessible to H_2S molecules making it a novel support material for active metal sites. Copper supported ETS-2 has been found to be a superior H_2S scavenger, outperforming the Ag, Ca, and Zn exchanged ETS-2 and a fully developed commercial H_2S adsorbent (BASF). A dynamic model based on the rigorous mass balance equations applied to the fixed-bed has analyzed H_2S column breakthrough experiments. Temperature-programmed desorption tests provided insight on the material characterization as well as on the relative magnitudes of the H_2S-material interactions. Sorption capacity of ETS-2 for Cu^{2+} ions from aqueous solution through the batch technique was also investigated. It

was experimentally shown that ion exchange is the major removal mechanism and up to 99% copper removal was achieved.

Low energy input regenerable moisture removal from CO_2 streams, which would be generated from a post-combustion capture (PCC) system, has been also studied. A desired desiccant for CO_2 drying should have a high moisture capacity at low partial pressure and high selectivity to provide through drying. It also needs to be economically efficient by being regenerable with waste heat and humid air. Engelhard Titanosilicate-10 (ETS-10) materials have been shown to reserve all of these characteristics. Ca-ETS-10 showed the highest moisture capacity for a temperature swing of 30-70 °C and a CO_2 feed stream of 50–100% relative humidity compared to that of commercial silica and 4A zeolite.

Preface

Chapter 3 of this thesis, with minor modification, is published in Ind. Eng. Chem. Res. 2012, 51, 12430−12434; coauthored by Sabereh Rezaei, Aida Tavana, James A. Sawada, Lan Wu, Abu S.M. Junaid and Steven M. Kuznicki. I was responsible for the data collection and analysis as well as the manuscript composition and edit. Aida Tavana assisted with the data collection, analysis and the first draft of the manuscript. James A. Sawada assisted with the manuscript edits. Lan Wu assisted with the synthesis part. Abu S.M. Junaid assisted with the data analysis. Steven M. Kuznicki was the supervisory author and was involved with concept formation.

Chapter 4 of this thesis, with minor modification, is published in Chem. Eng. Sci. 2015, 123, 444–449; coauthored by Sabereh Rezaei, Maria Ophelia D. Jarligo, Lan Wu and Steven M. Kuznicki. I was responsible for the data collection and analysis as well as the manuscript composition and edits. Maria Ophelia D. Jarligo contributed with the manuscript edits. Lan Wu assisted with the synthesis part. Steven M. Kuznicki was the supervisory author and was involved with concept formation.

Chapter 5 and 6 of this thesis are being prepared for submission for publication. Chapter 5 is coauthored by Sabereh Rezaei, Adolfo M. Avila and Steven M.

Kuznicki. I was responsible for the data collection, analysis and modeling as well as the manuscript composition. Adolfo M. Avila contributed in the modeling part manuscript composition. Steven M. Kuznicki was the supervisory author and was involved with concept formation. Chapter 6 is coauthored by Sabereh Rezaei and Steven M. Kuznicki. I was responsible for the data collection, analysis and the manuscript composition. Steven M. Kuznicki was the supervisory author and was involved with concept formation.

Chapter 7 of this thesis, with minor modification, is published in Sep. Purif. Technol. 120 (2013) 354–361; collaborated by Brenden Tanchuk and James A. Sawada, Sabereh Rezaei and Steven M. Kuznicki. The whole set up was designed by the first three authors for the first time. Brenden Tanchuk (Msc in Chemical Engineering) was responsible for building the set up and commissioning tests under James A. Sawada (Lab Manager University of Alberta) supervision and help. I was responsible for adsorption synthesis and adsorption experiments. The first three authors had equal contributions in the data interpretation part. Steven M. Kuznicki was the supervisory author and was involved with concept formation.

To my beloved parents and my dear brother

for their incessant love and support

Acknowledgements

First and above all I would like to express my wholehearted gratitude to God, the Almighty, for his countless mercy and showers of blessings in every aspect of my life. It is very hard to escape the feeling of God's existence in the science that is studied and learned.

I would like to express my sincere appreciation to my supervisor Prof. Steven Kuznicki, for his inspiring guidance, encouragement and support during my studies at the University of Alberta. Being in a big research group under his supervision enabled me to collaborate with different people.

I would also like to thank my dissertation committee, Prof. Rajender Gupta, Dr. Zaher Hashisho, Prof. William McCaffrey, Dr. Larry Unsworth and Prof. Michael Tsapatsis, for their valuable time and helpful comments.

My PhD oral defense was not possible without the kind assistance of Artin Afaqan when the session had conflict with my TA sessions.

I give especial thanks to Dr. Adolfo Avila for his support, inspiring guidance and valuable time he devoted to my research. My journey would not have been what it was without him.

And a very special thank you to my family. Words cannot express how grateful I am to my beloved mother, Zahra, and father, Mohammad Javad, for all of the sacrifices that they have made on my behalf. I am really proud of them and I will never forget the values they have taught me. I am forever indebted to them for their endless patience and encouragement. I am also grateful to my dear brother, Mohammad Hosein, who has always supported and encouraged me. My program was a collaborative effort with my family's love, constant prayers and support far away from home.

Sabereh Rezaei

March 2015

Table of Contents

List of Tables

List of Figures

Nomenclature

a	Deactivation rate term
a'	Molar area (surface area per mole of adsorbate)
A	Surface area
b	Langmuir equilibrium constant
c	Concentration in fluid phase
d_p	Particle diameter
D_L	Axial dispersion coefficient
D	Molecular diffusivity
E_{act}	Activation energy
E_{ads}	Adsorption energy
E_{diss}	Dissociation energy
F	Molar flow
K	Kinetic parameter
k_d	Deactivation constant

k_f	Mass transfer coefficient
k_H	Henry's constant
k_r	Reaction rate constant
L	Adsorbent bed length
m	value of n for full monolayer coverage (the saturation value)
n	Number of moles of adsorbate per unit mass of adsorbent
N	Specific amount of adsorbate during the breakthrough experiment
N'	Specific amount of adsorbate during the desorption time
N_z	The molar flux in z direction
P	Gas-phase pressure
dP	Pressure drop
q	Concentration in solid phase
R	Universal gas constant

S	Entropy
T	Temperature
t	Time
u_s	Superficial velocity
V	Volume
w	Adsorbent weight
x	Adsorbate mole fraction
y	Gas-phase mole fraction
z	Distance
Z	Compressibility factor

Greek Letters

ε	Void fraction
δ	Mass transfer boundary layer thickness
β	Heating rate
θ	Surface coverage
ρ	Density

μ	Viscosity
Π	Spreading pressure, adsorbed phase
φ	Energy of the adsorption system
μ'	Chemical potential
ν	Intrinsic fluid velocity
γ	Parameter for deactivation rate equation
λ	Parameter for deactivation rate equation

Abbreviations and Acronyms

BE	Binding energy
BET	Brunauer–Emmett–Teller
EDX	Energy Dispersive X-Ray analysis
eV	Electronvolt
FPD	Flame photometric detector
GC	Gas chromatograph
ICP	Binding energy
MFC	Mass flow controller

Mw	Molecular weight
ODE	Ordinary differential equations
PCC	Post combustion capture
PDE	Partial differential equations
PE	Potential energy
ppm	Parts per million
Re	Reynolds number
Sc	Schmidt number
SEM	Scanning electron microscopy
Sh	Sherwood number
TEG	Triethyleneglycol
TEM	Transmission electron microscopy
TGA	Thermogravimetric analysis
XRD	X-ray diffraction
XPS	X-rad photoelectron spectroscopy

Subscript and superscript

b	Bed
g	Gas phase
i	Species i
o	Initial value
p	Particle
sat	Saturation value

1. Introduction

1.1. Synopsis

The world's economy is relatively energy intensive and is strongly influenced by the prices of oil or fossil fuels such as petroleum and natural gas. Over the years, progressive interests have been focused on finding alternative energy sources to reduce reliance on fossil based energy. However, up to now petroleum still remains a primary source. According to the US Energy Information Administration (EIA) estimate for 2014, the world consumes 87.421 million barrels of oil each day [1]. Associated with the production of petroleum are contaminants, which are harmful to both oil processing and the environment. Therefore with the humongous volumetric demand for oil consumption there is a great necessity to address these contaminants.

One of the most common contaminants in petroleum production is acid gas. This refers to any gas stream containing significant amount of acidic gases such as hydrogen sulfide (H_2S) or carbon dioxide (CO_2) [2]. It is often found in fossil fuels. For instance a gas stream from one oil well in Canada has been reported to contain 90% of H_2S while others may have contents in tens of percent range [3]. In natural

gas the concentrations vary in a wide range from parts per million to 50 volume percent and higher, depending on the nature of the rock formation from which it comes [4]. H_2S threshold for natural gas is usually considered 4 ppmv under standard temperature and pressure [2, 5] however differs by country, agency or application.

1.2. The Necessity of Acid gas Removal

Hydrogen sulfide is a common contaminant that must be addressed in multiple aspects of petrochemical processing and combustion gas clean up [6]. This is especially important for high sulfur hydrocarbons such as Alberta's substantial oil sands resource as well (4% [7]). Gasification and use of natural gas in advanced power generation approaches also requires removal of contaminations such as sulfur. Crude oil and coal have up to 6 wt.% sulfur content depending on their sources [8].

During the combustion of natural gas or when H_2S is oxidized in air, sulfur dioxide (SO_2) is generated which reacts with water and produce acid rain which is harmful to the environment. In addition, acid rain can increase the rate of corrosion of important metallic structures such as bridges. Sulfur levels higher than 3 ppm can cause corrosion in the pipelines used for transporting natural gas and reduce the plant's lifetime in general [9].

During coal gasification processes H_2S is released making the resulting syngas the main product of gasification for electric power generation impure. Even at trace levels (sub ppm level), H_2S degrades the performance of many inorganic membranes that could be used to enhance the separation processes related to syngas and causes corrosion of gas turbines and pipelines. Thus the produced syngas should be scavenged completely before being applied in further processes [10]. Nickel and alumina catalysts used in steam reforming processes also get poisoned by H_2S.

Fuel cells, the promising candidates for electrical power generation also gets affected by H_2S when their hydrogen fuel is not cleaned up. The processed natural gas meets the environmental regulations, but the remaining H_2S content is still problematic for fuel cell applications. Since even at 0.1-1 ppm H_2S poison the anode catalyst of fuel cells. Thus acid gas removal plants such as gas sweetening and desulphurization plants are essential and are one of the major parts of industrial gas processing and transportation [11]. The design and development of adsorbents that remove H_2S from the gaseous streams up to sub ppm levels for different applications are therefore the main focus of this research.

Meanwhile, finding a solution for the generation of pure carbon dioxide streams produced from the combustion of natural gas or gasified coal, bitumen, biomass (syngas) for storage and compression is highly required [12]. Pure carbon dioxide generation is desirable primarily since it reduces the compression costs and eliminates other liquefaction and associated storage problems. One of the most

problematic issues associated with producing a pure CO_2 stream is moisture contamination since the presence of water in the CO_2 stream causes corrosion as well as difficulty with its separation from other combustion products. Water vapor that combines with CO_2 makes carbonic acid, which corrodes process equipment and piping. In addition at the high pressures required for pipeline distribution or for deep well injection gas hydrates may be created.

Although processes as to how water vapor is removed from CO_2 gas stream have not reported in many explorations, an effective thoroughly drying (below 10 ppmv) of CO_2 gas stream would prevent those issues. Therefore, carbon dioxide streams must be thoroughly dried before underground storage.

To sum up, acid gases must be removed or separated from the mixture of gases prior to use or distribution to reduce piping and equipment corrosion during transportation and maintenance problems in the pipelines, prevent atmospheric pollution and meet environmental standards [13, 14]. All gasification processes include an acid gas clean up step, regardless of the feedstock used or the ultimate use of the synthesis gas produced [11]. However in applications where the gasifier product is going to be a chemical feedstock, complete removal (sub ppm level) of carbon dioxide and sulfur species is required.

Given the importance of acid gas removal, the focus of this thesis is to develop new adsorbents to: first, reduce the H_2S to sub ppm levels; second, drying CO_2 streams thoroughly with a desiccant being able to regenerate with low energy input. This will be crucial to the future of the chemical processing industry and should be

viewed as an avenue for the discovery of next-generation adsorptive gas purification technologies.

1.2.1. Hydrogen sulfide removal

There has been continuous research and development of new methods and adsorbents in past decades for H_2S removal. Current available techniques for H_2S removal are absorption in liquids (such as alkanolamines, ammonia solutions, and alkaline salt solutions) and solid supported amines, the Claus process, and adsorption by activated carbon (AC) or metal oxides [8, 15].

Absorption in liquids can reduce H_2S concentration from percentage to ppm levels readily. However the challenging problem is to remove the last traces of H_2S from the process stream, which is the focus of this work. On the other hand, this method can experience operating difficulties such as high solvent losses, failure to meet sweet gas specification, foaming, corrosion, fouling of equipment and contamination of the solution [3]. Although the Claus process, which is the most significant gas desulfurizing process, has high efficiency of 94% - 97% and a relatively small ecological impact when coupled with a tail-gas treatment unit, the H_2S levels in this method cannot be reduced to ppm levels due to the equilibrium limitation of the reaction in the process [8].

Activated carbon, although it has high specific surface area and porous structure, its virgin form is not considered a good candidate for H_2S removal due to its low capacity [10]. However, it has been reported that its capacity for H_2S removal can

be improved to about 10 times by impregnation with copper or potassium hydroxide [16].

Reactive removal of H_2S is common when the gas stream must be polished down to sub-ppm levels [14]. Much of the previously reported work on reactive sequestration of H_2S has focused on using different forms of supported and unsupported metal oxides and mixed metal oxides, in efforts to improve the adsorbents capacity, thermal stability, and utilization. High dispersion of active sites can noticeably enhance the reaction between metal compounds and H_2S molecules [17]. The high surface area supports include zeolites [18-20], carbon sorbents [21, 22], SBA-15 and other mesoporous material supports [14, 19, 23-27].

The first and focal part of this research has been contributed to further improve the capacity and utilization of supported metal/metal oxide adsorbents for deep H_2S removal (to sub-ppm levels) for gas purification applications at different temperature ranges.

Engelhard Titanosilicate-2 (ETS-2) has been synthesized and used as a novel substrate material to load active ions for H_2S scavenging systems for the first time. ETS-2 has high external surface area and cation exchange capacity, which allow active ions to be highly dispersed and accessible to H_2S molecules [14]. It has been exchanged with different metal ions, Cu^{+2}, Ag^+, Zn^{2+}, Ca^{2+}. Room temperature H_2S removal capacity of the samples including the commercial sample shows Cu-ETS-2 has the highest capacity.

Several studies have been dedicated to the development of H_2S sorbents and measurements of the breakthrough curves, however the column dynamics are still poorly understood and differ for many of the sorbents studied. Much progress has been made for the column dynamics and interactions of gases with physisorbents without any chemical reaction included [28-32]. Less attention has been paid to the investigation of the adsorbent by a dynamic model, which considers both chemisorption of H_2S molecules on the surface and deactivation of the solid. Deactivation models [33, 34] were reported to be quite successful in predicting the reaction rates of such gas-solid non-catalytic reactions. However they have been used for the pseudo-steady state condition [34-40] in which the dynamic of the system is only considered in the activity term implicitly.

Part of this work is focused on better understanding of the transport phenomena occurring during the adsorption of ppm level H_2S on a copper-ETS-2 packed bed column. A continuum mechanics-based model was developed to support the analysis of experimental data obtained from dynamic column breakthrough tests. The model includes the chemical reaction term, which is affected by the deactivation of the solid phase. Temperature-programmed desorption (TPD) [41] experiments of H_2S on Cu-ETS-2 provided a further insight of the different H_2S-material interaction energy levels.

1.2.2. Drying of CO_2 Streams

Numerous researches have been done on the high levels of CO_2 emissions and their

7

direct effect on global warming and climate change in the last decade. Since the global production of CO_2 is projected to increase from 30 billion tons in 2008 to 43.2 billion tons by 2035 [42], various methods have been proposed to mitigate the environmental effect of rising CO_2 emissions. An appealing design is post combustion capture (PCC), which uses an adsorptive separation process to selectively remove and concentrate CO_2 from the combustion gas stream. The concentrated CO_2 is then compressed and permanently separated preventing significant volumes of CO_2 from releasing to the atmosphere. The combustion process may be modified to run on pure oxygen and/or through a turbine in an integrated gasification combined (IGC) cycle [43-45] to improve the efficiency of the separation. Through IGC systems a combustion stream with a high concentration of CO_2 is generated however such advantages come at increased cost and added process complexity.

Different types of adsorbents with a high selectivity for CO_2 over other atmospheric gases including zeolites [46-50], metal oxides [51-56], and solid-supported amines [57-61] have been investigated for recovering CO_2. Despite different characteristics of these materials, they all co-adsorb water to some extent which will be desorbed with the CO_2. But the moisture content needs to be reduced to trace levels prior to compression of the carbon dioxide streams to meet the requirements for underground carbon sequestration [62], and to prevent the formation of CO_2 hydrates [63].

An ideal desiccant for drying CO_2 streams should have a high water capacity at low moisture partial pressure and need low energy input for regeneration as well as high selectivity toward water over CO_2.

Liquid absorption drying systems such as triethylene glycol (TEG) are not good candidates for PCC/CO_2 sequestration due to the thermal input required in the reboiler (200°C) and the poor selectivity of the liquid [64, 65]. Zeolite temperature swing adsorption (TSA) drying systems used for drying natural gas have high moisture selectivity can generate gas streams having very low dew points, but similar to TEG systems, they require a regeneration step at temperatures greater than 200°C [66].

Silica gel desiccants, on the other hand can be regenerated at temperatures as low as 100°C, but the water adsorption capacity of silica gel decreases linearly with concentration [48]. The latter causes the adsorbent to have little capacity at trace levels of moisture and reduces the amount of the bed used for adsorption.

Engelhard Titanosilicate 10 (ETS-10) is a large-pored, titanium silicate molecular sieve include a mixture of silicon oxide tetrahedra and titanium oxide octahedral [67, 68]. The specific structure of ETS-10 combines the chemically passive characteristics of silica gel with the ion exchange capability of zeolite molecular sieves. Thus it displays a unique adsorption behaviour since it retains a high moisture capacity at low partial pressures at ambient temperatures, but rapidly loses moisture capacity as temperature increases [69].

ETS-10 has previously been identified as an air desiccant [69], though its use for drying CO_2 streams has not been investigated.

The last part of this research project will focus on the CO_2 drying performance of different forms of ETS-10 and compares them to commercial silica and zeolite 4A adsorbents.

Separation issues and challenges to be addressed by this thesis are highlighted in Figure 1-1.
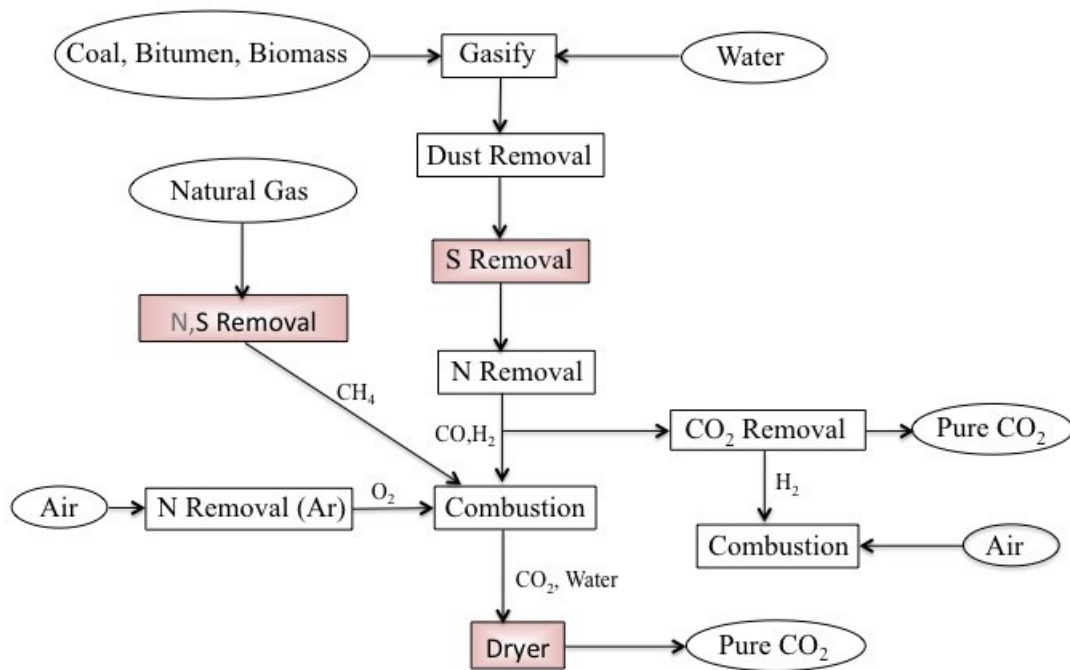
Figure 1- 1 Challenges of this research are highlighted

1.3. Framework of the Study

A concise review of available literatures on adsorption fundamentals including physisorption versus chemisorption concept, adsorption equilibrium, kinetics and adsorption dynamics are presented in chapter 2.

A novel Cu-based adsorbent is introduced and preparation using a high surface area titanosilicate (ETS-2) in chapter 3. It was tested for low concentrations H_2S removal at room temperature and its capacity and copper utilization was compared to a fully developed commercial H_2S adsorbents as well as Cu exchanged ETS-4 and 10. The effect of activation temperature on Cu-ETS-2 properties was investigated as well.

Breakthrough performances of metal-exchanged nanotitanate ETS-2 adsorbents for room temperature desulfurization are reported in chapter 4. A description of various applied characterization techniques for the morphology, structure and chemical properties of the synthesized adsorbents are discussed as well.

Chemisorption of H_2S on copper-ETS-2 is investigated in chapter 5. Adsorption test conditions followed by the mechanism of H_2S adsorption on Cu-ETS-2 are also presented. In this chapter, H_2S column breakthrough experiments are analyzed by a proposed model based on the rigorous mass balance equations for the fluid and solid phases. The model also includes the chemical reaction term, which is affected by the deactivation of the solid phase.

Chapter 6 discusses the Cu ions removal of from aqueous solutions by nanotitanate ETS-2. Different characterization tests such as XPS, EDX and ICP as well as copper removal tests at different solution PH have been conducted to study the adsorption mechanism.

Chapter 7 focuses on the modification of a molecular sieve as a low temperature regenerable desiccant that requires low thermal input, to be used in the process of drying CO_2 streams. Different ion exchanged forms of ETS-10 were used as desiccants for CO_2 drying. The manner in which the moisture capacity declines with temperature makes ETS-10 intensely suited toward low energy input CO_2 drying.

Finally in chapter 8, the conclusions and highlights of the major discoveries of the present study and recommendations for future studies are presented.

1.4. References

[1] *Short-Term Energy Outlook,*

Available: http://www.eia.gov/forecasts/steo/report/global_oil.cfm. (Accessed on Jan. 20th, 2015).

[2] NaturalGas. Available: http://naturalgas.org. (Accessed on Jan. 16th, 2015).

[3] F. Ullmann, *Ullmann's Encyclopedia of Industrial Chemistry. [Electronic Resource]*. New York]; 7th ed, 2010.

[4] *Gas Sweetening,*

Available:http://msdssearch.dow.com/PublishedLiteratureDOWCOM/dh_0039/0901b803800391f8.pdf?filepath=gastreating/pdfs/noreg/170-01395.pdf&fromPage=GetDoc. (Accessed on Jan. 20th, 2015).

[5] *Fundamentals of Stack Gas Dispersion*.

Available: http://www.air-dispersion.com/default.htm. (Accessed on Jan. 10th, 2015).

[6] Y. Elsayed, M. Seredych, A. Dallas and T. J. Bandosz, "Desulfurization of air at high and low H2S concentrations," *Chem. Eng. J.,* vol. 155, pp. 594-602, 2009.

[7] *Canada's Oilsands and Heavy Oil Deposits*.

Available: www.energy.gov.ab.ca/oilsands/pdfs/rpt_chops_app1.pdf. (Accessed on Jan. 20th, 2015).

[8] D. Stirling, *The Sulfur Problem [Electronic Resource] : Cleaning Up Industrial Feedstocks / Diane Stirling.* Cambridge, UK : Royal Society of Chemistry, 2000.

[9] T. Baird, P. J. Denny, R. Hoyle, F. Mcmonagle, D. Stirling and J. Tweedy, "Modified Zinc-Oxide Absorbents for Low-Temperature Gas Desulfurization," *Journal of the Chemical Society-Faraday Transactions*, vol. 88, pp. 3375-3382, 1992.

[10] S. K. Gangwal, "Chapter 11: Desulfurization for Fuel Cells," *Fuel Cells: Technologies for Fuel Processing,* pp. 317-360, 2011.

[11] *Chemical Solvent-Based Processes for Acid Gas Removal in Gasification Application*.

Available:http://msdssearch.dow.com/PublishedLiteratureDOWCOM/dh_003a/0901b8038003a89e.pdf?filepath=gastreating/pdfs/noreg/170-01406.pdf&fromPage=GetDoc. (Accessed on Jan. 17th, 2015).

[12] B. Tanchuk, J. A. Sawada, S. Rezaei and S. M. Kuznicki, "Adsorptive drying of CO2 using low grade heat and humid, ambient air," *Separation and Purification Technology,* vol. 120, pp. 354-361, 2013.

[13] B. D. Bhide, A. Voskericyan and S. A. Stern, "Hybrid processes for the removal of acid gases from natural gas," *J. Membr. Sci.,* vol. 140, pp. 27-49, 1998.

[14] S. Rezaei, A. Tavana, J. A. Sawada, L. Wu, A. S. M. Junaid and S. M. Kuznicki, "Novel Copper-Exchanged Titanosilicate Adsorbent for Low Temperature H2S Removal," *Ind Eng Chem Res,* vol. 51, pp. 12430-12434, 2012.

[15] Q. Xue and Y. Liu, "Removal of minor concentration of H2S on MDEA-modified SBA-15 for gas purification," *Journal of Industrial and Engineering Chemistry,* vol. 18, pp. 169-173, 2012.

[16] C. Huang, C. Chen and S. Chu, "Effect of moisture on H2S adsorption by copper impregnated activated carbon," *J. Hazard. Mater.,* vol. 136, pp. 866-873, 2006.

[17] D. Jiang, L. Su, L. Ma, N. Yao, X. Xu, H. Tang and X. Li, "Cu-Zn-Al mixed metal oxides derived from hydroxycarbonate precursors for H2S removal at low temperature," *Appl. Surf. Sci.,* vol. 256, pp. 3216-3223, 2010.

[18] D. Melo, J. de Souza, M. Melo, A. Martinelli, G. Cachima and J. Cunha, "Evaluation of the zinox and zeolite materials as adsorbents to remove H2S from natural gas," *Colloid Surf. A-Physicochem. Eng. Asp.,* vol. 272, pp. 32-36, 2006.

[19] D. Crespo, G. Qi, Y. Wang, F. H. Yang and R. T. Yang, "Superior sorbent for natural gas desulfurization," *Ind Eng Chem Res,* vol. 47, pp. 1238-1244, 2008.

[20] P. Kumar, C. Sung, O. Muraza, M. Cococcioni, S. Al Hashimi, A. McCormick and M. Tsapatsis, "H2S adsorption by Ag and Cu ion exchanged faujasites," *Microporous Mesoporous Mat.,* vol. 146, pp. 127-133, 2011.

[21] D. Nguyen-Thanh and T. Bandosz, "Activated carbons with metal containing bentonite binders as adsorbents of hydrogen sulfide," *Carbon,* vol. 43, pp. 359-367, 2005.

[22] F. Li, J. Wei, Y. Yang, G. H. Yang and T. Lei, "Preparation of Sorbent Loaded with Nano-CuO for Room Temperature to Remove of Hydrogen Sulfide," *Applied Mechanics and Materials,* vol. 475, pp. 1329-1333, 2014.

[23] P. Dhage, A. Samokhvalov, D. Repala, E. C. Duin, M. Bowman and B. J. Tatarchuk, "Copper-Promoted ZnO/SiO2 Regenerable Sorbents for the Room Temperature Removal of H2S from Reformate Gas Streams," *Ind Eng Chem Res,* vol. 49, pp. 8388-8396, 2010.

[24] Q. Xue and Y. Liu, "Removal of minor concentration of H2S on MDEA-modified SBA-15 for gas purification," *J. Ind. Eng. Chem.,* vol. 18, pp. 169-173, 2012.

[25] M. Hussain, N. Abbas, D. Fino and N. Russo, "Novel mesoporous silica supported ZnO adsorbents for the desulphurization of biogas at low temperatures," *Chem. Eng. J.,* vol. 188, pp. 222-232, 2012.

[26] X. Wang, T. Sun, J. Yang, L. Zhao and J. Jia, "Low-temperature H2S removal from gas streams with SBA-15 supported ZnO nanoparticles," *Chem. Eng. J.,* vol. 142, pp. 48-55, 2008.

[27] D. Montes, E. Tocuyo, E. Gonzaĺez, D. Rodriǵuez, R. Solano, R. Atencio, M. A. Ramos and A. Moronta, "Reactive H2S chemisorption on mesoporous silica molecular sieve-supported CuO or ZnO," *Microporous and Mesoporous Materials,* vol. 168, pp. 111-120, 2013.

[28] S. Guntuka, S. Farooq and A. Rajendran, "A- and B-Site substituted lanthanum cobaltite perovskite as high temperature oxygen sorbent. 2. Column dynamics study," *Ind Eng Chem Res,* vol. 47, pp. 163-170, 2008.

[29] Y. Xiao, S. Wang, D. Wu and Q. Yuan, "Experimental and simulation study of hydrogen sulfide adsorption on impregnated activated carbon under anaerobic conditions," *J. Hazard. Mater.,* vol. 153, pp. 1193-1200, 2008.

[30] S. N. Nobar and S. Farooq, "Experimental and modeling study of adsorption and diffusion of gases in Cu-BTC," *Chemical Engineering Science,* pp. 801, 2012.

[31] R. Haghpanah, A. Rajendran, S. Farooq, I. A. Karimi and M. Amanullah, "Discrete Equilibrium Data from Dynamic Column Breakthrough Experiments," *Ind Eng Chem Res,* vol. 51, pp. 14834-14844, 2012.

[32] K. B. Lee, A. Verdooren, H. S. Caram and S. Sircar, "Chemisorption of carbon dioxide on potassium-carbonate-promoted hydrotalcite," *Journal of Colloid & Interface Science,* vol. 308, pp. 30-39, 2007.

[33] N. Yaşyerli, T. Doğu, G. Doğu and i. Ar, "Deactivation model for textural effects of kinetics of gas-solid noncatalytic reactions "char gasification with CO2"," *Chemical Engineering Science,* vol. 51, pp. 2523-2528, 1996.

[34] S. Yasyerli, G. Dogu, I. Ar and T. Dogu, "Breakthrough Analysis of H 2 S Removal on Cu-V-Mo, Cu-V, and Cu-Mo Mixed Oxides," *Chem. Eng. Commun.,* vol. 190, pp. 1055, 2003.

[35] Y. Suyadal, M. Erol and H. Oguz, "Deactivation model for the adsorption of trichloroethylene vapor on an activated carbon bed," *Ind Eng Chem Res,* vol. 39, pp. 724-730, 2000.

[36] S. Yasyerli, G. Dogu, I. Ar and T. Dogu, "Activities of copper oxide and Cu-V and Cu-Mo mixed oxides for H2S removal in the presence and absence of hydrogen and predictions of a deactivation model," *Ind Eng Chem Res,* vol. 40, pp. 5206-5214, 2001.

[37] S. Yasyerli, I. Ar, G. Dogu and T. Dogu, "Removal of hydrogen sulfide by clinoptilolite in a fixed bed adsorber," *Chem. Eng. Process,* vol. 41, pp. 785-792, 2002.

[38] T. Kopac and S. Kocabas, "Deactivation models for sulfur dioxide adsorption on silica gel," *Adv. Environ. Res.,* vol. 8, pp. 417-424, 2004.

[39] H. F. Garces, H. M. Galindo, L. J. Garces, J. Hunt, A. Morey and S. L. Suib, "Low temperature H2S dry-desulfurization with zinc oxide," *Microporous Mesoporous Mat.,* vol. 127, pp. 190-197, 2010.

[40] T. Ko and H. Hsueh, "Removal of Hydrogen Sulfide by Iron-Rich Soil: Application of the Deactivation Kinetic Model for Fitting Breakthrough Curve," *Aerosol Air Qual. Res.,* vol. 12, pp. 1355-1361, 2012.

[41] K. J. Leary, J. N. Michaels and A. M. Stacy, "Temperature-programmed desorption: Multisite and subsurface diffusion models," *AICHE J.,* vol. 34, pp. 263, 02, 1988.

[42] *International Energy Outlook 2011.* Available: http://large.stanford.edu/courses/2011/ph240/nagasawa2/docs/0484-2011.pdf. (Accessed on Jan. 20th, 2015).

[43] C. Cormos, A. Padurean and P. S. Agachi, "GHGT-10: Technical evaluations of carbon capture options for power generation from coal and biomass based on integrated gasification combined cycle scheme," *Energy Procedia,* vol. 4, pp. 1861-1868, 2011.

[44] Y. Hu, H. Li and J. Yan, "Integration of Evaporative Gas Turbine with Oxy-Fuel Combustion for Carbon Dioxide Capture," *International Journal of Green Energy,* vol. 7, pp. 615-631, 2010.

[45] A. Kather and S. Kownatzki, "Assessment of the different parameters affecting the CO2 purity from coal fired oxyfuel process," *International Journal of Greenhouse Gas Control,* vol. 5, pp. S204-S209, 2011.

[46] C. O. Areán and M. R. Delgado, "Variable-temperature FT-IR studies on the thermodynamics of carbon dioxide adsorption on a faujasite-type H-Y zeolite," *Appl. Surf. Sci.,* vol. 256, pp. 5259-5262, 2010.

[47] Z. Liu, C. A. Grande, P. Li, J. Yu and A. E. Rodrigues, "Adsorption and Desorption of Carbon Dioxide and Nitrogen on Zeolite 5A," *Separation Science & Technology,* vol. 46, pp. 434-451, 02, 2011.

[48] Y. Wang and M. D. Levan, "Adsorption Equilibrium of Carbon Dioxide and Water Vapor on Zeolites 5A and 13X and Silica Gel: Pure Components," *J. Chem. Eng. Data,* vol. 54, pp. 2839-2844, 2009.

[49] Z. Zhao, X. Cui, J. Ma and R. Li, "Adsorption of carbon dioxide on alkali-modified zeolite 13X adsorbents," *International Journal of Greenhouse Gas Control,* vol. 1, pp. 355-359, 2007.

[50] A. Zukal, J. Mayerová and M. Kubu, "Adsorption of Carbon Dioxide on High-Silica Zeolites with Different Framework Topology," *Topics in Catalysis,* vol. 53, pp. 1361-1366, 11, 2010.

[51] J. Baltrusaitis, J. Schuttlefield, E. Zeitler and V. H. Grassian, "Carbon dioxide adsorption on oxide nanoparticle surfaces," *Chem. Eng. J.,* vol. 170, pp. 471-481, 2011.

[52] P. H. Chang, Y. P. Chang, S. Y. Chen, C. T. Yu and Y. P. Chyou, "Ca-Rich Ca-Al-Oxide, High-Temperature-Stable Sorbents Prepared from Hydrotalcite Precursors: Synthesis, Characterization, and CO2 Capture Capacity," *Chemsuschem,* vol. 4, pp. 1844-1851, 2011.

[53] G. S. Grasa and J. C. Abanades, "CO2 capture capacity of CaO in long series of carbonation/calcination cycles," *Ind Eng Chem Res,* vol. 45, pp. 8846-8851, 2006.

[54] H. Lu, P. G. Smirniotis, F. O. Ernst and S. E. Pratsinis, "Nanostructured Ca-based sorbents with high CO2 uptake efficiency," *Chemical Engineering Science,* vol. 64, pp. 1936-1943, 2009.

[55] G. Ramis, G. Busca and V. Lorenzelli, "Low-Temperature Co-2 Adsorption on Metal-Oxides - Spectroscopic Characterization of some Weakly Adsorbed Species," *Mater. Chem. Phys.,* vol. 29, pp. 425-435, 1991.

[56] S. P. Wang, S. L. Yan, X. B. Ma and J. L. Gong, "Recent advances in capture of carbon dioxide using alkali-metal-based oxides," *Energy & Environmental Science,* vol. 4, pp. 3805-3819, 2011.

[57] B. Arstad, H. Fjellvag, K. O. Kongshaug, O. Swang and R. Blom, "Amine functionalised metal organic frameworks (MOFs) as adsorbents for carbon dioxide," *Adsorption,* pp. 755, 2008.

[58] F. Chang, K. Chao, H. Cheng and C. Tan, "Adsorption of CO2 onto amine-grafted mesoporous silicas," *Separation and Purification Technology,* vol. 70, pp. 87-95, 2009.

[59] R. Chatti, A. K. Bansiwal, J. A. Thote, V. Kumar, P. Jadhav, S. K. Lokhande, R. B. Biniwale, N. K. Labhsetwar and S. S. Rayalu, "Amine loaded zeolites for carbon dioxide capture: Amine loading and adsorption studies," *Microporous and Mesoporous Materials,* vol. 121, pp. 84-89, 2009.

[60] C. Knöfel, J. Descarpentries, A. Benzaouia, V. Zeleňák, S. Mornet, P. L. Llewellyn and V. Hornebecq, "Functionalised micro-/mesoporous silica for the adsorption of carbon dioxide," *Microporous and Mesoporous Materials,* vol. 99, pp. 79-85, 2007.

[61] O. G. Nik, B. Nohair and S. Kaliaguine, "Aminosilanes grafting on FAU/EMT zeolite: Effect on CO2 adsorptive properties," *Microporous and Mesoporous Materials,* vol. 143, pp. 221-229, 2011.

[62] L. Marini, *Geological Sequestration of Carbon Dioxide. [Electronic Resource] : Thermodynamics, Kinetics, and Reaction Path Modeling.* Amsterdam ; Oxford : Elsevier, 2007.

[63] A. Y. Manakov, Y. A. Dyadin, A. G. Ogienko, A. V. Kurnosov, E. Y. Aladko, E. G. Larionov, F. V. Zhurko, V. I. Voronin, I. F. Berger, S. V. Goryainov, A. Y. Lihacheva and A. I. Ancharov, "Phase Diagram and High-Pressure Boundary of Hydrate Formation in the Carbon Dioxide-Water System," *J. Phys. Chem. B,* vol. 113, pp. 7257-7262, 2009.

[64] V. Hernandez-Valencia, M. W. Hlavinka, J. A. Bullin and I. N. C. Bryan, "Design glycol units for maximum efficiency," *Research & Eng.,* pp. 310-317, 1992.

[65] O. Aschenbrenner and P. Styring, "Comparative study of solvent properties for carbon dioxide absorption," *Energy & Environmental Science,* vol. 3, pp. 1106-1113, 2010.

[66] D. W. Breck, *Zeolite Molecular Sieves: Structure, Chemistry, and Use.* New York, Wiley, 1974.

[67] M. W. Anderson, O. Terasaki, T. Ohsuna, A. Philippou, S. P. MacKay, A. Ferreira, J. Rocha and S. Lidin, "Structure of the microporous titanosilicate ETS-10," *Nature,* pp. 347, 1994.

[68] S. M. Kuznicki, "Large-pored crystalline titanium molecular sieve zeolites,", 19910430; 1991.

[69] S. M. Kuznicki, K. A. Thrush and H. M. Garfinkel, "Use of crystalline molecular sieves containing charged octahedral sites in cyclic desiccating processes,", 1993.

2. Literature background

2.1. Summary

Adsorption is a process in which gas or liquid molecules/atoms adhere to the surface of a certain solid known as an adsorbent. It is known as a fundamental separation technique in chemical and petrochemical industries and has been studied and improved by many researchers in the past decades [1, 2]. Not only it has been widely employed for removal of low-concentration impurities and pollutants from fluid streams, it is also the major part of chromatography and catalytic-reaction processes [3]. Most industrially important reactions are catalytic and 90% of chemicals are produced through a heterogeneously catalyzed process where the surface reaction occurs between the two key steps of adsorption of reactant and desorption of product species [3, 4]. Various technologies have been developed and still developing to improve adsorption mechanism and reach an efficient and desired separation. These improvements include adsorption design and process cycle development and optimization, manipulation of the structure and chemistry of the adsorbent to provide greater attractive forces for specific applications (e.g. by adjusting the size of the pores, to control access to the adsorbent surface on the

basis of molecular size) as well as discoveries of new, porous, high-surface area adsorbent materials (e.g. molecular sieve zeolites) [5]. Commercial adsorbents can be classified by their natural structure (amorphous or crystalline[1]), by the nature of their surfaces (polar, nonpolar, or intermediate), by the sizes of their pores (micropores, mesopores, and macropores), or by their chemical composition. Besides physical properties such as particle size, density, void fraction, etc. are key factors. Deactivation of the adsorbents during the extended usage by reaction with impurities, reaction of adsorbates, or thermal damage is important to consider. All of these factors are important in the selection of the best adsorbent for any specific application [5].

Following the brief discussion on the importance of adsorption technique is the theory of adsorption as well as its equilibrium, kinetics and dynamics, which are explained in this chapter. The mechanism of hydrogen sulfide adsorption on metal/metal oxide surfaces and study of regenerable desiccants, which are the focal points of this thesis, will be addressed at the end of the chapter.

2.2. The concept and fundamentals of adsorption

Adsorption is a surface phenomenon in which the outer or the topmost boundary of

---

[1] Properties and applications of amorphous and crystalline adsorbents are tabulated in [6].

the solid adsorbent attracts molecules from a fluid phase. Due to the asymmetric nature of the surface (or imbalanced forces of intermolecular interaction), the outermost bonds are unsaturated [6] and interaction forces, reprehensive of the bulk properties, change abruptly. The surface then becomes capable of attracting particles from the gas phase with a specific reactivity. As a result of interacting forces between the particles from the fluid phase and surface of the solid phase, the potential energy (PE)[2] of the adsorbing molecule close to the solid surface reduces and fluid particles tend to concentrate in the interphase boundary. Adsorbed molecules/ atoms create a film of condensed phase on the adsorbent with higher molecular density compared to the fluid phase called adsorbate.

2.2.1. Adsorption forces

The strength of the surface bonding depends on the nature of the adsorbent and the adsorbing fluid and can be any where between van-der-Waals (<50 kJ/mole) to metallic and ionic bonds (>50 kJ/mole) [7]. Depending on the strength of the interaction forces, adsorption can be classified to physisorption (physical adsorption) and chemisorption (chemical adsorption) [1, 8].

Physisorption is the most common form of adsorption where adsorbate molecules are attached to the solid surface by relatively weak interactions known as van der Waals forces [6, 9]. Since physisorption is governed by week electrostatic forces (dipole or quadrupole interactions), molecules remain intact and can be easily freed

---

[2] Explained in section 2.2.3

by heating or dropping the system pressure [6, 10]. The structure and texture of the adsorbent is also unaffected.

Chemisorption, on the other hand, happens when a chemical interaction occurs between the fluid and the solid surface and /or by a chemical reaction occurring at the exposed surface [3, 6, 11]. Unlike physical adsorption, which occurs on all surfaces at a favorable range of physical conditions (i.e. temperature and pressure), chemisorption takes place only on certain active sites. The adsorbate molecules split into atoms, radicals, or ions, which create a chemical bond with the adsorption site and form a surface compound. The chemical bond involves transferring of electrons between the adsorbate and solid substrate and a substantial rearrangement of electron density. These strong chemical interactions can be either the extreme of virtually ionic (complete electron replacement) or covalent character (sharing electrons) [12]. Not only much higher amount of energy is required to reverse a chemical adsorption (compared to physisorption) because of the strong bonding, even a sufficient amount of energy may only carry away the surface compound [13].

Table 2-1 summarizes the typical characteristics of physical and chemical adsorptions. As it is mentioned in this table chemisorption is a monolayer process in which adsorbate molecules need direct contact with the active surface, but physisorption has the potential of forming multiple layers of adsorbed molecules under proper conditions.

Table 2- 1 Typical characteristics of physical and chemical adsorbents [6, 14].

	Chemisorption	Physisorption
Temperature Range (over which adsorption occurs)	Virtually unlimited (but a given molecule may effectively adsorb only over a small range)	Near or below the condensation point of the gas (e.g. Xe < 100 K, CO_2 < 200 K)
Adsorption Enthalpy	Wide range (related to the chemical bond strength) - typically 40 - 800 kJ mol^{-1}	Related to factors like molecular mass and polarity - typically 5-40 kJ mol^{-1} (similar to heat of liquefaction)
Nature of Adsorption	Often dissociative May be irreversible	Non-dissociative Reversible
Saturation Uptake	Limited to one monolayer	Multilayer uptake possible
Adsorption Kinetics	Very variable Often an activated process	Fast Non-activated process
Material Specificity (variation between substrates of different chemical composition)	Substantial variation between materials	Slight dependence upon substrate composition

Physisorption and chemisorption processes may happen simultaneously on a sample [13]; e.g. physisorption may occur on inactive sites of a heterogeneous adsorbent while chemisorption occurs on active sites, or a layer of physisorbed

molecules can be on top of an underlying chemisorbed layer and vice versa. Besides the same surface can display physisorption at one temperature and chemisorption at elevated temperatures. This is possible from the fact that physisorption weakens rapidly with temperature elevation however chemisorption gets improved at high temperature due to the activation energy required for the strong interactions.

2.2.2. Dissociative chemisorption

Chemisorption of diatomic molecules on adsorbent surfaces (such as hydrogen on copper surfaces [15]) usually occur through a rearrangement of the electronic configuration followed by the dissociation of the molecule into two atoms [4]; new adsorbate species. The absorbed molecule known as a precursor state diffuses across the surface to the chemisorption sites where the molecular bond is broken in favor of new bonds to the surface. The energy to overcome the activation potential of dissociation usually provided by the translational energy and vibrational energy [15].

2.2.3. Potential energy curve

Potential energy curve displays the variation of the energy $\varphi(z)$ of a adsorption system versus the distance of an adsorbing molecule from the surface (z). As a molecule approaches the surface feels the attraction to the surface, which eventually leads to a fundamental interaction. Upcoming very close to the surface, it feels the strong repulsive forces due to the electron density overlap, which cause

a rapid increase in the potential energy of the system.

Physisorption and chemisorption potential energy curves (Curve (a) and (b) in Figure 2.1 respectively) are qualitatively similar. However, physical forces make a shallow minimum in the PE curve at a relatively large distance from the solid surface (typically $z > 3$ Å) before the rapid increase in the total energy occurs [16]. As it can be seen in Figure 2-1 the potential energy diagram corresponding to dissociative chemisorption (curve (c)) can be explained as the combination of the potential for the physisorption of an un-dissociated molecule (curve (a)) and the chemisorption potential of two dissociated atomic specious (curve (b)) [8].
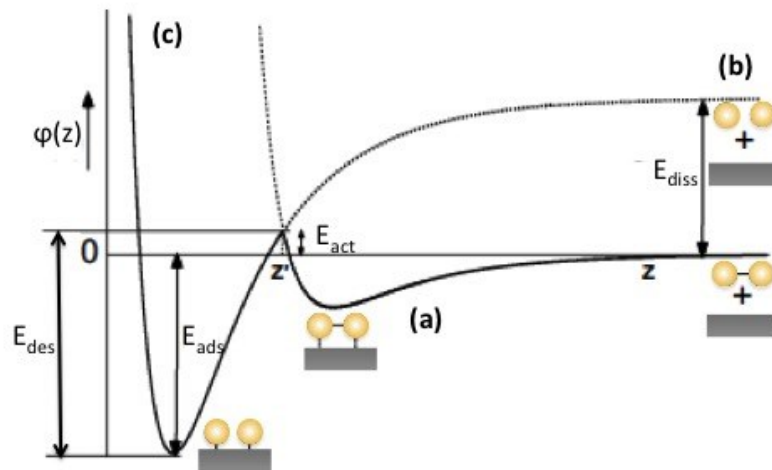
Figure 2- 1 Typical potential energy curve for a dissociative chemisorption of a diatomic molecule [8].

A substantial amount of energy is required for the dissociation of a diatomic

molecule equidistant (far) from an adsorbent surface[3]. Figure 2-1- curve (b) in shows two monatomic species after well separated from each other. When they approach the surface (z decreases) their electronic structures get perturbed and they both form chemical bonds with the surface (a deep chemisorption PE minimum). However the dissociation energy (E_{diss}) to break diatomic bond is very big. Alternatively the diatomic molecule is attracted to the surface through a physisorbate state, known as the precursor-mediated before bond dissociation [8]. Then electrons transfer from the surface to this molecule cause strong molecular bond and dissociation of the diatomic molecule to two monatomic species, which gets chemisorbed to the surface with total adsorption energy of E_{ads} (Figure 2-1 curve (c)).

Dissociative chemisorption is an activated process in which a molecule needs to overcome the energy barrier of E_{act}, which is lower than the dissociation energy (E_{diss}). This clearly shows why this mechanism is favorable in practice.

2.3. Adsorption equilibrium

An adsorbed molecule can leave the surface when it receives energy equal to or greater than the energy of adsorption. This phenomenon is the reverse of adsorption and is called desorption. When the number of molecules attracted by the surface

---

[3] e.g. E_{diss} for H_2 is reported 435 kJ mol^{-1} or 4.5 eV [16].

and staying there is equal to the number of molecules that are leaving the surface the system is at equilibrium [8].

The scientific basis for adsorption is the thermodynamics of adsorbent-adsorbate at equilibrium [1]. Thermodynamic description of adsorption equilibrium, applicable to physical adsorption and chemisorption, employs the Gibbs/Duhem equation [17] for the adsorbate as following [3]:

$$SdT - a'd\Pi + \sum_i x_i d\mu_i' = 0 \qquad\qquad (2-1)$$

where a' is the molar area (surface area per mole of adsorbate) and x_i is adsorbate mole fractions. Π is the spreading pressure, which is the two-dimensional analog of pressure [3].

Considering the equilibrium condition at a constant temperature and ideal gas condition for the gas phase lead to the Gibbs adsorption isotherm as follows:

$$-\frac{a'}{RT}d\Pi + d\ln P + \sum_i x_i d\ln y_i = 0 \qquad\qquad (2-2)$$

where y_i and P are gas-phase mole fraction and pressure respectively.

Experimental data for pure-gas adsorption are reported as number of moles of adsorbate per unit mass of adsorbent (n) at equilibrium as a function of P at constant temperature. Each set of data is known as equilibrium adsorption isotherm and gives information of how much material will be uptaken for a specific gas on a

particular solid adsorbent. There are two main methods to collect adsorption equilibrium data: volumetric and gravimetric method methods. The former is based on mass balance using two volume - calibrated vessels (manifold and sample holder). Monitoring of the pressure and the temperature, combined with an equation of state are required. The later method monitors the weight change of the adsorbent sample in a closed system on a balance. The uptake amount for a given adsorbent is a decisive parameter, since a high uptake usually means a desired/ high adsorbent efficiency. The respective uptake is often called adsorption capacity and characterized by the adsorption isotherm [7].

The adsorption isotherm can be correlated by an analytical relation between n and P consistent with equation $(2-2)$. Considering the compressibility-factor analog for an adsorbate as $Z = \pi a'/RT$, integration of equation $(2-2)$ from $n = 0$ and $P = 0$ to $n = n$ and $P = P$ for a pure chemical species yields to the following general relation between n and P

$$n = k_H P \ exp[\int_0^n (1 - Z)\frac{dn}{n} + 1 - Z] \qquad (2 - 3)$$

Z can be represented by an equation of state for the adsorbate, however the simplest such equation is the ideal-gas analog, $Z = 1$, the Henry's law for adsorption $n = k_H P$ is achieved and k_H is the Henry's constant.

The ideal-lattice-gas equation [3] is an equation of state, which is developed specifically for an adsorbate under the assumption that the surface of the adsorbate

is a two-dimensional lattice of energetically equivalent sites. Each adsorbent site may bind an adsorbate molecule and the bound molecules do not interact with each other. Therefore this model is therefore limited to one layer adsorption (monolayer coverage). Using this equation of state gives the wide known Langmuir isotherm as follows [3]:

$$n = \frac{k_H b' P}{b' + P} \qquad (2-4)$$

where $b' = m/k_H$ and m is the value of n for full monolayer coverage (the saturation value). When $P \rightarrow 0$, Henry law fulfills and at the other extreme, when $P \rightarrow \infty$, n approaches m.

Equation (2-4) can be written in terms of surface coverage θ, i.e., the fraction of occupied sites per available sites on the solid surface. Number of sites in monolayer adsorption is also represented as the fraction of surface sites occupied $\theta = n/m$ ($0 < \theta < 1$).

$$\theta = \frac{bP}{1+bP} \qquad (2-5)$$

where b is the Langmuir constant [18].

However, Langmuir isotherm's original derivation assumed elementary processes for adsorption and desorption and have rates at equilibrium [4]. Since Langmuir isotherm is written based on assumptions at low surface coverage, it fits well to n vs. P data as $\theta \rightarrow 0$ and as $n \rightarrow 0$. However the assumptions become unrealistic

at higher surface coverage and the Langmuir isotherm may provide an approximate overall fit to n vs. P data.

Foo K.Y. et al. presented other isotherm models such as Freundlich, BET, Toth, etc. [12, 19]. Freundlich equation is the earliest 2-parameter empirical model, which is not restricted to the formation of monolayer [4, 19]. Brunauer–Emmett–Teller (BET) [20] isotherm is based on the theory of multilayer adsorption and is most widely applied in the gas–solid equilibrium systems. Toth equation [3] is an empirical extension of the Langmuir isotherm with three parameters for adsorption on heterogeneous adsorbents. Sites are energetically different in heterogeneous adsorbents. Molecules prefer to adsorb onto sites of high energy, but as adsorption progresses, molecules then adsorb onto sites of decreasing interaction energy. Masel R. I. [4] derived the Langmuir isotherm expression for the case of dissociative adsorption.

The shape of the adsorption isotherm provides immediate information about how the adsorption process proceeds over a given surface and about the chemical and physical properties of the catalyst material. Most of the behavior seen during the adsorption of gases on solids can be classified into five general isotherms types [21], depending on the nature of the catalyst and the kind of interaction [7]. Figure 2-2 present these five types.

Type I describes a typical Langmuir isotherm, which is for the adsorption on microporous (micropore diameters < 2 nm [5, 12]) solids. It is not only observed for the adsorption of chemically active gases on metal surfaces but for non-polar

gases (e.g. methane, nitrogen) on zeolites. The more rectangular isotherms have larger Langmuir constants, which reflect stronger affinity for the adsorbate molecules within the micropores. Type II describes a BET adsorption mechanism such as adsorption of water vapor on γ-Al_2O_3, which includes condensation [7]. Type III is typical of polar molecules (e.g. H_2O or methanol) adsorption on a hydrophobic/ non-polar surface (e.g. like charcoal). It is begins rather repulsive interactions leading to a reduced uptake, while at high pressure, ongoing adsorption get facilitated due to capillary condensation in mesopores (micropore diameters between 2 and 50 nm [5, 12]).
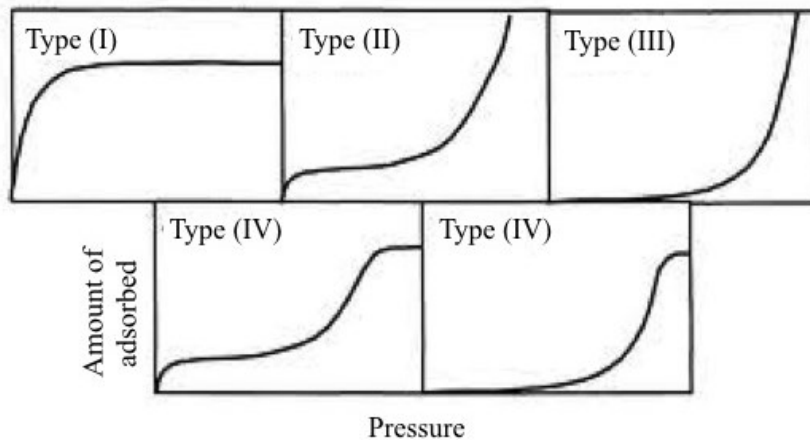
Figure 2- 2 The adsorption isotherms classification [21].

Type IV and Type V are similar to Type II and Type III, with the exception that they have finite limits as pressure reaches saturation pressure due to the finite pore volume of porous solids (capillary condensation effects) [7]. A schematic for the adsorptive molecules in type IV, which also includes type I, and II, is given in

Figure 2-3.
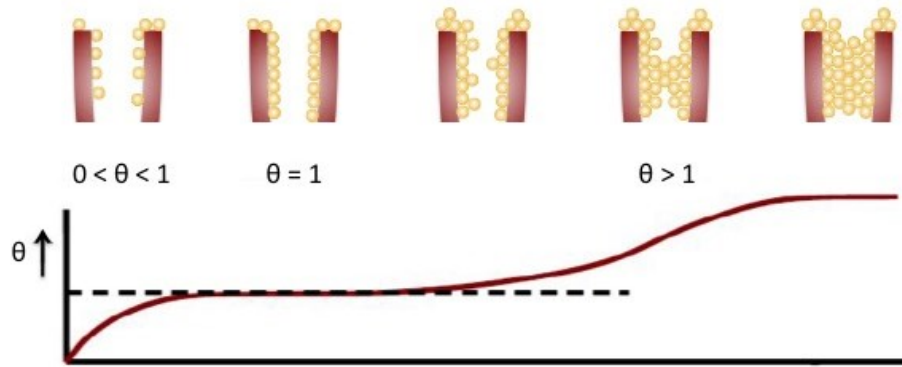
Figure 2- 3 A schematic for the adsorptive molecules on a solid surface at different pressure.

As it is illustrated in Figure 2-3 at very low gas pressures, relatively few molecules are adsorbed, and only a fraction of the adsorbent surface is occupied. As the gas pressure increases isothermally, surface coverage increases. Near the monolayer capacity all surface sites become covered, and higher pressures cannot increase the occupancy anymore. With further increase in pressure multilayer adsorption may take place. However it is also possible that multilayer adsorption happens on one part of a porous surface while vacant sites still remain on another part [7].

Monolayer or multilayer adsorption can be an experimental method to distinct between physisorption and chemisorption. However, for permanent gases above their critical temperature the isotherm is Type I and monolayer. In chemisorption the activation energy for adsorption of the first monolayer is much stronger than

33

the one for the second and subsequent layers. In physisorption, on the other hand, the activation energy for adsorption of the first layer is comparable to the heat of condensation of the next layers [7, 8].

2.4. Adsorption Kinetics

Once chemisorption is referred to a chemical reaction, it is associated with an activated energy, which can be expressed by the Arrhenius rate law [6]. However kinetics are more complex than this in practice. Indeed the activation energy usually varies with surface coverage due to the energetic heterogeneity or interphase interactions. Therefore more precise formulations have been proposed for the adsorption rate representation (Elovich equation [6]). Physisorption, on the other hand, is a process in which the rate is controlled by mass transfer resistance.

Figure 2-4 shows the contact between a porous adsorbent and a fluid phase with different resistances in the mass transfer; external film resistance and intraparticle diffusion resistance. Depending on the adsorption conditions, any one of these resistances may be dominant or a combination of them determines the overall rate of mass transfer.
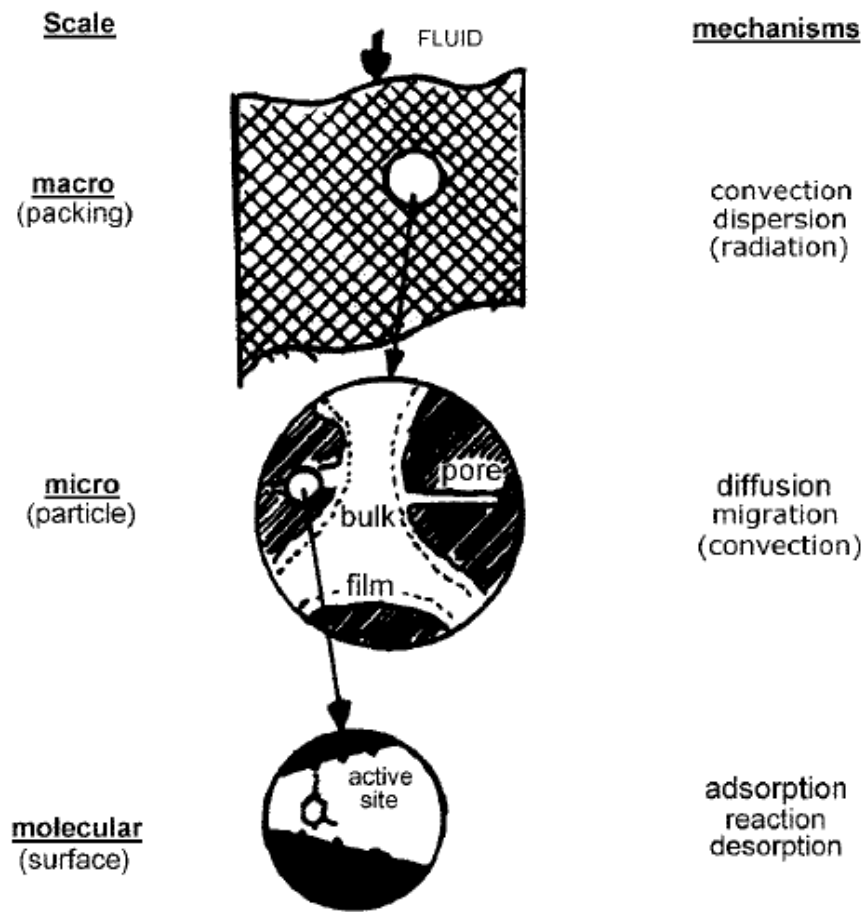
Figure 2- 4 Contact of a fluid phase and a porous adsorbent showing some of the possible mechanism [23].

External film resistance is based on the concept where fluid passing over the surface of an adsorbent particle develops a boundary layer in which the velocity parallel to the surface changed rapidly over a very short distance. Mixing occurs in the bulk stream but not very close to the surface. The adsorbing molecules diffuse through a stagnant boundary layer. If the thickness of the boundary layer (δ) is

small compared to the radius of curvature of the adsorbent particle, then the problem can be solved in one dimension as shown in Figure 2-5. Using the Fick's Law, the molar flux of component i in z direction is [22]:

$$N_{zi} = -D_i \frac{dc_i}{dz} \qquad (2-6)$$

Where D_i is diffusivity of component i in the fluid phase.

Due to the mass conservation the flux of i must be constant through the stagnant film. With the boundary condition depicted in Figure 2-5 the molar flux of i through the film can be simply written as:

$$N_{zi} = -\frac{D_i}{\delta} (c_i - c_i^s) = -k_f (c_i - c_i^s) \qquad (2-7)$$

Since the magnitude of δ is unknown, the mass-transfer coefficient (k_f) is normally used.

k_f is usually calculated from the following empirical correlation (applicable to a wide range of conditions [24])

$$Sh = \frac{k_f d_p}{D_i} = 2.0 + 0.6 Sc^{1/3} Re^{1/2} \qquad 0 < Re < 200 \qquad (2-8)$$

The dimensionless groups Sherwood (Sh), Reynolds (Re) and Schmidt (Sc) are defined as follows:

$$Sh = \frac{k_f d_p}{D_i} \qquad (2-9)$$

36

$$Re = \frac{\rho_g u_s d_p}{\mu_g} \qquad\qquad (2-10)$$

$$Sc = \frac{\mu_g}{\rho_g D_i} \qquad\qquad (2-11)$$
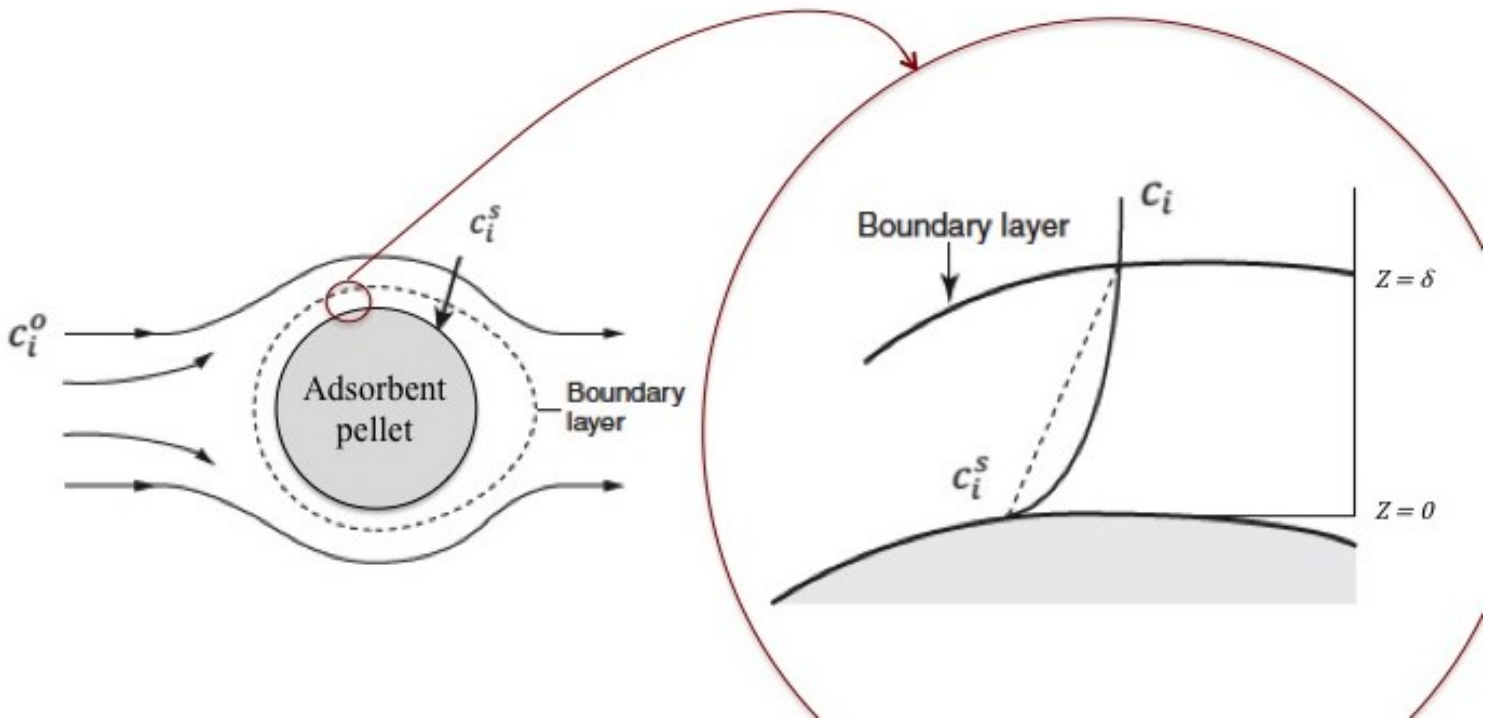
Figure 2- 5 Boundary layer around the surface of an adsorbent pellet.

Intraparticle diffusion resistance includes macropore and micropore diffusion resistances.

Macropore diffusion can be explained by different mechanisms such as bulk

molecular diffusion (dominant in liquid systems), Knudsen diffusion, surface diffusion, and Poiseuille flow.

Knudsen diffusion is dominant when adsorbing molecules collide with the pore wall more frequently than themselves. This happens when the pore diameter is smaller than the mean free path of adsorbing molecules. The mean free path changes inversely with pressure. At atmospheric pressure in pores of less than about 10 nm diameter Knudsen diffusion is dominant [6].

Micropore diffusion occurs in very small pores where the pore diameter is not much bigger than the molecular diameter. Under this condition the diffusing molecule is not able to escape from the force field of the pore wall, then steric effects and the effects of non-uniformity in the potential field are dominant.

Poiseuille flow, which is defined as a flow through the pore under the influence of the pressure gradient, is not usually dominant since most of the time pressure gradients are kept small enough [6].

2.5. Adsorption Dynamics

A good understanding of the dynamic behaviour of the adsorption processes is necessary for the process design and optimization. A dynamic model, which predicts the outlet concentration for any defined change in the system, can

generally be represented by the axial dispersed plug flow model. According to a mass balance for an element of the column the basic differential equation governing the dynamic behavior is as follows [6, 23]:

$$\frac{\partial c_i}{\partial t} + \nabla.(c_i\vec{u_s}) = \nabla.(D_L\nabla c_i) + r_i \qquad\qquad (2-12)$$

which represents the accumulation for specious i is either due to the flux (in-out) across the volume boundary by convection and dispersion or by the consumption through the chemical reaction.

Since for the adsorption systems two phases exist it may be necessary to distinguish between the conditions in the fluid and on the adsorbent surface.

The overall rate of mass transfer for component i over a solid particle is governed by a mass transfer rate expression, which must satisfy the boundary conditions imposed by the equilibrium isotherm, and it must be thermodynamically consistent so that the mass transfer rate be zero at equilibrium. The simplest case is the famous linear driving force expression [25, 26].

When a chemical reaction also occurs on the solid surface, the consideration of the heterogeneous reaction concept is required. This will be addressed in section 2.6.

Since both the equilibrium concentration and the rate coefficients are temperature dependent, when the system is non-isothermal and heat effects are important an energy balance is required and all equations are coupled.

2.5.1. Pressure drop

The prediction of pressure drop in an adsorbent bed is important since when pressure drop is high adsorbent may be fluidized or the excessive force may crush the particles [5]. The most commonly used pressure drop equations are those calculate pressure drop based on Darcy's law [27]:

$$\frac{dP}{dz} = 150 \, (1 - \varepsilon_b)^2 \mu_g v / \varepsilon_b{}^2 d_p^2 \qquad (2 - 13)$$

2.6. Chemical active surfaces

Since in adsorption the uptake amount is highly dependent on the fluid phase concentration, removal of a trace impurity is a crucial issue. An effective technique is to preload the adsorbent with a reactant to enhance the adsorption interactions through a chemisorption and strong bonding (see Figure 2-6). Although physisorption has been used extensively in industry, a number of commercially significant processes employ chemisorption for gas purification. Chemisorption is an important step, the adsorbed molecule forming an intermediate surface compound that is more receptive to chemical reaction [28].

Obviously the higher external surface area of the adsorbent provide higher contact and the higher performance is achieved.

Some examples include:

Desulfurization. An old method for removal of sulfur compounds involves contacting gases containing H_2S with metal oxides loaded on a various type of molecular sieves to adsorb the sulfur in the form of metal sulfide [5].

Mercury Removal. Trace amounts of mercury can be removed from industrial gases, down to low concentrations using activated carbon adsorbent containing sulfur, and allowing reactions involving the formation of mercuric sulfide to adsorb mercury from the gas [5].
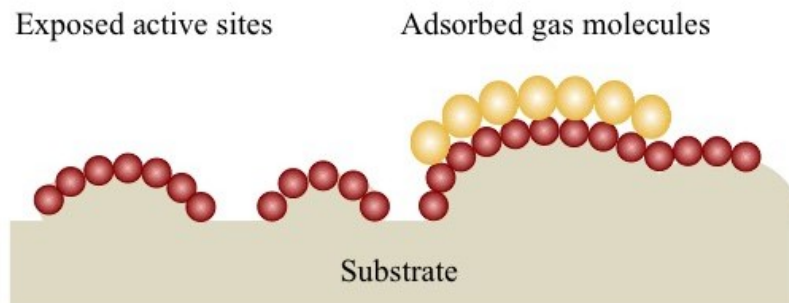
Figure 2- 6 Schematic image of a preloaded adsorbent.

For a heterogeneous non-catalytic reaction system in which a gas contacts a solid and reacts with it, the modification of the kinetic expressions resulting from the mass transfer between phases as well as the contacting patterns of the reacting phases should be considered [29].

41

2.6.1. Shrink core model

The shrinking unreacted core model is a simple mathematical representation of the rate equation, which approximates the reaction progress closely to what really takes place for a wide variety of situations [29, 30].

In this model reaction occurs first at the outer layer of the particle and then moves into the solid. Thus and, at any time there exists an unreacted core of material which shrinks in size during reaction (Figure 2-7).
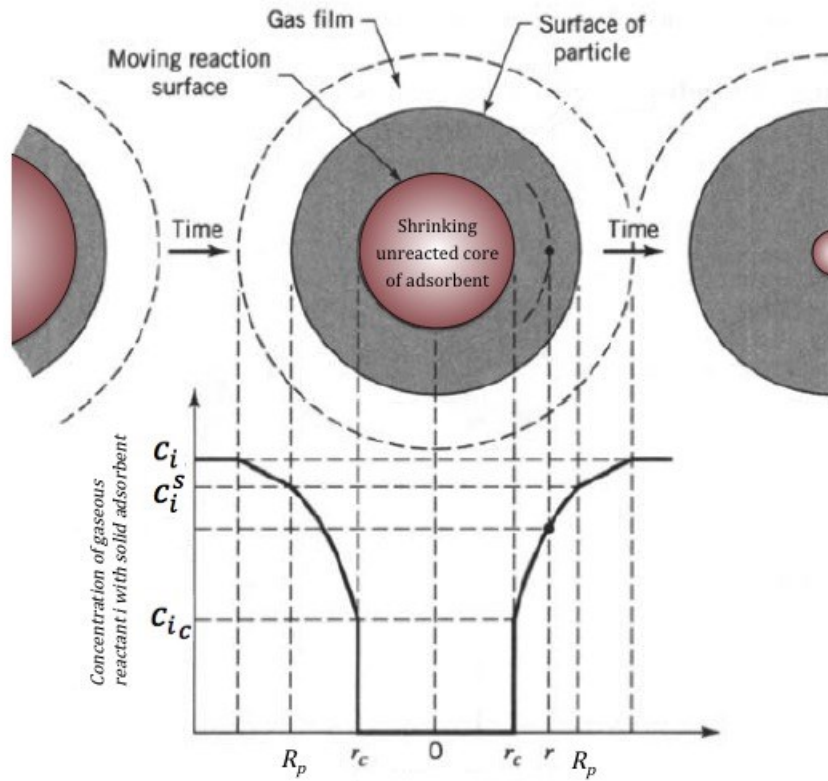
Figure 2- 7 Shrinking unreacted-core model [29].

The rate expression for the gaseous reactant i includes the combination the following resistances [29]:

I. Diffusion of gaseous reactant i through the gas film surrounding the particle to the surface of the solid.

II. Penetration and diffusion of i through a surface solid layer to the surface of the unreacted core.

III. Reaction of gaseous i with solid at this reaction surface.

However for the small adsorbent particles considered in this thesis the second resistance is smaller than the other two and step I and III are rate-controlling.

When the resistance of the gas film controls no gaseous reactant is present at the particle surface; thus, the concentration driving force, $c_i - c_i^s$, becomes c_i, and is constant at all times during reaction of the particle. On the other hand when chemical reaction controls, the progress of the reaction is proportional to the gas phase concentration of spacious i, which is available on the solid surface [29].

In the situations where the combined effects of the tow resistances are important, two limiting cases of diffusion and reaction on a sphere adsorbent particle are considered. On a stationary interface, molar flux of component i equals the rate of reaction. For a simple first-order reaction, the kinetics depend on the surface rate constant, k_r, and the concentration of i at the surface c_i^s:

$$k_f \, (c_i - c_i^s) = -r_i^s = k_r \, c_i^s \tag{2-14}$$

Thus

$$-r_i^s = \frac{k_r k_f c_i}{k_f + k_r} \qquad (2-15)$$

When reaction is rapid ($k_r \gg k_f$), the rate of mass transfer to the surface limits the overall rate of reaction. Under these circumstances:

$$-r_i^s \approx k_f c_i \qquad (2-16)$$

To increase r_i^s (the rate of reaction per unit surface area of solid sphere), c_i and/or k_f need to be increased.

According to equation (2-8), k_f rises for an increase in gas velocity and for smaller particles. For Stockes regime ($Re \ll 1$), equation (2-8) reduces to

$$k_f = \frac{2D_i}{d_p} \qquad (2-17)$$

When Re and Sc are sufficiently large that the number 2 in equation (2-8) be negligible with respect to the second term on the right hand side[31]:

$$k_f = 0.6 \frac{D_i}{d_p} Sc^{1/3} Re^{1/2} \qquad (2-18)$$

$$k_f = 0.6 \frac{D_i^{2/3}}{(\mu_g/\rho_g)^{1/6}} \frac{u_s^{1/2}}{d_p^{1/2}}$$

$$k_f = 0.6(TermI)(TermII) \qquad (2-19)$$

Term I is a function of the physical properties $(D_i, \mu_g/\rho_g)$, which depend on temperature and pressure only. Diffusivity always increases with increasing temperature for both gas and liquid systems however; the kinematic viscosity (μ_g/ρ_g) increases rapidly with temperature for gases and decreases exponentially with temperature for liquids. Term II is a function of flow conditions and particle size. Thus, to increase k_f and k_f consequently, we need to either increase the velocity of the fluid phase or decrease the particle size.

On the other hand when reaction is slow ($k_r \ll k_f$), the rate of reaction on the surface limits the overall rate of reaction. Under these circumstances:

$$-r_i^s \approx k_r c_i \qquad\qquad (2-20)$$

In this case the reaction rate is independent of the velocity of the fluid and for the solid sphere considered here, independent of particle size [31].

Figure 2-8 shows the change in reaction rate with Term II in equation (2-19). At low velocities the mass transfer boundary layer thickness is large and diffusion limits the reaction. At high velocities, the boundary layer thickness is smaller, and the mass transfer across the boundary layer no longer limits the rate of reaction. Also for a given velocity, reaction-limiting conditions can be achieved by using very small particles. However, with decreasing the particle size, the greater the pressures drop in a packed bed is gained.
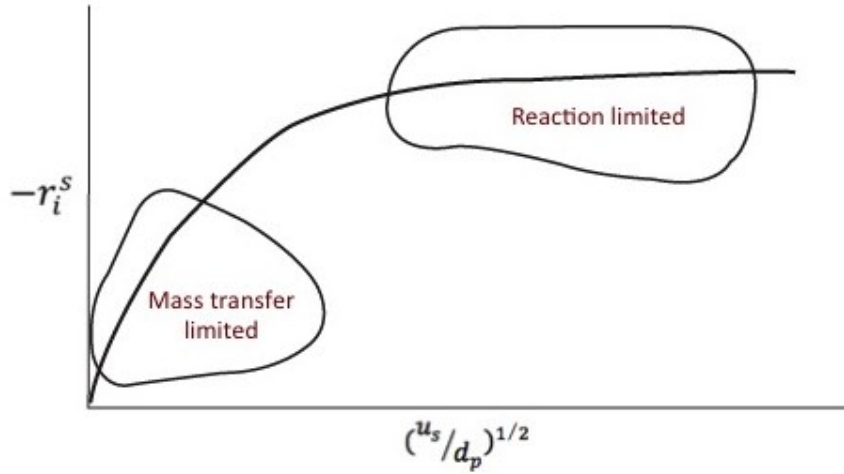
Figure 2- 8 Regions of mass transfer–limited and reaction–limited reactions [31].

2.6.2. Deactivation of active sites on the solid surface

Activity of the solid reactant can occur in the following ways: i) The reactant may produce a side product which deposits on and deactivates the surface. ii) The reaction product may decompose or react further to produce a material that later deposits on and degrades the surface. iii) An impurity in the feed may deposit on and deactivate the surface. iv) Pore mouth blocking by deposited solid, v) Thermal degradation, etc [29, 32].

The change in number of working active sites with the reaction extent is represented by the variation of an activity term for the solid pellet at any time as follows [29, 33]:

$$a = \frac{r_i}{r_i^o} \tag{2-21}$$

46

where r_i^o is rate of reaction for specious i on fresh pellet. In general rate of deactivation may be written as:

$$\frac{da}{dt} = -k_d c_i^\gamma a^\lambda \qquad (2-21)$$

where k_d is the deactivation constant. The simplest case is when $\gamma = 0 \ or \ 1$ and $\gamma = 1$ [34].

The deactivation rate term is introduced into the rate expression and takes into account the changes in surface area, pore volume, and activity of the solid reactant due to the reaction [35].

2.7. Adsorption techniques for acid gas removal

2.7.1. H$_2$S dissociation on metal activated surfaces

It has been shown that transition-metal ions [36-41], metal oxides [42] and TiO$_2$ surface [43] enhance H$_2$S adsorption by facilitating its dissociation to HS$^-$ and S$^-$ ions. HS$^-$ may further react with metal oxide and form sulfide products [44]:

$$H_2S(ads) + 2(*) \rightarrow H^+(*) + HS^-(*) \qquad (2-22)$$

$$HS^-(*) + MO \rightarrow MS + OH^-(*) \qquad (2-23)$$

where M is transition-metal.

Thus the initiation steps in the dissociation mechanism proceed as follows [36-38, 40]: i) Molecular adsorption of hydrogen sulfide on solid surface, ii) Dissociative chemisorption of adsorbed H_2S to HS^- and S^- ions.

These steps occur spontaneously at room temperature and continue by second hydrogen separation on metal surfaces. The corresponding thermodynamic parameters for every stage energy profile of the sequence of the entire events are listed in Table 2-2. It shows the first three reactions are the stoichiometric reaction and occur spontaneously at room temperature. The overall reaction occurs at a low temperature with a complete conversion and selectivity for the hydrogen sulfide [36, 38].

2.7.2. Effective regenerable moisture removal

A solid desiccant is simply an adsorbent, which has a high affinity and capacity for moisture removal. The main requirements for an efficient desiccant are a highly polar surface and a high specific area. The most commonly used desiccants are silica gel, activated alumina, and the aluminum rich zeolites (4A or 13X) [6]. Since the moisture isotherms for these materials have different shapes (Figure 2-9), they have been used for different particular applications.

Table 2- 2 Quantum-chemical calculations of the thermodynamic parameters of the sequential stages of the catalytic hydrogen sulfide decomposition at room temperature [36, 38].

Stage	Reaction	ΔH_{298}	ΔS_{298}	ΔG_{298}
I	Molecular adsorption: $2M + 2H_2S(g) \rightarrow 2M - 2H_2S(ads)$	-12.7	-39.6	-0.9
II	Dissociative chemisorption: $2M - 2H_2S(ads) \rightarrow 2M - SH(ads) + 2H(ads)$	-16.0	2.2	-16.6
III	The removal of the first hydrogen molecule: $2M - SH(ads) + 2H(ads) \rightarrow 2M - (\psi - S_2)(ads) + 2H(ads) + H_2(g)$	-0.2	-21.9	6.3
IV	The removal of the second hydrogen molecule: $2M - (\psi S_2)(ads) + 2H(ads) \rightarrow 2M - (\psi - S_2)(ads) + H_2(g)$	25.5	35.1	15.0
V	Recombination: $2M - (\psi S_2)(ads) \rightarrow 2M + (1/4)S_8(ads)$	-19.6	-29.0	-11.0
	Overall catalytic reaction: $2H_2S(g) \rightarrow 2H_2(g) + (1/4)S_8(ads)$	-23.0	-53.2	-7.2
	Gas-phase reaction: $2H_2S(g) \rightarrow 2H_2(g) + (1/4)S_8(g)$	15.8	10.3	18.9
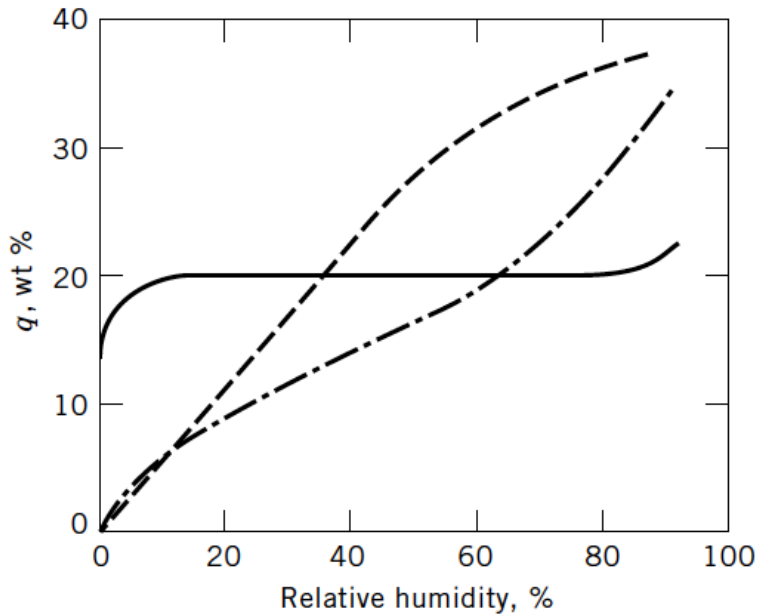
Figure 2- 9 Adsorption equilibrium isotherms for moisture on three commercial adsorbents: pelletized 4A zeolite (solid line), silica gel (dashed line), and a typical activated alumina (dot dashed line) [6].

The rectangular form of the moisture isotherm on zeolites shows their high affinity and high capacity at low moisture partial pressure.

The major disadvantage of zeolite desiccants is that a high temperature is required for regeneration, which makes their use uneconomic when temperatures are typically greater than 200 °C [45]. An effective regenerable desiccant is a desirable adsorbent capable of two things: substantially drying a gas stream at relatively low water concentration (classical molecular sieve zeolites); and reactivating under mild conditions (amorphous gel-type desiccants). Titanosilicate desiccants can potentially provide a high degree of drying with regeneration at much lower temperatures and energy inputs than other desiccants [46].

50

2.8. Conclusions

Adsorption capacity of an adsorbent for a particular adsorbing molecule is highly dependent on the interaction between adsorbent and adsorbate molecules. Chemisorption is known as a brand of adsorption with strong interaction. Loading active compounds on high surface area substrates take the advantage of both chemisorption and high accessibility of the sites. The adsorption process also needs to be optimized to use the separation potential of the adsorption system efficiently. Development of novel adsorbents as well as process technologies is then growing in recent years and still crucial to the chemical processing industry.

2.9. References

[1] R. T. Yang, *Gas Separation by Adsorption Processes.* Boston : Butterworths, 1987.

[2] T. E. Whyte, C. M. Yon and E. H. Wagener, *Industrial Gas Separations.* Washington, D.C. : American Chemical Society, 1983.

[3] J. M. Smith and H. C. Van Ness, *Introduction to Chemical Engineering Thermodynamics.* New York, McGraw-Hill, 2d ed, 1959.

[4] R. I. Masel, *Principles of Adsorption and Reaction on Solid Surfaces.* New York : Wiley, 1996.

[5] "Adsorption, Gas Separation," *Kirk-Othmer Encyclopedia of Chemical Technology,* pp. 617, 2007.

[6] "Adsorption" *Kirk-Othmer Encyclopedia of Chemical Technology,* pp. 582, 2007.

[7] *Modern Methods in Heterogeneous Catalysis Research*. Available: http://www.fhi-berlin.mpg.de/acnew/department/pages/teaching/pages/teaching__wintersemester__2010_2011/klaus_christmann__adsorption__101105.pdf. (Accessed on Jan. 8th, 2015).

[8] Z. Renju, "Desorption of gases from graphitic and porous carbon surfaces," 2004.

[9] C. N. Satterfield, *Mass Transfer in Heterogeneous Catalysis.* Malabar, Fla. : R. E. Krieger Pub. Co.,1981.

[10] R. T. Yang, *Adsorbents : Fundamentals and Applications.* Hoboken, N.J.: Wiley-Interscience, 2003.

[11] J. R. Schrieffer and R. Gomer, "Induced covalent bond mechanism of chemisorption," *Surf Sci,* vol. 25, pp. 315-320, 1971.

[12] D. W. Breck, *Zeolite Molecular Sieves: Structure, Chemistry, and Use.* New York, Wiley, 1974.

[13] *Chemisorption*.

Available: http://www.micromeritics.com/Repository/Files/Chemisorption_Poster.pdf. (Accessed on Jan. 20th, 2015).

[14] *The Surface Analysis Forum*.

Available: http://www.uksaf.org/home.html. (Accessed on Jan. 16th, 2015).

[15] C. T. Rettner, D. J. Auerbach, J. C. Tully and A. W. Kleyn, "Chemical dynamics at the gas-surface interface," *J. Phys. Chem.,* vol. 100, pp. 13021-13033, 1996.

[16] *An Introduction to Surface Chemistry*.

Available: http://www.chem.qmul.ac.uk/surfaces/scc/. (Accessed on Jan. 20th, 2015).

[17] A. L. Myers, "Thermodynamics of adsorption in porous materials," *AICHE J.,* vol. 48, pp. 145-160, 2002.

[18] I. Langmuir, "The Adsorption of Gases on Plane Surfaces of Glass, Mica And Platinum," *J. Am. Chem. Soc.,* vol. 40, pp. 1361-1403, 1918.

[19] K. Y. Foo and B. H. Hameed, "Insights into the modeling of adsorption isotherm systems," *Chem. Eng. J.,* pp. 2, 2010.

[20] S. Brunauer, P. H. Emmett and E. Teller, "Adsorption of Gases in Multimolecular Layers," *J. Am. Chem. Soc.,* vol. 60, pp. 309-319, 1938.

[21] *The Adsorption of Gases and Vapors, Volume I.*

Available: https://archive.org/details/adsorptionofgase031704mbp. (Accessed on Jan. 10th, 2015).

[22] M. E. Davis and R. J. Davis, *Fundamentals of Chemical Reaction Engineering. [Electronic Resource]*. Boston : McGraw-Hill, International ed, 2003.

[23] H. A. Jakobsen, "Fixed Bed Reactors," Department of Chemical Engineering Norwegian University of Science and Technology, 2011.

[24] N. Wakao and T. Funazkri, "Effect of fluid dispersion coefficients on particle-to-fluid mass transfer coefficients in packed beds: Correlation of sherwood numbers," *Chemical Engineering Science,* vol. 33, pp. 1375-1384, 1978.

[25] S. N. Nobar and S. Farooq, "Experimental and modeling study of adsorption and diffusion of gases in Cu-BTC," *Chemical Engineering Science,* pp. 801, 2012.

[26] R. Haghpanah, A. Rajendran, S. Farooq, I. A. Karimi and M. Amanullah, "Discrete Equilibrium Data from Dynamic Column Breakthrough Experiments," *Ind Eng Chem Res,* vol. 51, pp. 14834-14844, 2012.

[27] R. Haghpanah, A. Majumder, R. Nilam, A. Rajendran, S. Farooq, I. A. Karimi and M. Amanullah, "Multiobjective Optimization of a Four-Step Adsorption Process for Postcombustion CO2 Capture Via Finite Volume Simulation," *Ind Eng Chem Res,* vol. 52, pp. 4249-4265, 2013.

[28] *Introduction to Chemical Adsorption Analytical Techniques and their Applications to Catalysis.*

Available:
http://www.micromeritics.com/repository/files/intro_to_chemical_adsorption.pdf.
(Accessed on Jan. 20th, 2015).

[29] O. Levenspiel, *Chemical Reaction Engineering; an Introduction to the Design of Chemical Reactors*. New York, Wiley, 1962.

[30] "A grain size distribution model for non-catalytic gas-solid reactions," 20140118, 1993.

[31] H. S. Fogler, *Elements of Chemical Reaction Engineering.* Upper Saddle River, NJ : Prentice Hall PTR, 4th ed, 2006.

[32] C. H. Bartholomew, "Mechanisms of catalyst deactivation," *Applied Catalysis A: General,* vol. 212, pp. 17-60, 2001.

[33] N. Yaşyerli, T. Doğu, G. Doğu and i. Ar, "Deactivation model for textural effects of kinetics of gas-solid noncatalytic reactions "char gasification with CO2"," *Chemical Engineering Science,* vol. 51, pp. 2523-2528, 6, 1996.

[34] S. Yasyerli, G. Dogu, I. Ar and T. Dogu, "Activities of copper oxide and Cu-V and Cu-Mo mixed oxides for H2S removal in the presence and absence of hydrogen and predictions of a deactivation model," *Ind Eng Chem Res,* vol. 40, pp. 5206-5214, 2001.

[35] H. F. Garces, H. M. Galindo, L. J. Garces, J. Hunt, A. Morey and S. L. Suib, "Low temperature H2S dry-desulfurization with zinc oxide," *Microporous Mesoporous Mat.,* vol. 127, pp. 190-197, 2010.

[36] A. N. Startsev, I. I. Zakharov, O. V. Voroshina, A. V. Pashigreva and V. N. Parmon, "Low-temperature decomposition of hydrogen sulfide under the conditions of conjugate chemisorption and catalysis," *Doklady Physical Chemistry,* vol. 399, pp. 283-286, 2004.

[37] Y. M. Choi, C. Compson, M. C. Lin and M. Liu, "A mechanistic study of H2S decomposition on Ni- and Cu-based anode surfaces in a solid oxide fuel cell," *Chemical Physics Letters,* vol. 421, pp. 179-183, 2006.

[38] I. I. Zakharov, A. N. Startsev, O. V. Voroshina, A. V. Pashigreva, N. A. Chashkova and V. N. Parmon, "The molecular mechanism of low-temperature decomposition of hydrogen sulfide under conjugated chemisorption-catalysis conditions," *Russian Journal of Physical Chemistry A,* vol. 80, pp. 1403-1410, 2006.

[39] D. R. Alfonso, "First-principles studies of H2S adsorption and dissociation on metal surfaces," *Surf Sci,* vol. 602, pp. 2758-2768, 2008.

[40] Q. L. Tang, S. R. Zhang and Y. P. Liang, "Influence of Step Defects on the H2S Splitting on Copper Surfaces from First-Principles Microkinetic Modeling," *Journal of Physical Chemistry C,* vol. 116, pp. 20321-20331, 2012.

[41] S. H. Chen, S. Q. Sun, B. J. Lian, Y. F. Ma, Y. G. Yan and S. Q. Hu, "The adsorption and dissociation of H2S on Cu(100) surface: A DTF study," *Surf Sci,* vol. 620, pp. 51-58, 2014.

[42] J. A. Rodriguez, S. Chaturvedi, M. Kuhn and J. Hrbek, "Reaction of H2S and S2 with metal/oxide surfaces: band-gap size and chemical reactivity," *J Phys Chem B,* pp. 5511, 1998.

[43] A. Fahmi, J. Ahdjoudj and C. Minot, "A theoretical study of H2S and MeSH adsorption on TiO2," *Surf Sci,* vol. 352–354, pp. 529-533, 1996.

[44] J. Sun, S. Modi, K. Liu, R. Lesieur and J. Buglass, "Kinetics of zinc oxide sulfidation for packed-bed desulfurizer modeling," *Energy Fuels,* vol. 21, pp. 1863-1871, 2007.

[45] B. Tanchuk, J. A. Sawada, S. Rezaei and S. M. Kuznicki, "Adsorptive drying of CO2 using low grade heat and humid, ambient air," *Separation and Purification Technology,* vol. 120, pp. 354-361, 2013.

[46] S. M. Kuznicki, K. A. Thrush and H. M. Garfinkel, "Use of crystalline molecular sieves containing charged octahedral sites in cyclic desiccating processes" WO1993000152 A1, 1993.

3. A novel copper-exchanged titanosilicate adsorbent for low temperature H$_2$S removal

3.1. Summary

The H$_2$S removal capacity of copper loaded on a number of titanosilicate supports was investigated. Copper supported on Engelhard Titanosilicate-2 (Cu-ETS-2) has been found to be a superior H$_2$S scavenger for maintaining H$_2$S levels below 0.5 ppm because of its high cation exchange capacity and copper dispersion. Cu-ETS-2 demonstrated higher utilization at room temperature when compared to fully developed commercial H$_2$S adsorbents. In addition it was found that the adsorption capacity of Cu-ETS-2 is maintained over a wide range of activation temperatures.

3.2. Introduction

Hydrogen sulfide (H_2S) is a common contaminant in hydrocarbon process streams. In addition to being found in the process streams of coal gasification plants, wastewater treatment plants and petrochemical plants, it is present in natural sources such as hot springs, volcano gases and natural gas. This odorous, colorless, toxic gas is corrosive and poisonous, and has a negative impact on pipelines and catalysis, and ceramic membranes used in syngas separations. Even at levels as low as 3 ppm, severe pipeline corrosion is predicted in the presence of H_2S [1]. Nickel or alumina catalysts, used in steam reforming processes are poisoned by the trace amounts of H_2S in natural gas. PEM fuel cells have anode Pt catalysts that are susceptible to H_2S at even lower levels (0.1-1 ppm), which requires the incoming hydrogen gas to be essentially free of H_2S [2].

Conventional techniques for H_2S removal are absorption in liquids (alkaloamines, ammonia solutions, and alkaline salt solutions), solid supported amines, the Claus Process, and by reaction on activated carbon or metal oxides [3, 4]. Reactive removal of H_2S is common when the gas stream must be polished down to sub-ppm levels.

Much of the previously reported work on reactive sequestration of H_2S has focused on using different forms of supported and unsupported metal oxides and mixed metal oxides, in efforts to improve the adsorbents capacity, thermal stability, and utilization.

Westmoreland et al. have conducted a thermodynamic survey of 28 elements of the periodic table and found that Fe, Zn, Mo, Mn, V, Ca, Sr, Ba, Co, Cu and W oxides are all possible candidates for high temperature desulfurization [5]. The study was focused on selecting materials that would be functional at temperatures between 360°C and 1560°C.

A great deal of effort has been applied to enhancing the adsorptive performance of metal oxides through heteroatom doping. Ayala et al. used zinc ferrite for the desulfurization of coal gases at 538°C [6]. Mixed oxides of copper with Cr, Ce, Al, Mg, Mn, Ti and Fe were also investigated and it was found that $CuO\text{-}Cr_2O_3$ and $Cu\text{-}CeO_2$ were the most efficient desulfurization adsorbents at 650°C [7].

In order to further enhance the utilization of the active metals, a higher degree of metal dispersion is required. Active chemicals (metals/metal oxides) can be loaded on different supports such as Al_2O_3, TiO_2, SiO_2, and zeolites in order to gain more surface areas and improve structural stability.

Tzu-Hsing Ko et al. compared adsorption capacities of Mn, Fe, Cu, Co, Ce and Zn supported on $\gamma\text{-}Al_2O_3$ for H_2S removal in syngas at 500°C-700 °C and found that 100% utilization was achieved using copper and manganese [8]. Gasper-Galvin et al. studied copper, molybdenum and manganese supported on SP-115 zeolite for desulfurization purposes and observed an increase in the mechanical strength of the adsorbents [9]. Copper supported on SiO_2 and natural zeolite (major phases consisting of mordenite and clinoptilolite) was also investigated and compared to pure copper oxide by Kyotani et al. This study showed almost the same

58

breakthrough capacities for copper supported on SiO_2 (15 wt.% copper) and zeolite (20 wt.% copper) as of that for pure copper oxide [10].

Less attention has been paid to H_2S removal from gas streams at room temperature. H_2S removal at room temperature is useful when the gas stream's temperature is low and in applications such as on-board fuel processing of proton exchange membrane fuel cells. A comparative study of different metal oxides (Ag, Cu, Zn, Co, Ni, Ca, Mn and Sn) has been conducted by Mei Xue et al. which showed that the hydrous CuO has the highest H_2S uptake capacity using 10 ppm H_2S in N_2 at room temperature [11]. Yang et al. doped ZnO/SiO_2 with eight different transition metals and compared the H_2S capacities with ZnO/SiO_2 at room temperature. It was shown that copper doped ZnO/SiO_2 had the highest H_2S capacity which was double that of ZnO/SiO_2 [12]. Baird et al. also demonstrated that copper and cobalt dopants enhance the sulfur removal capacity of ZnO at room temperature [1].

At low temperatures H_2S can only react with the first monolayer of metal oxides[1], thus selecting the most reactive metals and applying them to supports that yield the highest surface areas can significantly enhance utilization at these temperatures.

Based on the superior H_2S adsorption performance of Cu-based compounds at room temperature, a novel Cu-based adsorbent was prepared using a non-porous, high surface area titanosilicate as the support (Cu-ETS-2). Titanosilicate-2 (ETS-2) has a high surface area and a high cation exchange capacity making it a suitable support to allow Cu ions a high degree of accessibility toward H_2S.

59

This novel adsorbent was tested for the adsorption of low concentrations of H_2S at room temperature and the copper utilization was compared to commercial, low temperature H_2S adsorbents as well as copper-exchanged Engelhard Titanosilicate-4 (ETS-4) and Engelhard Titanosilicate-10 (ETS-10). The effect of activation temperature on the H_2S capacity of Cu-ETS-2 was also investigated.

3.3. Materials and Methods

3.3.1. Adsorbent preparation

ETS-2, ETS-4 and ETS-10 were hydrothermally synthesized as cited in the literature [13]. The method for ETS synthesis includes the addition of sources of silica, sources of titanium, and sources of alkalinity such as sodium and/or potassium hydroxide and water. Sources of potassium fluoride can be used optionally to improve the solubility of a solid titanium source. Sodium silicate (28.7% SiO_2, 8.9% Na_2O) was the source of silica in ETS-2, ETS-4 and ETS-10.

The source of titanium for ETS-2 was solid Ti_2O_3, while solubilized $TiCl_3$ was used in ETS-4 and ETS-10 synthesis.

For the ion exchange experiments a quantity of the as-synthesized powdered material was mixed with a copper nitrate salt solution. The weight proportion of adsorbent (ETS-2/4/10) to salt and water was 1:2:10. The salt was first dissolved in

the quantity of water then the adsorbent was added and the mixture agitated to create a slurry. The vessel containing the slurry was then placed in an oven at 80°C for approximately 18 hours. Afterward, the exchanged samples were filtered and washed with de-ionized water and dried at 80°C overnight. Adsorbent granules were generated by mixing the Cu-exchanged powder with Ludox HS-40 colloidal silica (10:4 wt/wt ratio). The relatively dry mixture was placed in a cylindrical mold (2.54 cm diameter) and compressed in an axial press to a pressure of 6 metric tons for about 1 minute. The disk formed at this step was crushed and sieved to obtain 20-50 mesh particles.

Prior to analysis, samples were activated in air by heating them in a muffle furnace at a rate of ~4° /min and an isothermal dwell of 2 hrs.

Commercial samples of R3-11G (36 wt.% CuO), R3-12 (40 wt.% ZnO and 40 wt.% CuO), Zinc Oxide (100 wt.% ZnO) were provided by BASF Chemical Company and were sieved to 20-50 mesh particles and used as received.

3.3.2. Adsorption experiments

A sample of 50 mg of the pelletized adsorbent was packed between plugs of glass wool in a stainless steel column of 4 cm length and 0.38 cm inside diameter. The adsorbent was exposed to a continuous flow of 100 ml/min of the 10 ppm H_2S (balance N_2) mixture. The flow rate was controlled by needle valves and was measured using a bubble flow meter. The outlet of the bed was connected to a Gas Chromatograph (GC) equipped with MXT-1 column (60 m length, 0.53 mm ID)

provided by Restek and a FPD detector. The H_2S concentration was monitored continuously during the experiments at 4 min intervals. The breakthrough point was determined when an H_2S concentration of 0.5 ppm was measured at the outlet of the bed. The FPD detector from SRI is specified to be able to detect H_2S at 200 ppb. In our experiments, the typical baseline signal was 5 counts. The area of the integrated peak increased to 55 counts at 10 ppm H_2S at the outlet. This suggests our detection limit is in line with the instrument specification.

3.3.3. Characterization tests

3.3.3.1. Surface area measurements

The specific surface area of the samples was determined by N_2 adsorption using an Autosorb-1 volumetric system from Quantachrome Instruments. The surface area of the adsorbent was calculated using the BET method. Since ETS-2 material is not microporous but is composed of platelets having an exposed surface, multilayer adsorption can occur and the BET theory is best applied for the surface area measurements. A t-plot calculation was done to measure the proportion of micropores in the material.

3.3.3.2. Powder X-ray diffraction (XRD) analysis

The crystalline structures of the adsorbents were examined by XRD measurements using a Rigaku Geigerflex Model 2173 diffractometer equipped with a cobalt

(λ=1.79021Å) rotating anode source and a graphite monochromator for filtering the K-beta wavelengths.

3.3.3.3. Transmission electron microscopy (TEM)

The image and selected area electron diffraction (SAED) of Cu-ETS-2 and ETS-2 particles were investigated by a JEOL 2010 and JEOL 2100 with Lab6 filament transmission electron microscopes (TEM), respectively. Samples in powder form were dispersed in methanol in an ultrasonic bath for 10 minutes. One or two drops of each of these suspensions were then placed on a Carbon Type B, Au grid (300 mesh) and dried prior to analysis.

3.3.3.4. Energy dispersive X-ray spectroscopy (EDX)

The point specific elemental analysis of Cu-ETS-2 particles was done with EDX, which was attached to TEM instrument used in this study.

3.3.3.5. Atomic absorption spectrophotometry (AAS)

Atomic absorption spectrophotometry was performed for investigating the copper content (wt. %) in Cu-ETS-2, Cu-ETS-4 and Cu-ETS-10. A quantity of material was weighed using a balance with 0.1 mg resolution. Nitric acid was then added to the sample to extract the copper species and build-up 10 millilitres of solution. The copper concentration in the solution was measured with VARIAN 220FS atomic absorption spectrophotometer afterward.

3.4. Results and discussion

3.4.1. Characterization of Cu-ETS-2 before H_2S exposure

TEM analysis of the ETS-2 and Cu-ETS-2 samples identified a substantial amorphous component in both ETS-2 and Cu-ETS-2 (Figure 3-1). Card-like components are also seen in the TEM images, which are assigned to an impurity phase. The SAED patterns confirm that only the card-like phase is crystalline.

The TEM images of Cu-ETS-2 (Figure 3-1-b) indicate that the copper exchange process does not change the morphology of ETS-2 (Figure 3-1-a) and the XRD patterns (Figure 3-2) likewise indicate that the structure of the sample is unaffected by the ion exchange process. The low-intensity peaks present in the powder XRD patterns suggest a minor fraction of crystalline impurity is present and the broadening of those peaks further suggest that the crystal sizes should be on the nano-meter scale. The XRD data of Cu-ETS-2 also confirms the high atomic dispersion of copper ions in the ETS-2 structure, since no diffraction peaks for copper compounds are detected.

Point specific elemental analysis of Cu-ETS-2 particles was collected by EDX attached to TEM instrument and the results were used to determine on which component the exchanged copper resided. The ratios of sodium to titanium and copper to titanium of each component in the Cu-ETS-2 TEM results are summarized in Table 3-1. The crystalline component of the exchanged sample

64

contains predominately sodium ions. Due to the low copper content, the impurity phase (with the card-like morphology) will not measurably contribute to the H_2S capacity of the sample. The amorphous component, however, displays the hallmark ion exchange characteristics of the nano-titanate and has a significantly higher copper content compared to the crystalline component. Table 3-1 also shows that copper to titanium ratio in the amorphous component is almost 10 times higher than the one for the crystalline component, making the amorphous component principally responsible for H_2S adsorption.

The XRD and TEM results suggest that the samples studied contain predominately x-ray amorphous ETS-2 and contain a minor portion of inactive, crystalline impurity.
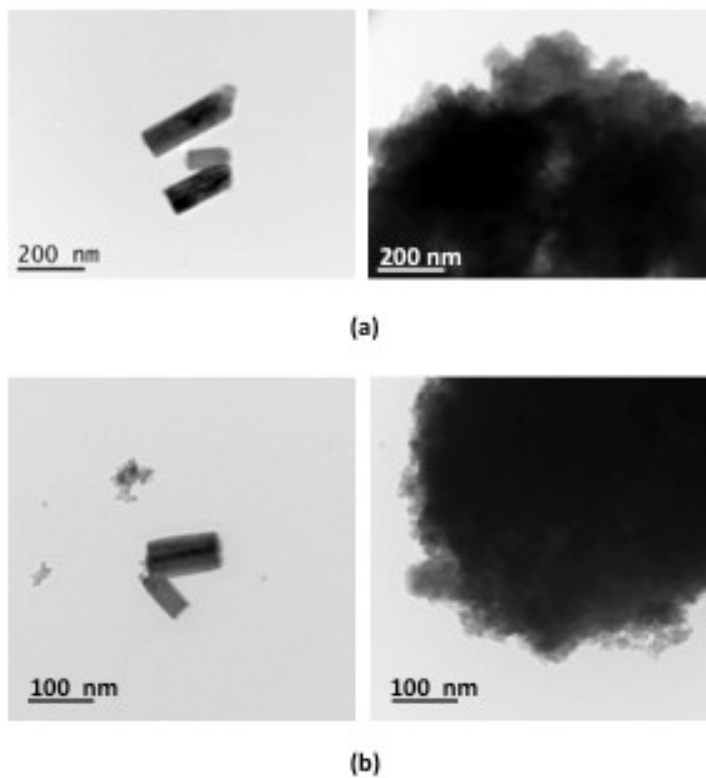
Figure 3- 1 TEM images of ETS-2 (a) and Cu-ETS-2 (b)

Table 3- 1 Elemental ratios derived from EDX analysis results for Cu-ETS-2

Elemental Ratios	crystalline impurity	amorphous component
Cu : Ti	0.02	0.21
Na : Ti	0.15	0.05
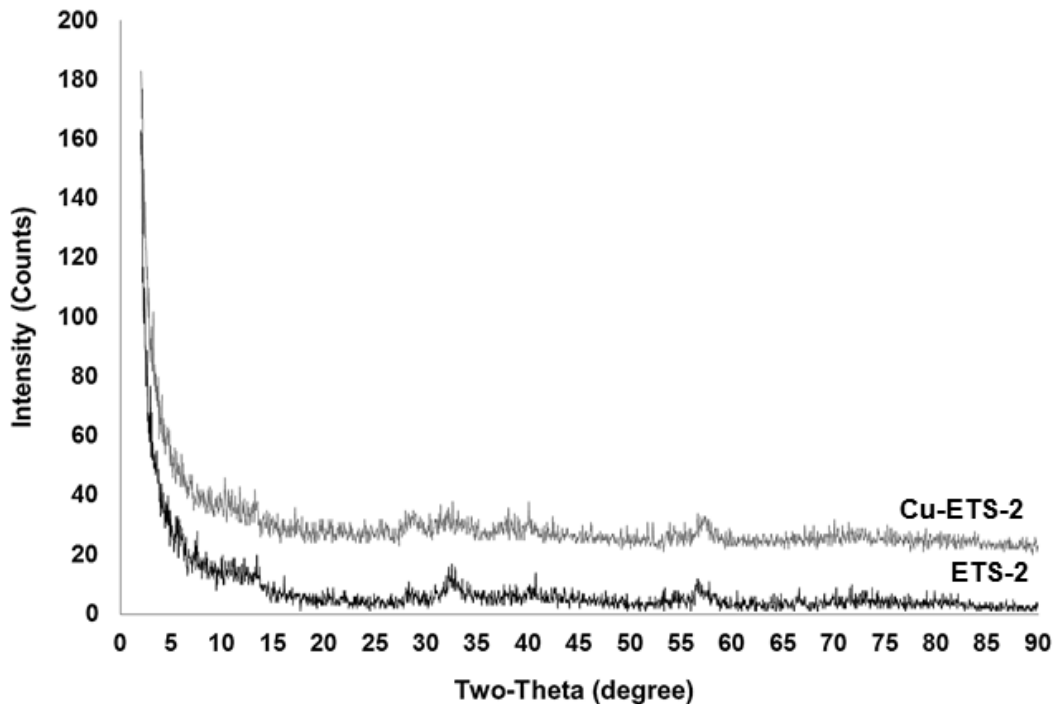
Figure 3- 2 XRD patterns of ETS-2 and as-prepared Cu-ETS-2

The XRD patterns for samples of Cu-ETS-2 exposed to different activation temperatures are shown in Figure 3-3.

The patterns in Figure 3-3 show that Cu-ETS-2 undergoes a phase change at higher activation temperatures. The XRD pattern of Cu-ETS-2 activated at 700°C shows reflections for anatase (TiO_2) and copper oxide (CuO). The intensities of the XRD reflections suggest a bulk conversion where the amorphous phase in Cu-ETS-2 gradually changes at temperatures in excess of 400°C.
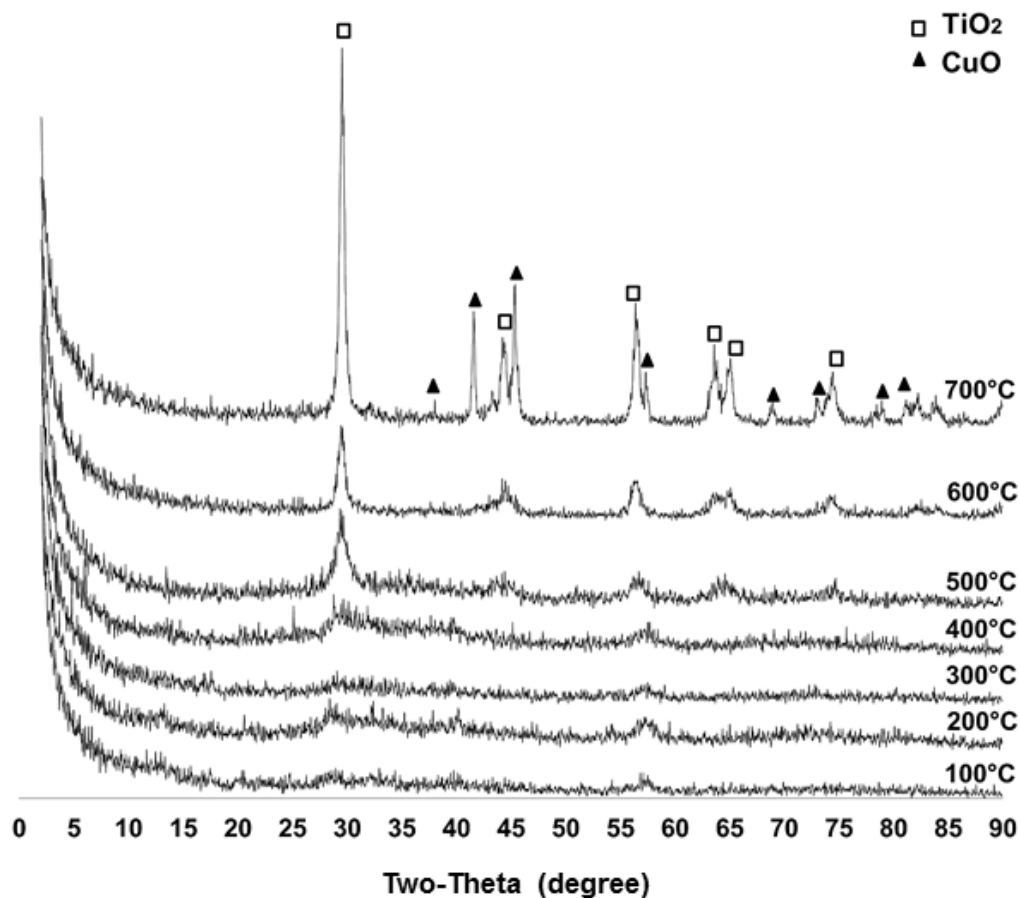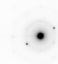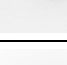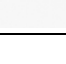
Figure 3- 3 XRD patterns of Cu-ETS-2 activated at different temperatures

A TEM/SAED survey of these samples agreed with the XRD results and showed that the previously amorphous regions gradually change to crystalline material although their morphology did not change significantly. The card-like components maintain their structure and morphology up to 700 °C after which they are no longer observed in the samples (Table 3-2).

68

Table 3- 2 TEM/SAED survey of Cu-ETS-2 samples activated at different temperatures.

Activation temperature	Diffraction pattern of impurity phase (card-like phase)	Structure	Diffraction pattern of amorphous phase	Structure
25 °C		Single crystal		Amorphous
100°C		Single crystal		Amorphous
200°C		Single crystal		Amorphous
300°C		Single crystal		Amorphous
400°C		Crystalline		Amorphous
500°C		Crystalline		Crystalline
600°C		Crystalline		Crystalline
700°C	No card- like phase	NA		Crystalline

The thermal stability of ETS-4 and ETS-10 has been reported in the literature. Naderi et al. investigated the thermal stability of ETS-4 by studying the XRD patterns of the sample activated at different temperatures in air [14]. The authors showed that a partial loss of crystallinity is observed at temperatures $\geq 200°C$. The complete collapse of the crystalline structure was observed at 500°C. Thus copper exchanged ETS-4 will not be stable at temperatures higher than 200°C. However, ETS-10 is stable at a wider temperature range, up to 550°C [15]. Another study also showed that copper exchanged ETS-10 is stable up to 550°C [16].

Surface area measurements were collected for ETS-2, as-prepared Cu-ETS-2, and the commercial H_2S adsorbent samples (Table 3-3). Given that Cu-ETS-2 is predominantly non-crystalline, its surface area must be derived from the external surface of very finely divided platelets that make up the material.

Table 3- 3 Specific surface area of ETS-2, Cu-ETS-2 and commercial samples

Sample	Specific surface area (m^2/g)
ETS-2	230
Cu-ETS-2	187
R3-11G[a]	152
R3-12[b]	118
ZnO	28

[a] 36 wt.% CuO. [b] 40 wt.% CuO + 40 wt.% ZnO.

The t-plot calculation for ETS-2 indicates that the micropore volume and area are equal to 0 cc/g and 0 m^2/g, respectively. This result confirms that ETS-2 is not a microporous material.

3.4.2. Adsorption tests

3.4.2.1. H$_2$S breakthrough capacities of Cu-ETS-2 versus Cu-ETS-4 and Cu-ETS-10

Comparison of the H$_2$S breakthrough capacities on the range of supports (Cu-ETS-2, Cu-ETS-4 and Cu-ETS-10) is given in Table 3-4. All breakthrough experiments were carried out on an equivalent mass of adsorbent under the same test conditions. The H$_2$S capacity was defined as the time it took to measure an outlet concentration of 0.5 ppm H$_2$S. The copper utilization was calculated by converting the breakthrough time to moles of H$_2$S, and then dividing that value by the moles of copper on the adsorbent sample, as measured by atomic adsorption. The blue-green Cu-ETS-2 granules were converted to dark olive green after H$_2$S exposure.

The low copper utilization in Cu-ETS-4 can be explained by a pore blockage effect. In crystalline materials with very small pores and channels in their structure the copper sites nearest the external surface of the crystals react first. When the H$_2$S reacts to form copper sulfide the occluded sulfur partially blocks the pore openings, impeding gas access to the rest of the crystal [10]. The high copper utilization of Cu-ETS-10 was anticipated since ETS-10 has a larger pore diameter that will allow

the gas passage even if the channel is partially blocked. The atomic dispersion of copper in the microporous framework allows for complete utilization of the metal.

Table 3- 4 Cu-ETS-2, Cu-ETS-4 and Cu-ETS-10 breakthrough capacities and copper utilizations

Adsorbent[a]	H_2S breakthrough capacity (mg H_2S/g of adsorbent)	Copper loading wt.%	% Copper utilization
Cu-ETS-2	47	12.5	71
Cu-ETS-4	11	4.8	44
Cu-ETS-10	45	8.4	98

[a] All adsorbents were activated at 100°C.

Unlike Cu-ETS-4 and Cu-ETS-10, which have crystalline microporous frameworks, Cu-ETS-2 is composed of finely divided platelets. The nano-sized platelets provide the material with its relatively high external surface area. The substantial, but incomplete, copper utilization for Cu-ETS-2 may be due to inconsistencies in the sample structure that may not allow some of the exchanged copper ions to react with H_2S, or may be the result of active copper sites being blinded due to copper sulfide formation on the surface of the particles.

3.4.2.2.H$_2$S breakthrough capacity of Cu-ETS-2 versus commercial adsorbents

Cu-ETS-2, activated at 100°C, demonstrated superior H$_2$S breakthrough capacity per gram compared to the ZnO and R3-12 (40 wt.% ZnO + 40 wt.% CuO) commercial adsorbents. The breakthrough times presented in Figure 3-4 show that, under the specified test conditions, Cu-ETS-2 is capable of maintaining a column outlet concentration of H$_2$S of less than 0.5 ppm for ~27 hours. The only commercial sample with longer breakthrough time is R3-11G sample (36 wt.% CuO).
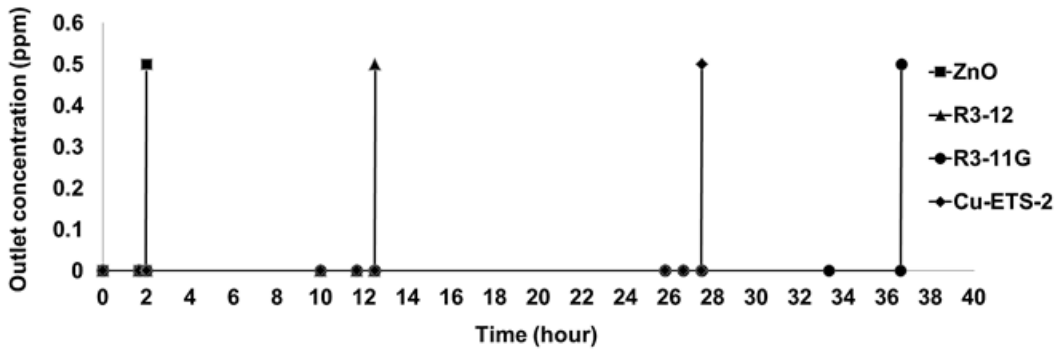
Figure 3- 4 Comparison of the breakthrough times for 50 mg of Cu-ETS-2 and commercial H$_2$S adsorbents

Table 3-5 shows that, despite having the highest capacity, R3-11G suffers from low utilization of copper species (41 wt.%). This is likely due to the dense copper sulfide phase formed during the sulfidation, which blinds the particle to further reaction with H$_2$S [10]. The data also shows that Cu-ETS-2 has the highest

utilization amongst all the samples. The significant improvement in Cu utilization

in Cu-ETS-2 compared to the rest of the samples is caused by an increase in the

degree of dispersion of active species on the ETS-2 support via ion-exchange.

Table 3- 5 Cu-ETS-2 versus commercial samples

Adsorbent	Loading wt.%		% Utilization
	Copper	Zinc	
Cu-ETS-2	12.5	-	71
R3-11G	29	-	41
R3-12	32	32	6.5
ZnO	-	80	0.8

3.4.2.3. *Effect of activation temperature on H_2S capacity of Cu-ETS-2*

In order to investigate the effect of activation temperature on H_2S breakthrough

capacity of Cu-ETS-2, H_2S adsorption tests were conducted for samples activated

at different temperatures.

Figure 3-5 shows that the H_2S capacity of Cu-ETS-2 remains relatively unchanged

after the material has been exposed to temperatures of up to 500°C. The decrease in

capacity after 500 °C correlates with an increase in the intensity of anatase

reflections seen in the XRD patterns (Figure 3-3) and is assigned to a re-crystallization event which renders Cu-ETS-2 inactive toward H_2S.
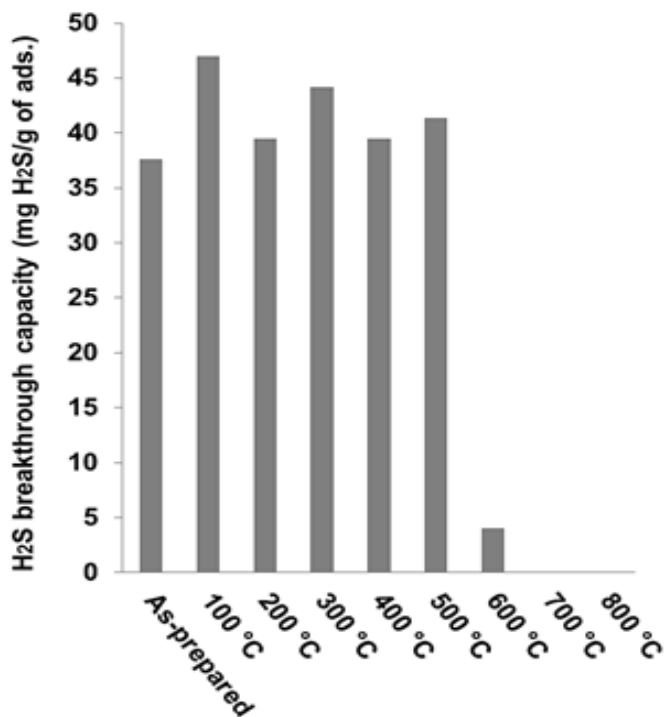
Figure 3- 5 Breakthrough capacity of Cu-ETS-2 activated at different temperatures

3.5. Conclusions

The data collected demonstrates that, at room temperature, Cu-ETS-2 is an H_2S adsorbent with a high gravimetric H_2S capacity and high copper utilization. This adsorbent maintains its capacity over a wide range of activation temperatures. The copper utilization in Cu-ETS-2 is higher than that of highly developed commercial

75

samples due to its high surface area and the degree of copper dispersion in ETS-2. The non-porous nature of the ETS-2 structure takes advantage of the ion exchange characteristics of microporous frameworks.

3.6. References

[1] T. Baird, P. J. Denny, R. Hoyle, F. Mcmonagle, D. Stirling and J. Tweedy, "Modified Zinc-Oxide Absorbents for Low-Temperature Gas Desulfurization," Journal of the Chemical Society-Faraday Transactions, vol. 88, pp. 3375-3382, 1992.

[2] D. A. Berry, D. Shekhawat and J. J. Spivey, *Fuel Cells. [Electronic Resource] : Technologies for Fuel Processing.* Amsterdam ; Boston : Elsevier, 2011.

[3] D. Stirling, *The Sulfur Problem [Electronic Resource] : Cleaning Up Industrial Feedstocks / Diane Stirling.* Cambridge, UK : Royal Society of Chemistry, 2000.

[4] Q. Xue and Y. Liu, "Removal of minor concentration of H2S on MDEA-modified SBA-15 for gas purification," *Journal of Industrial and Engineering Chemistry,* vol. 18, pp. 169-173, 2012.

[5] Westmoreland P.R. , Harrison D.P., " Evaluation of candidate solids for high-temperature desulfurization of low-Btu gases," *Environmental Science and Technology,* vol. 10, pp. 659, 1976.

[6] R. E. AYALA and D. W. MARSH, "Characterization and Long-Range Reactivity of Zinc Ferrite in High-Temperature Desulfurization Processes," *Ind Eng Chem Res,* vol. 30, pp. 55-60, 1991.

[7] J. Abbasian, A. H. Hill, J. R. Wangerow, M. Flytzani-Stephanopoulos, L. Bo and C. Patel, "Development of novel copper-based sorbents for hot-gas cleanup. [Quarterly] technical report, 1992.

[8] T. Ko, H. Chu and L. Chaung, "The sorption of hydrogen sulfide from hot syngas by metal oxides over supports," *Chemosphere,* vol. 58, pp. 467-474, 2005.

[9] Gasper-Galvin L. D., Atimtay A. T., Gupta R. P., " Zeolite-Supported Metal Oxide Sorbents for Hot-Gas Desulfurization," *Ind. Eng. Chem. Res.,* vol. 37, pp. 4157, 1998.

[10] T. Kyotani, H. Kawashima, A. Tomita, A. Palmer and E. Furimsky, "Full paper: Removal of H2S from hot gas in the presence of Cu-containing sorbents," *Fuel,* vol. 68, pp. 74-79, 1989.

[11] M. Xue, R. Chitrakar, K. Sakane and K. Ooi, "Screening of adsorbents for removal of H2S at room temperature," *Green Chem.,* vol. 5, pp. 529-534, 2003.

[12] H. Yang and B. Tatarchuk, "Novel-doped zinc oxide sorbents for low temperature regenerable desulfurization applications," *AICHE J.,* 2010.

[13] S. M. Kuznicki, "Large-pored crystalline titanium molecular sieve zeolites,", 19910430; 19910430, 1991.

[14] M. Naderi and M. W. Anderson, "Phase transformation of microporous titanosilicate ETS-4 into narsarsukite," *Zeolites,* vol. 17, pp. 437-443, 1996.

[15] M. W. Anderson, O. Terasaki, T. Ohsuna, P. Malley, A. Philippou, S. P. Mackay, A. Ferreira, J. Rocha and S. Lidin, "Microporous Titanosilicate Ets-10 - a Structural Survey," Philosophical Magazine B-Physic of Condensed Matter Statistical Mechanics Electronic Optical and Magnetic Properties, vol. 71, pp. 813-841, 1995.

[16] A. Gervasini, C. Picciau and A. Auroux, "Characterization of copper-exchanged ZSM-5 and ETS-10 catalysts with low and high degrees of exchange," *Microporous and Mesoporous Materials,* vol. 35, pp. 457-469, 2000.

4. Breakthrough Performances of Metal-Exchanged Nanotitanate ETS-2 Adsorbents for Room Temperature Desulfurization

4.1. Summary

Engelhard Titanosilicate-2 (ETS-2) has shown to be a promising substrate to load active sites for deep H_2S removal (to sub-ppm levels) for gas purification applications at room temperature. Because of the high external surface area and the cation exchange capacity of ETS-2, active sites can be highly dispersed and very accessible to H_2S molecules making it a novel support material for metal-oxide H_2S adsorbents. In this paper, we report the room temperature H_2S breakthrough performances of ETS-2 metal exchanged with Ag, Ca, Cu and Zn in comparison to a fully developed commercial H_2S adsorbent (R3-11G, 36 wt% CuO, BASF). The results indicate the following trend for H_2S uptake capacities at room temperature: Cu-ETS-2>Ag-ETS-2>Zn-ETS-2≈R3-11G>Ca-ETS-2≈Na-ETS-2. Cu exchanged ETS-2 displays the highest H_2S capacity of 29.7 mg H_2S/g adsorbent compared to the other investigated materials, making it the most promising metal-exchanged ETS-2 for room temperature desulfurization.

4.2. Introduction

Hydrogen sulfide (H_2S) is one of the major contaminants in various industrial gas streams that cause a number of negative effects such as corrosion of the pipelines, generation of harmful environmental emissions, etc. Its removal is therefore extremely necessary [1-4]. Even at very low concentrations (<1 ppm) H_2S has detrimental effects on many industrial catalysts (such as those used in reforming processes and fuel cells) and ceramic membranes (used in syngas separations) [5-7]. In addition, during the combustion process of biogas it causes corrosion in thermal or thermo-catalytic conversion devices [4] as well as resulting in other environmental hazards like acid rain [3, 8].

To improve the separation efficiency and for particular applications (e.g. natural gas sweetening and refining desulfurization of fuel cell system products) there is an increasing requirement for gas purification and H_2S scavenging at low temperatures (<200 °C). In particular, H_2S removal at room temperature for such applications is essential since both reforming and fuel cell catalysts are susceptible to H_2S at levels as low as 0.1-1 ppm [4, 7]. Among the currently used methods for H_2S removal, the adsorptive technique is the simplest and the most efficient and cost effective at low concentration and temperature [4, 9-11]. It is capable of reducing sulfur concentration in the process streams to sub ppm levels [7].

Adsorption processes using various metal and mixed metal oxides have been studied for room temperature [8, 12] and relatively low temperature (<400 °C)

desulfurization [13-15], focusing more on high surface area pure zinc oxide or mixed with other metal-oxides[3, 8, 12-15]. From the differences in the intrinsic reactivity of metal oxides with H_2S by thermodynamic driving force ZnO, CuO, Ag_2O and CaO have shown favorable sulfidation at room temperature [8, 12].

High dispersion of reactive sites can considerably enhance the reaction between metal compounds and H_2S molecules [3]. An approach for improving desulfurization capacity at room temperature is to load reactive sites on high surface area supports, which include zeolites [16-18], carbon sorbents [19, 20], SBA-15 and other mesoporous material supports [17, 21-24]. Cu-ZnO/SiO_2 and Cu supported titanosilicate have been studied for adsorptive removal of H_2S at room temperature as well [7, 25].

To further improve the capacity and utilization of supported metal-oxide adsorbents, Engelhard Titanosilicate-2 (ETS-2) is used as a novel substrate material to load active ions for deep H_2S removal (to sub-ppm levels) for gas purification applications at room temperature. ETS-2 has high external surface area and cation exchange capacity, which allow active ions to be highly dispersed and accessible to H_2S molecules [7].

In the present investigation we have exchanged Na-ETS-2 (native form) with metal ions Cu^{+2}, Ag^+, Zn^{2+}, Ca^{2+}. Their H_2S adsorption and room temperature H_2S removal capacities were then determined and compared to that of a commercial sample. Different characterization techniques such as X-ray diffraction, scanning

electron microscopy with EDX and BET surface area measurements have also been applied to carefully investigate phases and structures of the tested materials.

4.3. Experimental

4.3.1. Preparation of the precursor

Na-ETS-2 was hydrothermally synthesized using a commercial source of titanium (Titanium (III) Chloride Solution 20 % stabilized, Fisher Scientific, Canada) with the following formulation: 13.2 g of sodium hydroxide (97wt.%+ NaOH, Fisher Scientific, Canada) and 4.2 g sodium fluoride (99 wt.%+ NaF, Fisher Scientific, Canada) mixed in 10 g of de-ionized water (resistivity >18 MΩ cm). This mixture was then added to 10.4 g of sodium silicate (28.8 % SiO_2, 9.14 % Na_2O, Fisher Scientific, Canada), followed by the addition of 38.1 g of titanium trichloride (20 % w/w solution in 2N hydrochloric acid, Fisher Scientific, Canada). Finally, the reaction mixture was sealed into a 125 mL Teflon-lined autoclave (Parr Instrument Company, Illinois, USA) and reacted at 100 °C for 7 days. The autoclave was quenched to ambient temperature. The precipitate was washed and filtered by de-ionized water, and then dried in a forced-air oven at 80 °C for 24 hours.

In order to prepare the Ag and Cu exchanged forms of ETS-2, high external surface area Na-ETS-2 (253 m^2/g) was exchanged with nitrate salts (Fisher Scientific, Canada and Anachemia Chemicals, Canada, respectively). For the Zn and Ca

81

exchanged forms, Na-ETS-2 was exchanged with the chloride salts (Fisher Scientific, Canada). The ion exchange procedure was done by mixing a quantity of as synthesized ETS-2 with the salt dissolved in deionized water (weight proportion 1:2:10). Obtained slurry was kept in an oven at 80 °C for approximately 18 h following by filtering and washing with deionized water and dried at 80 °C overnight. The exchanged powders were pressed into binderless pellets, which were then crushed and sieved to 1.19 mm to 0.595 mm (No. 16 to 30 mesh) fraction for use in the H_2S removal test experiments. The commercial sample R3-11G (BASF, New Jersey, USA) was also sieved to obtain the same particle size.

4.4. Adsorption tests

A sample of 30 mg of each adsorbent was packed between plugs of glass wool in a stainless steel column of 3.8 mm (inner diameter). A certified gas mixture 10 ppm H_2S in He (Praxair, Canada) was passed through the column at a continuous flow of 100 mL/min. The feed flow rate was controlled with a mass flow controller (MFC, Alicat Scientific, Arizona, USA). The outlet concentration of the bed recorded at 7 min intervals was monitored using a gas chromatograph (GC) equipped with MXT-1 column 60 m in length and 0.53 mm inner diameter (Restek, Bellefonte, USA) and a flame photometric detector (FPD, SRI Instruments, Canada). The FPD detector is specified to be able to detect H_2S at 200 ppb.

The H2S breakthrough capacity of each adsorbent ($q(t)$) was calculated by using the H2S concentration in the inlet gas (c^o), the gas flow rates (F_{in} and F_{out}, inlet and outlet respectively), bed volume (V_b), column void fraction (ε_b), breakthrough time (t_∞), mass of adsorbent (w), H2S molecular weight (Mw) and is reported as (mg H2S) / (g adsorbent) through the following equation:

$$\frac{Mw}{w} \int_0^{t_\infty} (F_{in} - F_{out}) dt = q(t) + c^o\, V_b\, \varepsilon_b\, \frac{Mw}{w} \qquad\qquad (4-1)$$

Reproducibility was confirmed by repeating the breakthrough experiments at least twice and the testing system error was considered by averaging the measurements for each sample.

4.4.1. Microstructure characterization

The X-ray diffraction (XRD) was conducted to observe the material structures of the tested samples using a Rigaku Geigerflex 2173 (Rigaku Corporation, Tokyo, Japan) with a vertical goniometer. The elemental analysis of the adsorbents was performed using a Zeiss EVO MA 15 (Zeiss, Goettingen, Germany) equipped with a Bruker Silicon Drift Detector for Energy Dispersive X-Ray analysis (EDX). The BET specific surface area data was collected by an ASAP 2020 instrument (Micromeritics Instrument Corporation). Scanning electron microscopy was performed using a high resolution Hitachi S-5500 Series SEM (Hitachi, Japan) equipped with EDX.

4.5. Results

4.5.1. H₂S breakthrough performance

Figure 4-1 demonstrates the H_2S breakthrough capacities for all adsorbents using equation 4-1. Blank correction is neglected due to the prompt H_2S response obtained from the empty column tested with the glass wool. Negligible H_2S removal capacity of the base material Na-ETS-2 confirms that it does not have any role in H_2S removal and has been chosen properly as an inactive substrate to only expose active metal sites toward H_2S molecules. The data also show that among different exchanged forms of ETS-2, Cu exchanged ETS-2 has the highest H_2S removal capacity followed by Ag-ETS-2. The latter's performance is slightly higher than the commercial R3-11G which has almost the same capacity as Zn-ETS-2. Ca exchanged ETS-2 shows minor H_2S uptake capacity under the current experimental conditions.
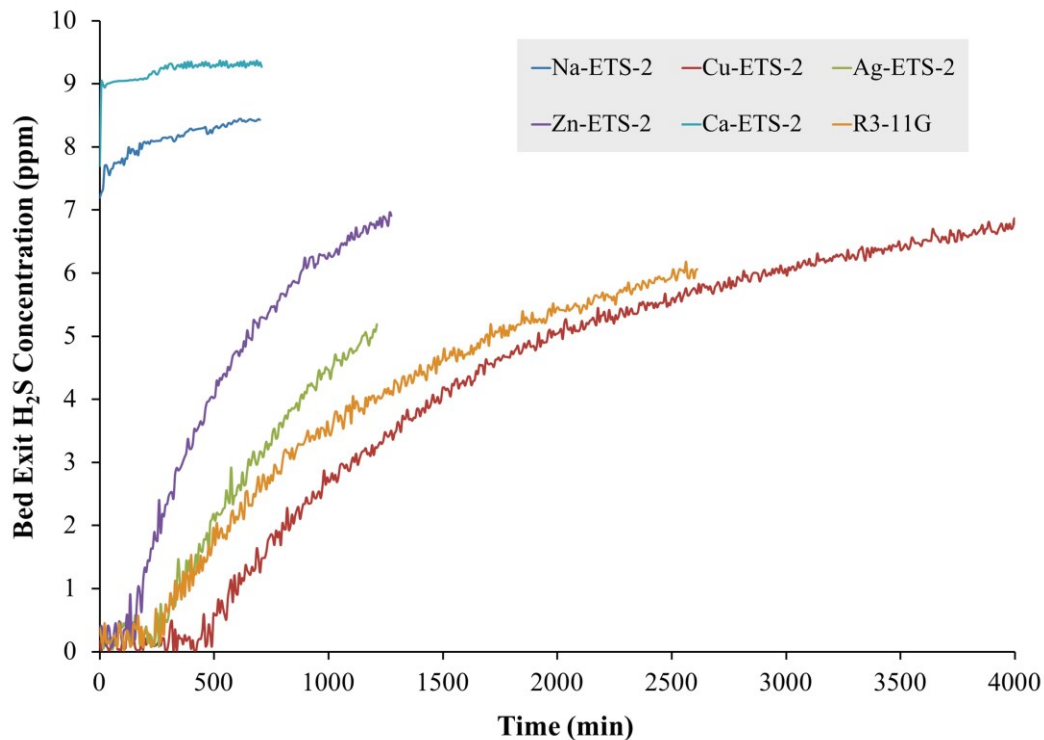
Figure 4- 1 H$_2$S breakthrough profiles of different tested adsorbents.

4.5.2. Phase formation and morphology

While the sulfidation of CuO, Ag$_2$O, ZnO and CaO is thermodynamically favorable at room temperature, it is noticeably different for each oxide (ΔG_{298}, -132.35 kJ/mol, -233.02 kJ/mol, -81.96 kJ/mol, -70.40 kJ/mol, HSC thermodynamic software). H$_2$S removal capacity of the studied samples does not follow the same trend of the metal oxide affinities to reaction with H$_2$S. This simply indicates that several other factors may influence the H$_2$S removal capacity of a metal-exchanged form of ETS-2 (see discussion in section 4.6).

Figure 4-2 shows the XRD patterns of the native and the different metal exchanged forms of ETS-2. The native form is cryptocrystalline as evidenced by low broad peaks in the XRD profile, which are characteristic of nano particles of anatase [25]. It can be seen that no significant crystalline peaks are visible for the rest of the samples, indicating that Na-ETS-2 structure is able to accommodate Ag, Ca, Cu and Zn during the ion exchange process without having any significant effect on its nano structure.
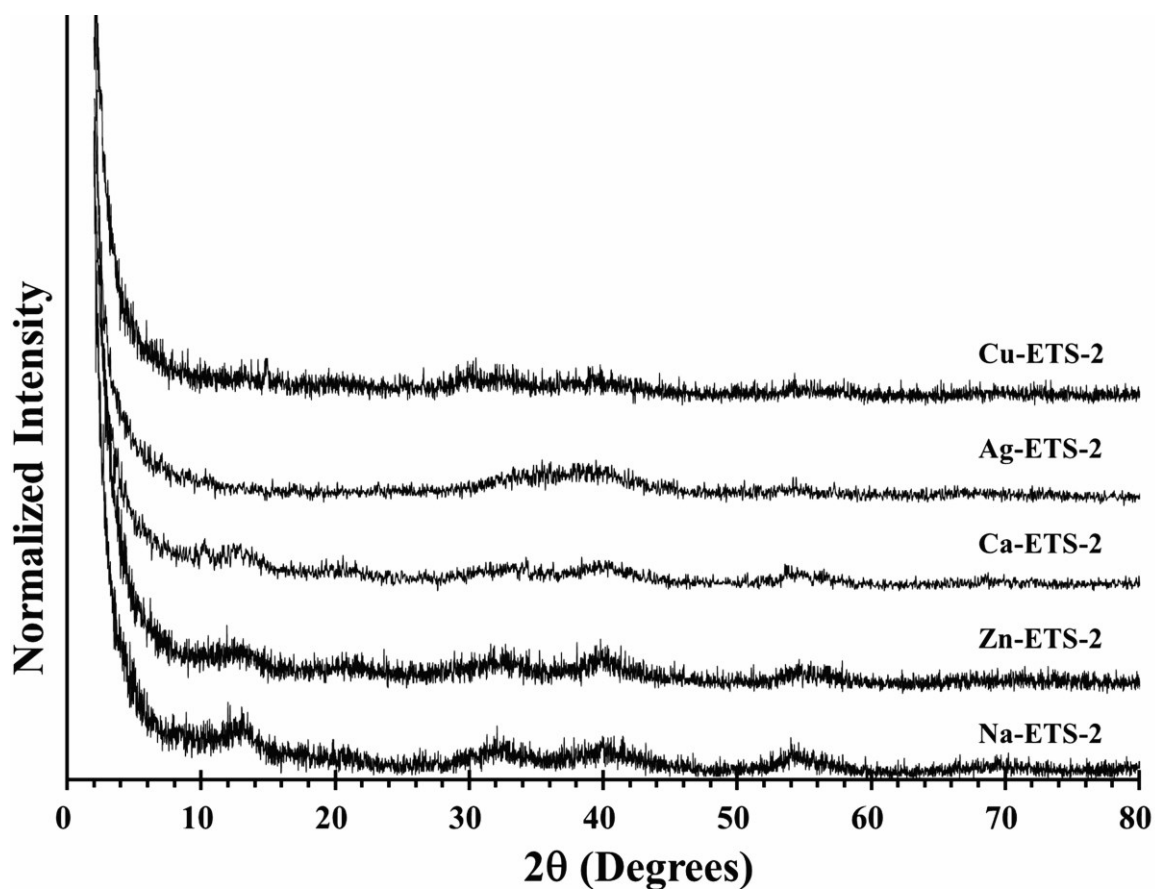
Figure 4- 2 XRD patterns for different ion exchanged forms of ETS-2.

Previously we have found that for Cu-ETS-2 at high temperature above 500°C structural changes occur [7]. In the presence of H_2S, structural changes start to occur from 350 °C. However, the removal capacity still shows promising values up to 650 °C after which sintering progresses leading to loss of copper adsorption sites [25].

The external surface areas of all the tested adsorbents are given in Table 4-1. Results show that besides Ag-ETS-2, all samples have very high surface area.

Table 4- 1 External surface area of different ion-exchanged forms of ETS-2 and a commercial sample R3-11G.

Adsorbent	BET surface area (m²/g)
Cu-ETS-2	250
Ag-ETS-2	173
Zn-ETS-2	297
Ca-ETS-2	293
R3-11G	264

Metal content of the samples have been determined through energy dispersive x-ray Spectroscopy (EDX). Results are given in Table 4-2. From the EDX results it can be seen that Ag-ETS-2 has very high Ag content. The metal loading for Cu and Zn are similar while Ca-ETS-2 has the lowest metal content.

Table 4- 2 Elemental analysis derived from EDX results for different adsorbents.

Adsorbent	Ion	Norm. wt%
Cu-ETS-2	Cu	13.2
Ag-ETS-2	Ag	39.0
Zn-ETS-2	Zn	14.3
Ca-ETS-2	Ca	8.1
R3-11G[4]	Cu	28.5

Based on the SEM images presented in Figure 4-3 the copper exchange process seems to enlarge the dendritic structure on the surface of ETS-2 while the particle morphology remains the same. Zn-ETS-2 also shows close morphology to the un-exchanged substrate material ETS-2. The Ag and Ca exchange processes change the physical structure of ETS-2 significantly. The particles have become highly agglomerated.

Figure 4-4 shows the metal dispersion on Cu-ETS-2, Ag-ETS-2, Zn-ETS-2 and Ca-ETS-2 samples. Metal sites are well dispersed on ETS-2 and exposed to H_2S molecules.

---

[4] MDS provided by BASF
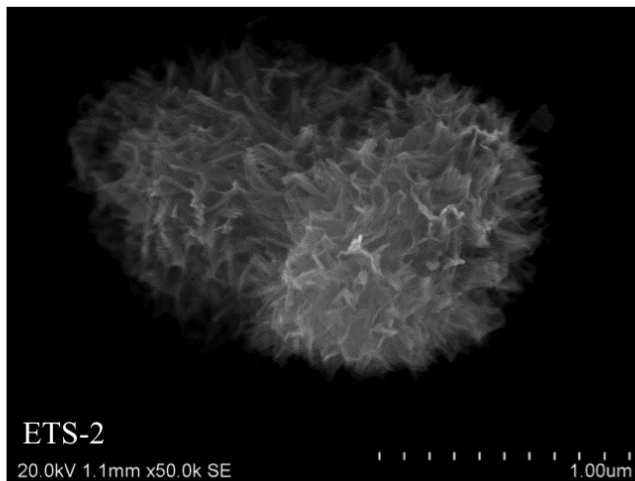
(a)
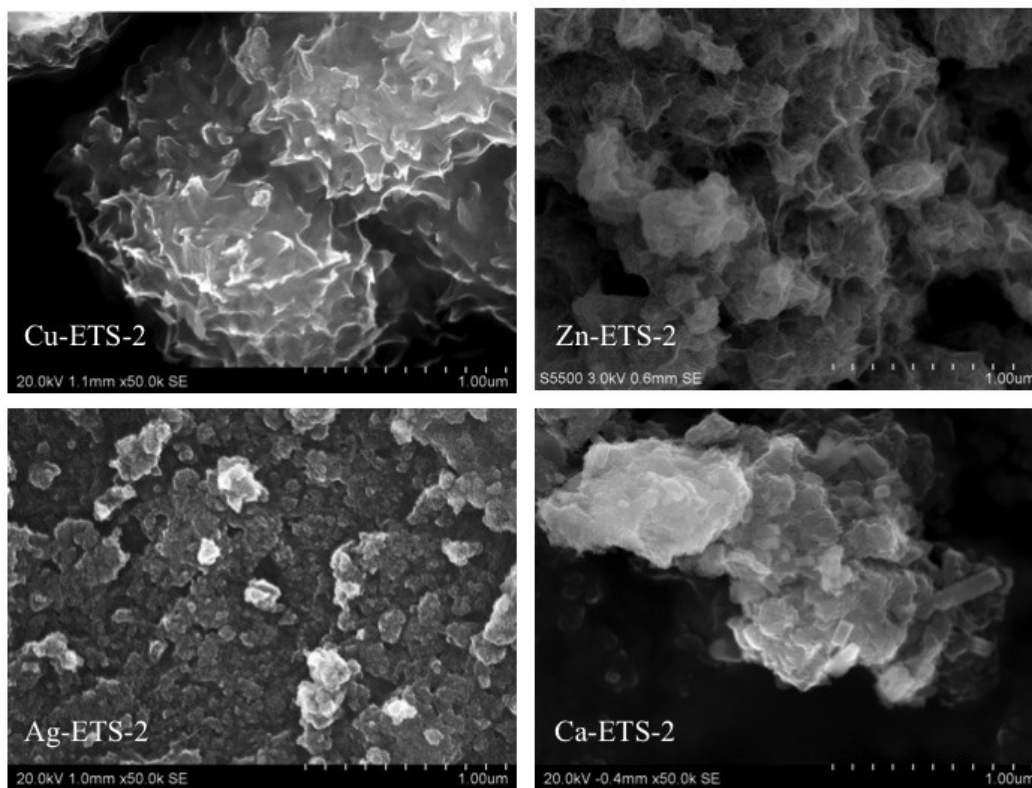
(b)

Figure 4- 3 SEM images for: a) Na-ETS-2 and b) Cu, Ag, Zn and Ca-ETS-2.
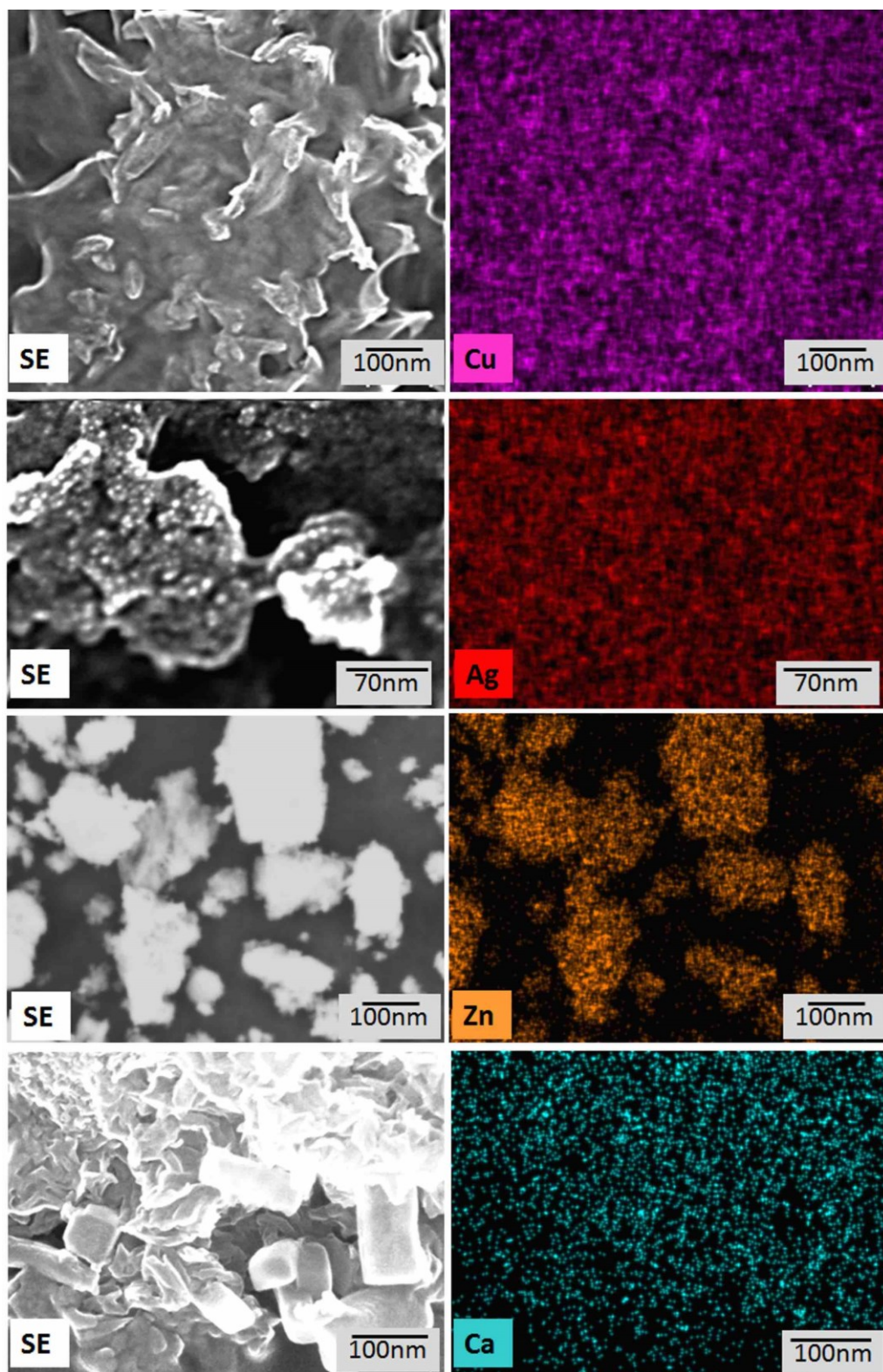
Figure 4- 4 Metal dispersion on Cu, Ag, Zn and Ca-ETS-2. L- secondary electron images and R- corresponding elemental maps.

90

4.6. Discussion

Several factors may influence the room temperature breakthrough performance of metal-oxide adsorbents. Among them are physical structure, external surface area and both number and affinity of the adsorption sites [3]. The high metal content (Table 4-2) of Ag-ETS-2 but rather low H_2S removal capacity could be attributed to its low surface area (Table 4-1). In addition, a lot of the Ag molecules are not in their active form for reaction with H_2S. A high resolution SEM image of this sample in Figure 4-5 clearly shows the presence of inactive sites of metallic silver dots on Ag-ETS-2.

From Figure 4-4 it can be seen that silver is well dispersed on Ag-ETS-2 as the other metal ions on other samples. Ag-ETS-2 compared to other adsorbents form highly agglomerated particles as shown in Figure 4-3. This also explains the lower surface area of Ag-ETS-2 compared to the other samples presented in Table 4-1. Agglomeration changes some physical properties like surface area and the adsorption capacity tends to decrease with increasing agglomeration [22].
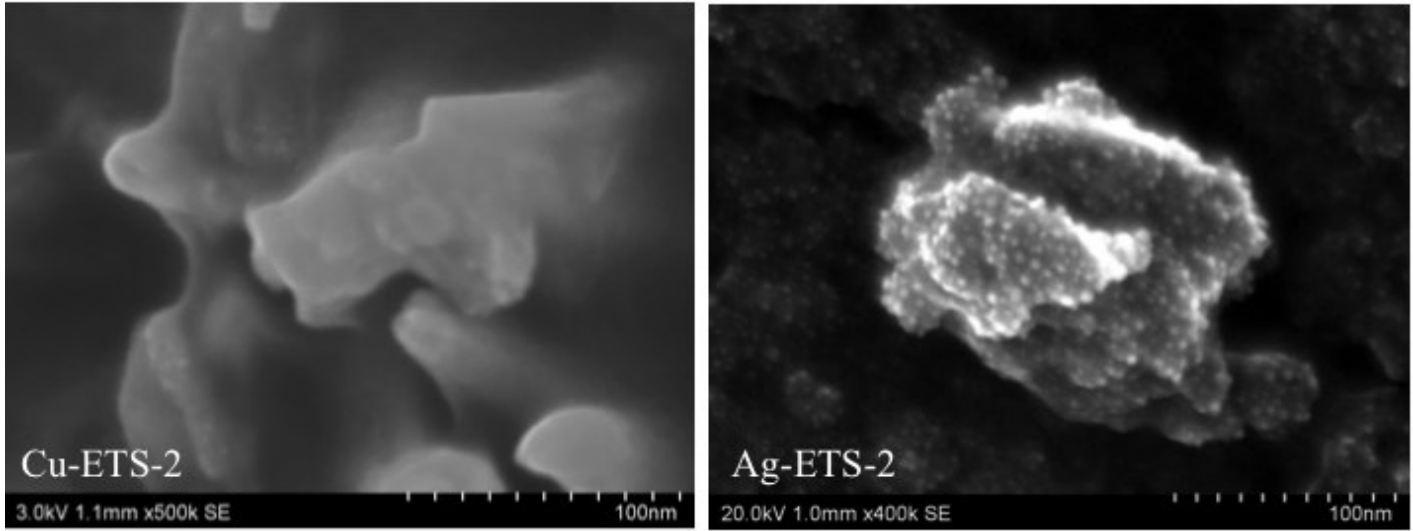
Figure 4- 5 High-resolution SEM image of Cu-ETS-2 and Ag-ETS-2.

The formation of some tetragonal particles can be observed in the Ca-ETS-2 morphology (Figure 4-6). Figure 4-7 shows an EDX line scan through a tetragonal particle indicated by an arrow in Figure 4-6.
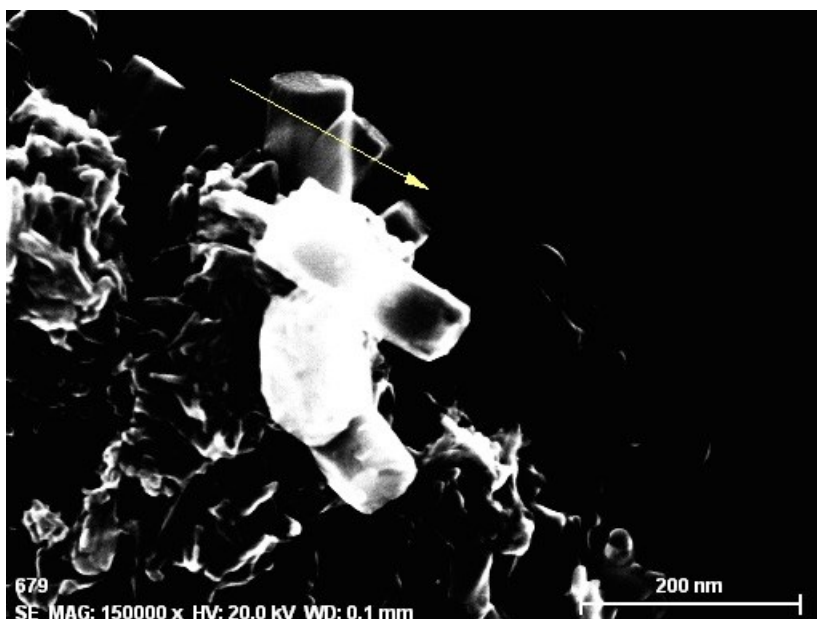
Figure 4- 6 High-resolution SEM image of Ca-ETS-2.
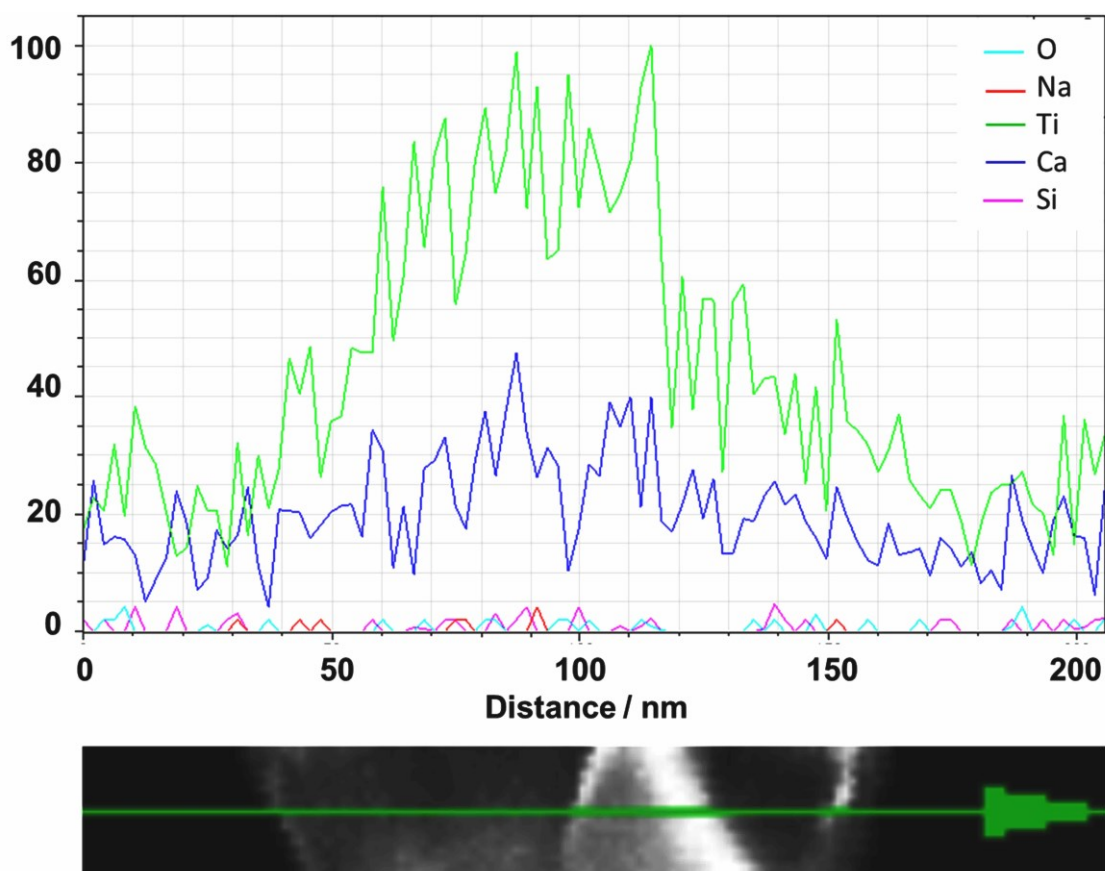
Figure 4- 7 EDX line scan through a tetragonal particle on Ca-ETS-2.

It can be seen that these particles are Ti-rich with very low Ca loading. This means that these particles can be considered as inactive sites for the purpose of this study. This observation is in good agreement with the low metal content in Ca-ETS-2 reported in Table 4-2. The low affinity of CaO for the reaction with H_2S in section 4.5.2 in addition to low metal loading compared to the other samples could probably cause the negligible H_2S removal capacity of Ca-ETS-2.

Among tested adsorbents, Cu-ETS-2 and Zn-ETS-2 show similar physical structures and amount of metal loading as well as surface area while their H_2S removal capacities are more different. Another factor, which strongly influences their breakthrough performances, is their thermodynamic property at room temperature. CuO is thermodynamically favorable for sulfidation than ZnO as indicated by their previously mentioned ΔGs. Moreover the sulfidation of ZnO requires more rearrangement of the anions than CuO, which results in slower rate of the lattice diffusion of the anions, or exchange of dissociated parts of H_2S with the lattice oxide [3].

High resolution SEM results for Cu-ETS-2 and spent sample (after H_2S adsorption) are given in Figure 4-8. It can be seen how surface structure is changed after H_2S adsorption when agglomerated particles are formed.
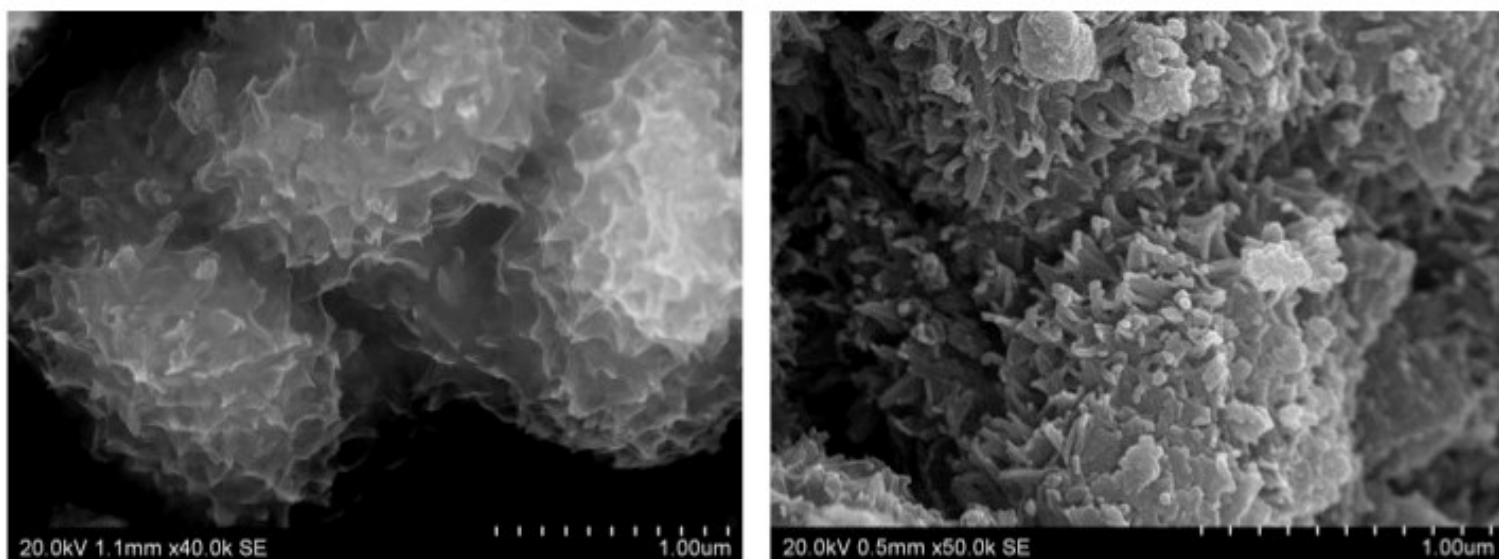
Figure 4- 8 SEM results for Cu-ETS-2 samples before (left hand side) and after (Right hand side) H$_2$S treatment at room temperature.

4.7. Conclusions

High surface area and cation exchange capacity nanotitanate ETS-2 was used as support material and cation-exchanged with Ag, Ca, Cu and Zn for potential adsorbents of sub-ppm levels of H$_2$S at room temperature. Breakthrough experimental results show that Cu-ETS-2 has the most promising performance as adsorbent material outperforming even the commercial sample. It has a high sulfur adsorption capacity of 29.7 mg H$_2$S/g adsorbent. Lower H$_2$S removal capacities for silver, zinc and calcium samples can be attributed to the presence of inactive sites such as metallic silver dots and the rigidity of physical structure of the material which lower thermodynamically favorable sulfidation reactions.

95

4.8. References

[1] S. Yasyerli, G. Dogu, I. Ar and T. Dogu, "Dynamic analysis of removal and selective oxidation of H2S to elemental sulfur over Cu-V and Cu-V-Mo mixed oxides in a fixed bed reactor," *Chemical Engineering Science,* vol. 59, pp. 4001-4009, 2004.

[2] Y. Elsayed, M. Seredych, A. Dallas and T. J. Bandosz, "Desulfurization of air at high and low H2S concentrations," *Chem. Eng. J.,* vol. 155, pp. 594-602, 2009.

[3] D. Jiang, L. Su, L. Ma, N. Yao, X. Xu, H. Tang and X. Li, "Cu-Zn-Al mixed metal oxides derived from hydroxycarbonate precursors for H2S removal at low temperature," *Appl. Surf. Sci.,* vol. 256, pp. 3216-3223, 2010.

[4] S. P. Hernández, M. Chiappero, N. Russo and D. Fino, "A novel ZnO-based adsorbent for biogas purification in H2 production systems," *Chem. Eng. J.,* vol. 176–177, pp. 272-279, 2011.

[5] D. A. Bhandari, N. Bessho and W. J. Koros, "Dual layer hollow fiber sorbents for trace H2S removal from gas streams," *Chemical Engineering Science,* vol. 94, pp. 256-264, 2013.

[6] G. Monteleone, M. De Francesco, S. Galli, M. Marchetti and V. Naticchioni, "Deep H2S removal from biogas for molten carbonate fuel cell (MCFC) systems," *Chem. Eng. J.,* vol. 173, pp. 407-414, 2011.

[7] S. Rezaei, A. Tavana, J. A. Sawada, L. Wu, A. S. M. Junaid and S. M. Kuznicki, "Novel Copper-Exchanged Titanosilicate Adsorbent for Low Temperature H2S Removal," *Ind Eng Chem Res,* vol. 51, pp. 12430-12434, 2012.

[8] M. Xue, R. Chitrakar, K. Sakane and K. Ooi, "Screening of adsorbents for removal of H2S at room temperature," *Green Chem.,* vol. 5, pp. 529-534, 2003.

[9] L. Zhou, M. Yu, L. Zhong and Y. Zhou, "Feasibility study on pressure swing sorption for removing H2S from natural gas," *Chemical Engineering Science,* vol. 59, pp. 2401-2406, 2004.

[10] F. Gholampour and S. Yeganegi, "Molecular simulation study on the adsorption and separation of acidic gases in a model nanoporous carbon," *Chemical Engineering Science,* vol. 117, pp. 426-435, 2014.

[11] S. Velu, X. Ma and C. Song, "Zeolite-based adsorbents for desulfurization of jet fuel by selective adsorption," in *ACS Division of Fuel Chemistry, Preprints,* 2002, pp. 447-448.

[12] C. L. Carnes and K. J. Klabunde, "Unique chemical reactivities of nanocrystalline metal oxides toward hydrogen sulfide," *Chemistry of Materials,* vol. 14, pp. 1806-1811, 2002.

[13] T. Baird, K. Campbell, P. Holliman, R. Hoyle, M. Huxam, D. Stirling, B. Williams and M. Morris, "Cobalt-zinc oxide absorbents for low temperature gas desulfurisation," *J. Mater. Chem.,* vol. 9, pp. 599-605,1999.

[14] C. Babé, M. Tayakout-Fayolle, C. Geantet, M. Vrinat, G. Bergeret, T. Huard and D. Bazer-Bachi, "Crystallite size effect in the sulfidation of ZnO by H2S: Geometric and kinetic modelling of the transformation," *Chemical Engineering Science,* vol. 82, pp. 73-83, 2012.

[15] A. Moezzi, A. M. McDonagh and M. B. Cortie, "Zinc oxide particles: Synthesis, properties and applications," *Chem. Eng. J.,* vol. 185–186, pp. 1-22, 2012.

[16] D. Melo, J. de Souza, M. Melo, A. Martinelli, G. Cachima and J. Cunha, "Evaluation of the zinox and zeolite materials as adsorbents to remove H2S from natural gas," *Colloid Surf. A-Physicochem. Eng. Asp.,* vol. 272, pp. 32-36, 2006.

[17] D. Crespo, G. Qi, Y. Wang, F. H. Yang and R. T. Yang, "Superior sorbent for natural gas desulfurization," *Ind Eng Chem Res,* vol. 47, pp. 1238-1244, 2008.

[18] P. Kumar, C. Sung, O. Muraza, M. Cococcioni, S. Al Hashimi, A. McCormick and M. Tsapatsis, "H2S adsorption by Ag and Cu ion exchanged faujasites," *Microporous Mesoporous Mat.,* vol. 146, pp. 127-133, 2011.

[19] D. Nguyen-Thanh and T. Bandosz, "Activated carbons with metal containing bentonite binders as adsorbents of hydrogen sulfide," *Carbon,* vol. 43, pp. 359-367, 2005.

[20] F. Li, J. Wei, Y. Yang, G. H. Yang and T. Lei, "Preparation of Sorbent Loaded with Nano-CuO for Room Temperature to Remove of Hydrogen Sulfide," *Applied Mechanics and Materials,* vol. 475, pp. 1329-1333, 2014.

[21] Q. Xue and Y. Liu, "Removal of minor concentration of H2S on MDEA-modified SBA-15 for gas purification," *J. Ind. Eng. Chem.,* vol. 18, pp. 169-173, 2012.

[22] M. Hussain, N. Abbas, D. Fino and N. Russo, "Novel mesoporous silica supported ZnO adsorbents for the desulphurization of biogas at low temperatures," *Chem. Eng. J.,* vol. 188, pp. 222-232, 2012.

[23] X. Wang, T. Sun, J. Yang, L. Zhao and J. Jia, "Low-temperature H2S removal from gas streams with SBA-15 supported ZnO nanoparticles," *Chem. Eng. J.,* vol. 142, pp. 48-55, 2008.

[24] D. Montes, E. Tocuyo, E. Gonza͘ez, D. Rodri͘uez, R. Solano, R. Atencio, M. A. Ramos and A. Moronta, "Reactive H2S chemisorption on mesoporous silica molecular sieve-supported CuO or ZnO," *Microporous and Mesoporous Materials,* vol. 168, pp. 111-120, 2013.

[25] P. Dhage, A. Samokhvalov, D. Repala, E. C. Duin, M. Bowman and B. J. Tatarchuk, "Copper-Promoted ZnO/SiO2 Regenerable Sorbents for the Room Temperature Removal of H2S from Reformate Gas Streams," *Ind Eng Chem Res,* vol. 49, pp. 8388-8396, 2010.

5. Chemisorption of H$_2$S on Copper-ETS-2 packed-column: experiment and modeling

5.1. Summary

Copper supported on Engelhard Titanosilicate-2 (ETS-2) has been shown to be a promising adsorbent for deep H$_2$S removal (to sub-ppm levels) for gas purification applications at room temperature. Because of the high external surface area and the cation exchange capacity of ETS-2, Cu ions are highly dispersed and very accessible to H$_2$S molecules. In this study, H$_2$S column breakthrough experiments are analyzed by a dynamic model based on the rigorous mass balance equations applied to the fixed-bed. The proposed model also includes the chemical reaction term, which is affected by the deactivation of the solid phase. Temperature-programmed desorption tests provided insight on the material characterization as well as on the relative magnitudes of the H$_2$S-material interactions.

5.2. Introduction

Sulfidation reactions between metal oxides and H_2S have been widely applied in the industrial H_2S removal plants in wide range of working temperatures [1-6]. At room temperature high surface area materials such as zeolites [7-9], carbon sorbents [10, 11], mesoporous and silica material [8, 12-15] are frequently used as supports to load metal/metal oxides and improve H_2S uptake by high dispersion of active sites. Recently, a unique titanosilicate material has been synthesized and loaded active sites for deep H_2S removal (to sub-ppm levels) for gas purification applications at room temperature [16, 17]. Cu-ETS-2 displayed the most promising adsorbent in comparison to a fully developed commercial H_2S adsorbent and other tested metal-exchanged ETS-2. Also, Cu-ETS-2 has the chemical environment favorable for decomposition of H_2S. Since it has been shown that a transition-metal ion [18-23], metal oxides [24] and TiO_2 surface [25] enhance H_2S adsorption by facilitating its dissociation to HS^- and S^- ions, which may further react and form sulfide products [26].

Although several studies have been dedicated to the development of H_2S sorbents at low temperatures and measurements of the breakthrough curves, the column dynamics are still poorly understood and differ for many of the sorbents studied. Much progress has been made for the column dynamics and interactions of gases with physisorbents without any chemical reaction included [27-30] and less attention to chemisorption and surface reactions [31]. Less attention has been paid

to the investigation of the adsorbent by a dynamic model, which considers both chemisorption of H_2S molecules on the surface and deactivation of the solid.

In general, textural variations of solid reactants, changes in active surface area, reactivity of the solid and formation of a dense product layer over the solid reactant cause a significant decrease in activity of the solid reactant during reaction [32, 33]. Deactivation models [34, 35] were reported to be quite successful in predicting the reaction rates of such gas-solid non-catalytic reactions. However it has been used for the pseudo-steady state condition [36-42] in which the dynamic of the system is only considered in the activity term implicitly.

The objective of this work is to gain a better understanding of the transport phenomena occurring during the adsorption of ppm level H_2S on a copper-ETS-2 packed bed column. Breakthrough adsorption experiments at room and higher temperatures up to 250°C were performed. A continuum mechanics-based model was developed to support the analysis of experimental data obtained from dynamic column breakthrough tests. The model includes the chemical reaction term, which is affected by the deactivation of the solid phase. Temperature-programmed desorption (TPD) [43, 44] experiments of H_2S on Cu-ETS-2 provided a further insight of the different H_2S-material interaction energy levels.

5.3. Experimental

5.3.1. Materials

Synthesis of ETS-2 and the ion exchange procedure to make the copper exchanged ETS-2 were followed as explained previously [17]. The final solid powder was pressed into a binderless dense disk and then was crushed and sieved with the 0.297 mm to 0.595 mm (No. 30 to 50 mesh) fraction for use in the column dynamic sulfidation test experiments.

5.3.2. Adsorption tests

A process flow diagram of the experimental setup for the H_2S breakthrough tests is included as Figure 5-1. The adsorption experiment was carried out by flowing a certified H_2S + He gas mixture (Praxair) of known composition (10 ppm H_2S) through the packed bed at different temperatures. The feed gas inlet flow rate was set up at 100 sccm by using a mass flow controller (MFC, scaled for 0-700 cc/min gas flows, Alicat Scientific). Packed-bed properties and test conditions are given in Table 5-1.

102
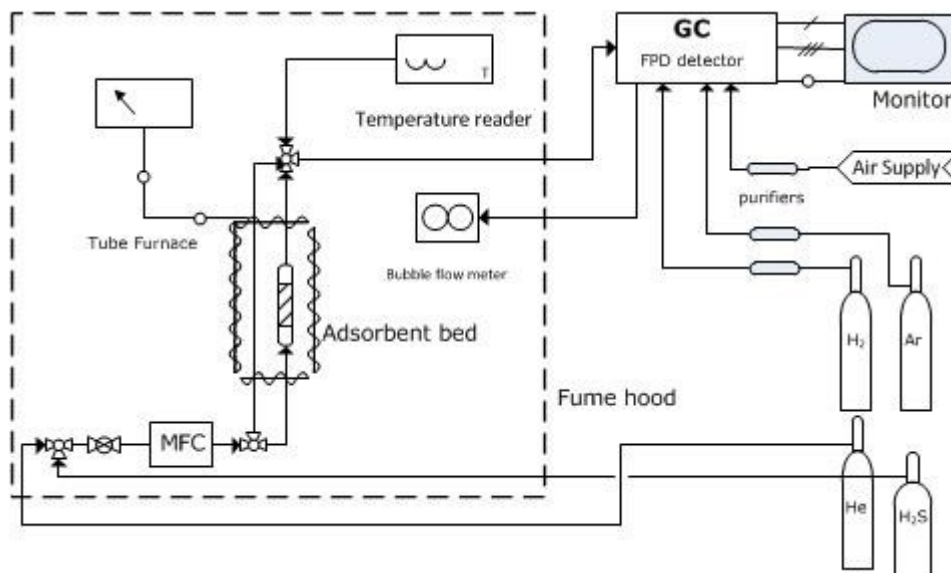
Figure 5- 1 Schematic flow diagram of test apparatus.

The bed exit gas stream was sent to a gas chromatograph (GC) equipped with MXT-1 column (Restek) and a FPD detector to determine the H_2S concentration [16]. The H_2S mole fraction, $y(t)$, in the column exit was recorded as a function of time until the effluent gas H_2S composition approached the column inlet y_{in} (H_2S breakthrough profiles). Blank correction is neglected due to the prompt H_2S response for the empty column including glass wool.

The spent column was then purged by flowing inert He (purity: 99.995%, Praxair) through it and simultaneously was heated at the rate ($\beta=10°C/min$) up to 500 °C in order to facilitate the desorption of H_2S molecules. Then it was cooled down to near-ambient temperature. For the temperature program, the packed

column was heated externally with a tube furnace[5] (Barnstead Thermolyne-21100) attached with 4836-Temperature controller (Parr Instrument Company, USA). Another K-type thermocouple was also inserted inside the tubes to monitor the temperature at the column exit.

Table 5- 1 Packed-bed properties and operation conditions

Packed bed	
Bed Length $[cm]$	$L_b = 0.24$
Adsorbent Weight $[mg]$	$w = 30$
Bed internal diameter $[cm]$	$d_b = 0.38$
Bed void fraction	$\varepsilon_b = 0.37$
Packed bed density $[g/cm^3]$	$\rho_b = 1.1$

Operation condition	
Temperature $[°C]$	T=25,150 1nd 250
Pressure $[\,kPa]$	$P = 101.3$
Gas flowrate $[standard^6\ cm^3/min]$	$Q = 100$

---

[5] Tube furnace axial temperature profile is given in the appendix.
[6] $25°C$ and $101.3\ kPa$

The entire tubing from H_2S cylinder to GC was made of Sulfinert tubes (Restek) to prevent any sulfidation on the tubing. Flow rate of the GC exit gas was measured using a bubble flow meter. In order to assure safe lab experiments, the whole experimental set-up was located inside the fume hood.

5.4. Mass transport model for the H_2S breakthrough simulation

5.4.1. System modeling

For the modeling of the experimental results of diluted H_2S flowing through a packed bed column of copper-ETS-2 adsorbent material, a reasonable number of decisions were made as explained below

1) One dimensional model. Concentration gradient along the axial direction of the bed is only considered.

2) Negligible axial dispersion effects.

3) Ideal gas law is valid in a gas stream of very low concentration of H_2S in He (10 ppm) at ambient condition.

4) No heat effects are considered. Heat effects associated with adsorption and reaction can be considered negligible in a dilute adsorption regime.

5) The pressure drop along the bed is negligible. The pressure drop calculated

based on Darcy's law[7] [45] was less than 1%.

6) Mass transfer resistance in the gas phase is negligible. (This assumption has been justified in the Appendix section.)

With these assumptions, the continuity equation applied within the packed bed for H₂S species (i subscript) can be expressed as:

$$\varepsilon_b \frac{\partial c_i}{\partial t} + \varepsilon_b \nabla (c_i v) + \rho_b \frac{\partial q_i}{\partial t} = 0 \tag{5-1}$$

where c_i is the H₂S concentration in the gas phase $[mol/cm^3]$ and q_i is the H₂S adsorbed in the solid phase $[mol/g]$. v is the interstitial velocity which remains essentially constant at low H₂S level and can be taken out of the divergence. ρ_b is the bed density $[g/cm^3]$.

In the interaction associated with H₂S removal by the sorbent Cu-ETS-2, two sequential steps were assumed to occur:

First, molecules from the gas adsorbs on the copper site (of an energetically homogeneous sorbent) reversibly:

$$\frac{\partial [H_2 S]}{\partial t} = -K_f [H_2 S][1 - \theta] + K_b \theta \tag{5-2}$$

where parameters K_f and K_b represent the specific rate constants for the forward and backward chemisorption reaction, respectively and θ represents the fraction of

---

[7] $\frac{dP}{dl} = 150 (1 - \varepsilon_b)^2 \mu_g v / \varepsilon_b^2 d_p^2$

the sorption sites on the chemisorbent that are occupied by the chemisorbed H_2S molecules at time t $(\theta = q_i/q_i^{sat})$. At equilibrium the reaction kinetic rate for the first step is equal to zero, which describes the Langmuirian mechanism of chemisorption [31]:

$$\theta = \frac{b \, c_i}{1 + b \, c_i} \tag{5 − 3}$$

where b is the ratio of the specific rate constants for the forward and backward chemisorption reactions. When there is no H_2S concentration gradient in the gas phase, the H_2S concentration in the vicinity of the solid phase (close to the interphase) is equal to the H_2S concentration in the bulk gas phase (c_i).

At low H_2S concentrations, the Langmuir isotherm model equation (5-2) is in the linear form of Henry's equilibrium as follows:

$$q_i = k_H \, c_i \tag{5 − 4}$$

And equation (1) can be rewritten as:

$$(\varepsilon_b + \rho_b k_H)\frac{\partial c_i}{\partial t} + \varepsilon_b v \frac{\partial c_i}{\partial z} = 0 \tag{5 − 5}$$

The second step is sulfidation reaction of the chemisorbed H_2S particles on the surface. The consumption of H_2S molecules due to surface reactions in the adsorbed phase is then presented in the following kinetic expression:

$$r_i = -k_r q_i \, a \tag{5 − 6}$$

where k_r is the kinetic rate constant.

When chemical reaction is an effective step, equation (5-1) or (5-5) is in the form of:

$$(\varepsilon_b + \rho_b k_H)\frac{\partial c_i}{\partial t} + \varepsilon_b v \frac{\partial c_i}{\partial z} = \rho_b r_i \qquad (5-7)$$

This equation means that any change in the H₂S concentration is associated with the convective mass transport along the bed and the surface interactions in the adsorbed phase.

Equation (5-6) considers a deactivation rate term a that takes into account the change in the surface area and activity of the solid reactant because of the decomposed H₂S on the surface or further potential of the sulfidation reaction [31, 32]. Then the overall effect of all these factors on the kinetic rate is expressed by the variation of an activity term introduced into the rate expression.

In this work change of surface activity and solid reactant consumption with time is considered proportional to the activity and species concentration as follows [33, 34]:

$$\frac{da}{dt} = -k_d\, c_i\, a \qquad (5-8)$$

where k_d is the deactivation constant. Using equation (5-4), (5-6), (5-7) the problem to solve is defined through the following PDE equation with the corresponding initial and boundary conditions:

$$(\varepsilon_b + k_H)\frac{\partial c_i}{\partial t} + \varepsilon_b v \frac{\partial c_i}{\partial z} = -\rho_b\, K\, c_i\, a \qquad\qquad (5-9)$$

$$@ \begin{cases} t = 0 & c_i = 0 & for \quad all\ z \\ z = 0 & c_i = c_i^o & for \quad t > 0 \end{cases}$$

where K is defined as a kinetics parameter which includes the product of the reaction rate and henry constants. c_i^o represents the H$_2$S concentration in the column inlet.

5.4.2. Numerical resolution

A numerical method is used to replace the spatial derivative with an algebraic approximation. This effectively removes the derivatives from the partial differential equation (5-9) and the model has been converted to a system of approximating ordinary differential equations (ODEs). Then equation (5-8) and (5-9) can be integrated simultaneously by standard and well-established numerical algorithms for initial value ODEs (ode15s in MATLAB_R2013a). Then an optimization function (fminsearch) is used to minimize the error between the breakthrough model and the experimental breakthrough curves.

5.4.3. Mass balance for the breakthrough / desorption dynamics

The H$_2$S bed capacity at sufficient long time for the breakthrough ($N_i(t)$, mol/g) was calculated considering the following mass balance in the column with integration between 0 and t

$$\int_0^t F_{in} y_{in} dt - \int_0^t F_{out} y_{out} dt = N_i(t).V_b.\rho_b + c_i^o.V_b.\varepsilon_b \qquad (5-10)$$

and considering:

$$F_{out} = F_{He} + F_{H2S,out} = F_{He} + F_{out} y_{out} \qquad (5-11)$$

$$F_{in} = F_{He} + F_{H2S,in} = F_{He} + F_{in} y_{in} \qquad (5-12)$$

then

$$F_{He} \left[\int_0^t \frac{1}{1/y_{in}-1} dt - \int_0^{t_\infty} \frac{y_{out}/y_{in}}{1/y_{in}-y_{out}/y_{in}} dt \right] = N_i(t).V_b.\rho_b + c_i^o.V_b.\varepsilon_b \qquad (5-13)$$

where V_b is the bed volume and F_{in} and F_{out} represent the inlet and outlet molar flow rates.

Analogously, the effluent gas H₂S composition, $y(t)$, was measured as a function of time during the regeneration process. The specific amount of H₂S removed from the column at time t, ($N_i'(t)$, mol/g) could be calculated by the following mass balance with an integration between 0 and t

$$\int_0^t F_{out} y_{out} dt = N_i'(t).V_b.\rho_b + c_i^o.V_b.\varepsilon_b \qquad (5-14)$$

$$F_{He} \int_0^t \frac{y_{out}/y_{in}}{1/y_{in} - y_{out}/y_{in}} dt = N_i'(t).V_b.\rho_b + c_i^o.V_b.\varepsilon_b \qquad (5-15)$$

Then the total amount of H₂S removed from the column can be calculated till when the effluent gas hydrogen sulfide mole fraction approaches zero.

110

5.5. Results and discussion

5.5.1. H$_2$S breakthrough concentration profiles on Copper-ETS-2

The H$_2$S breakthrough experiment results at different temperatures (25, 100 and 250°C) are given in Figure 5-2, it shows that breakthrough times are longer as the column temperature increases.
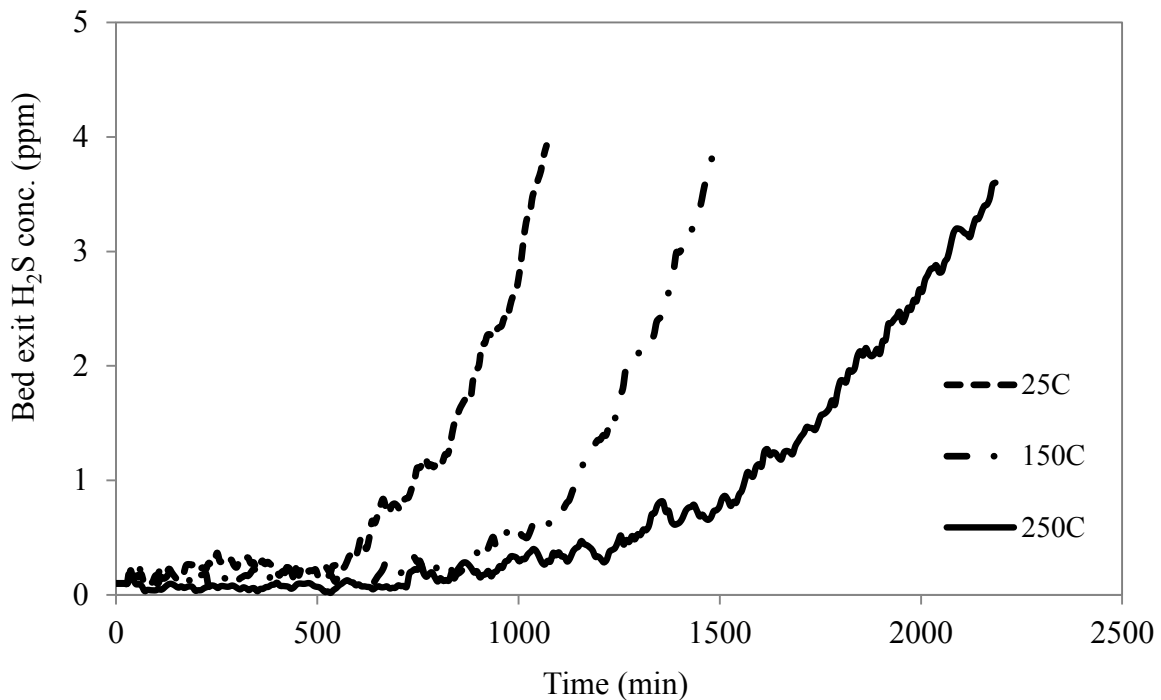
Figure 5- 2 H$_2$S breakthrough curves for Cu-ETS-2 at 25°C, 150°C and 250°C.

The experimental data have been fitted by the chemisorption model in diluted conditions presented in equation (5-5). Fitting curves are shown together with

experimental data in Figure 5-3 and the fit parameters are given in Table 5-2 show that Henry chemisorption constant increases with an increase in the temperature, which is indicating a temperature activated process. The magnitude of the interaction between the H_2S molecule and the copper sites associated with the parameter k_H increased as the bed temperature increased.
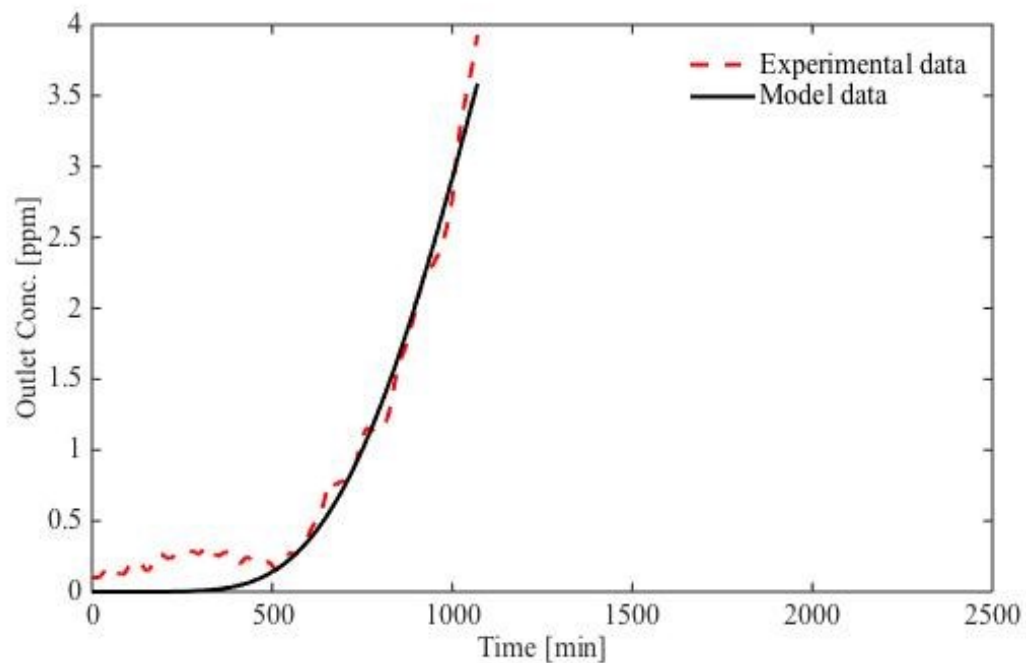
(a)
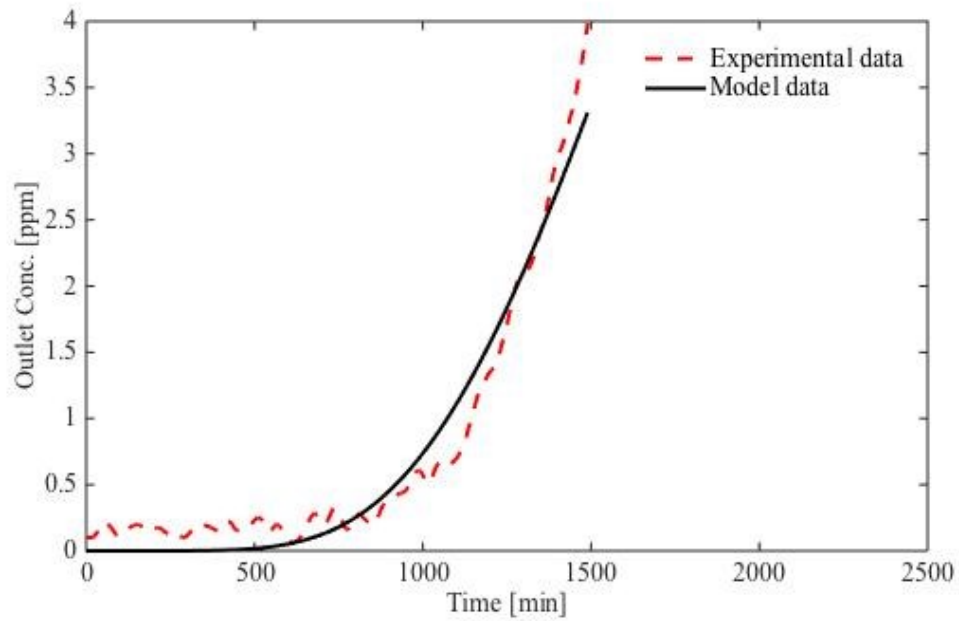
(b)
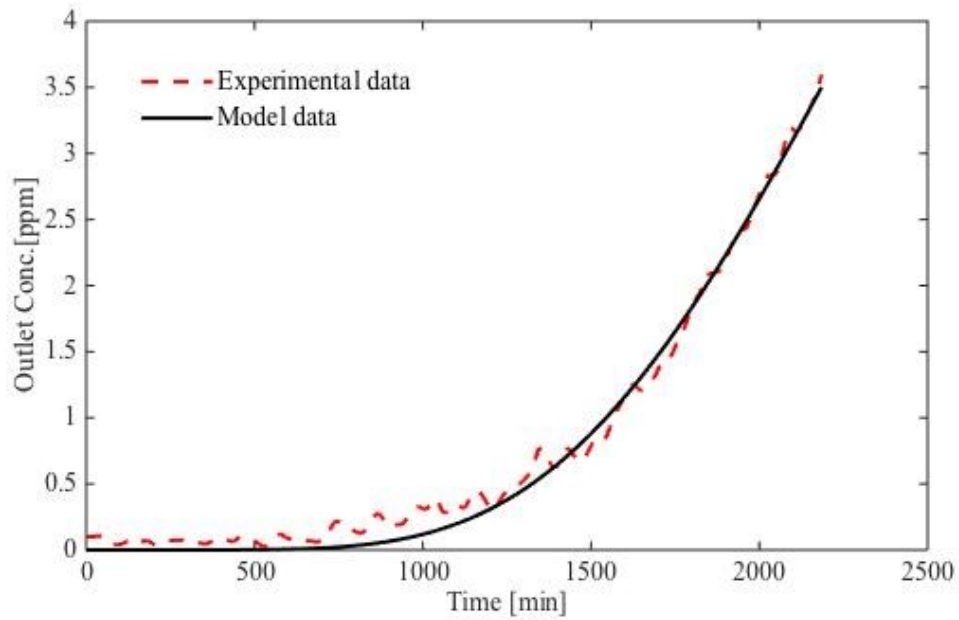
(c)

Figure 5- 3 The experimental data have been fitted by the chemisorption model at 25°C
(a), 150°C (b) and 250°C (c).

113

Table 5- 2 Henry's law constant at different temperatures.

Temperature [°C]	$k_H * 10^{-6}[ml\ of\ gas/g\ of\ solid]$
25	5.37
150	9.67
250	19.52

The experimental data could be fitted as well by the proposed model in equation (5-9). This model includes the reaction rate term. Model parameters are given in Table 5-3. As temperature increases from 25°C to 250°C, kinetic parameter increases, this is in good agreement with the breakthrough capacity trend at these temperatures. Cu-ETS-2 has higher affinity/interaction for H_2S removal at higher temperature, which is a sign of chemisorption processes.

Table 5- 3 Kinetics and deactivation parameters of Cu-ETS-2 at 25°C, 100°C and 250°C.

Temperatures [°C]	$K * 10^{-4} [\frac{ml}{min.\,g}]$	$k_d * 10^4$
25	3.17	6.45
150	5.2	6.22
250	5.65	3.18

Besides, deactivation parameter (k_d) follows an expected trend; at 25°C with the lowest H$_2$S removal capacity, Cu-ETS-2 has the lowest k_d which means the adsorbent deactivates faster at this temperature. Thus when adsorption capacity is higher, adsorbent deactivates slower (higher k_d).

A sensitivity analysis has been undertaken for the proposed model to check which parameter is more effective. Figure 5-4 and 5-5 display the change for H$_2$S breakthrough curves for kinetic and deactivation parameters within 30% error of the optimized value. As it can be seen these two parameters do not have minor effect on the outlet concentration.
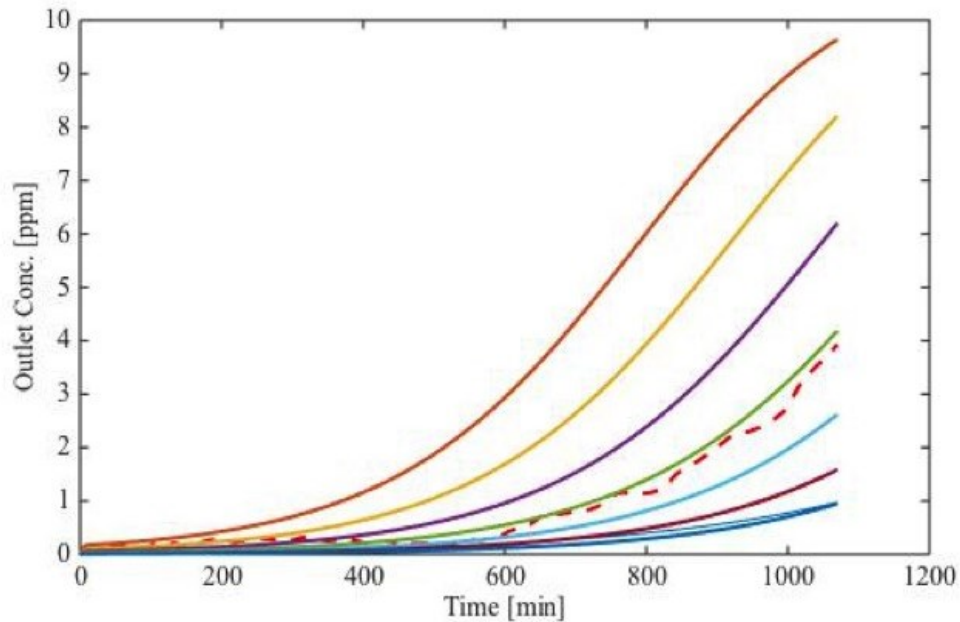
Figure 5- 4 Sensitivity analysis for kinetic parameter (K) within 30% error of the optimized value (green line); experimental data (dashed line).
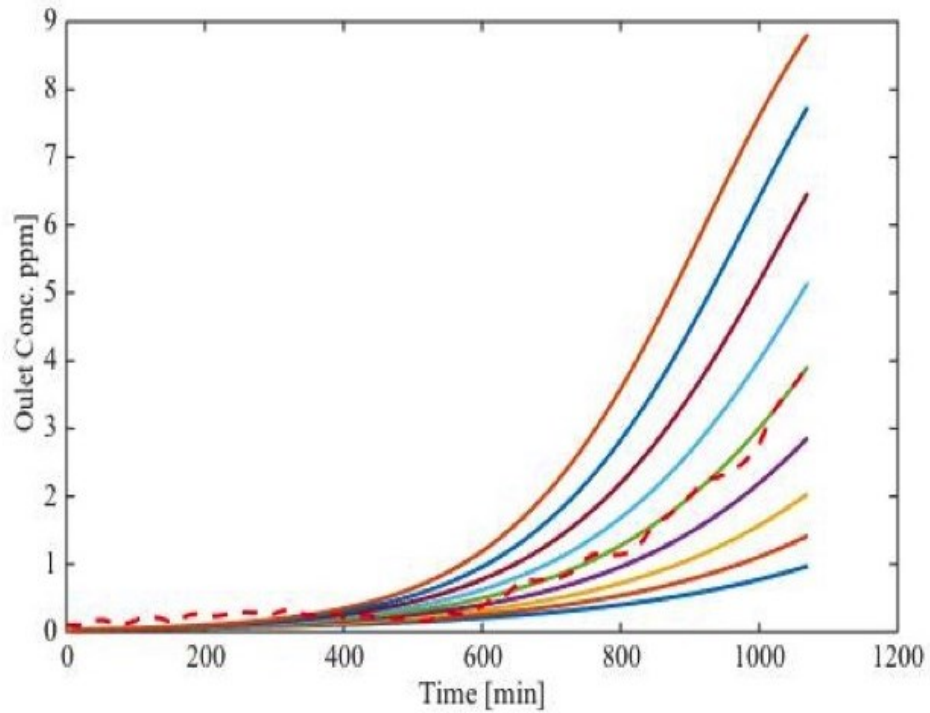
Figure 5- 5 Sensitivity analysis for deactivation parameter (k_d) within 30% error of the optimized value (green line); experimental data (dashed line).

The same study is done for the henry constant. Figure 5-6 shows even within 70% error deviation from the optimized value, equation (5-9) is not sensitive to the k_H value for the reaction model. Unlike Figure 5-4 and 5-5 all curves in Figure 5-6 are overlaid. Thus a fair assumption for a steady state solid phase can be considered to have equation (5-9) simplified as follows:

$$\varepsilon_b \frac{\partial c_i}{\partial t} + \varepsilon_b v \frac{\partial c_i}{\partial z} = -\rho_b \, K \, c_i \, a \qquad (5-16)$$

The simulation result for equation (5-16) gives the same parameters (K and k_d) presented in Table 5-3. This is in good agreement with the sensitivity analysis

outcome that k_H is not an effective parameter in the model and three parameter model (equation (5-9)) can be reduced to equation (5-16).
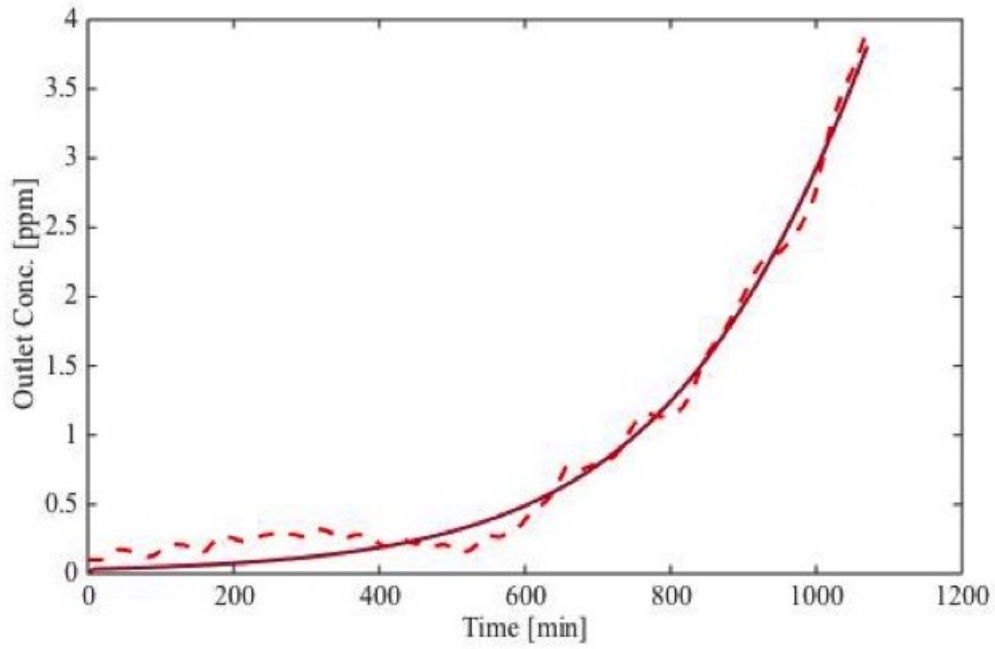
Figure 5- 6 Sensitivity analysis for deactivation parameter (k_H) within 70% error of the optimized value; experimental data (dashed line).

5.5.2. Desorption experiments of H₂S on spent Cu-ETS-2

Figure 5-7 show the temperature program desorption curve at 10°C/min and a maximum temperature of 500°C. The maximum temperature is selected in the way to prevent H₂S decomposition. Since it has been reported that Hydrogen sulfide decomposition is a highly endothermic process (ΔH_{298} = 20.25 kcal/mol) at temperature below 527°C and its total conversion does not exceed 1.5–2 % [46].
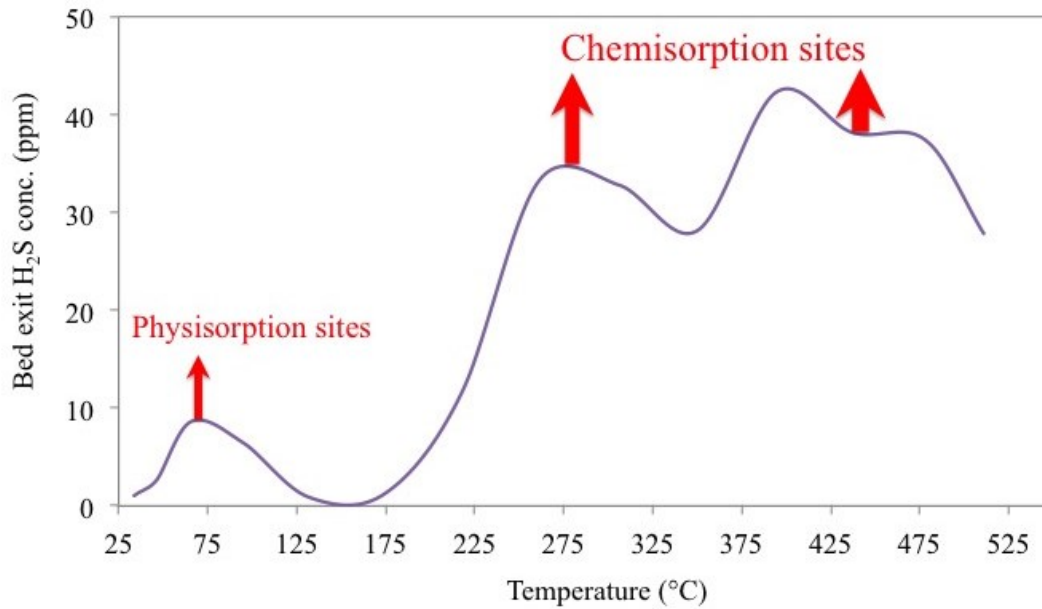
Figure 5- 7 Temperature program desorption curve of H$_2$S under He with the heating rate of 10°C/min.

As temperature increases, H$_2$S molecules get desorbed at different temperatures. This indicates that there are adsorption sites with different interaction energies on the surface of Cu-ETS-2 [47]. The small peak below 150°C can be most probably assigned to low energy interaction sites which can be associated with physisorption sites on the solid.

It has been shown that at room temperature, H$_2$S adsorption is accompanied by dissociation on metallic Cu and copper oxide and mainly interacts with the metal centers of the oxides [24], which proceeds by two stepwise reactions [18-20, 22]:

$$Cu + H_2S_g \xrightarrow[\text{Molecular adsorption}]{} \{Cu - SH_{2\ ads}\}$$

$$\xrightarrow[\text{Dissociative adsorption}]{} \{(Cu - SH)_{ads} + H_{ads}\}$$
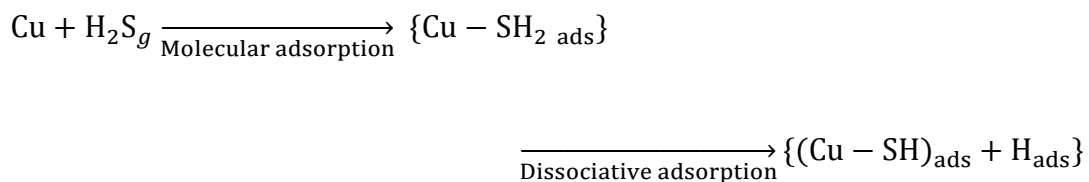
These steps occur spontaneously and continue by second hydrogen separation and further metal sufide formation step [26].

TiO$_2$ surface, on the other hand promotes H$_2$S dissociation according to the large Bronsted acid-base reaction [25].

Thus at room temperature H$_2$S strongly adsorbs and dissociative on the Cu-ETS-2 surface; mostly on metal active sites or very little on the titanate substrate.

H$_2$S molecules chemisorbed on copper sites requires more energy for desorption and they start to desorb at higher temperature than 150°C. The presence of consecutive peaks as the desorption temperature increases from 150 up to 500°C suggests that copper sites on the surface provide different energy interactions and chemisorption is a key interaction in the process.

The amount of adsorbed H$_2$S obtained from the desorption curve (Figure 5-7) through equation (5-15) is $5.69\ mg\ H_2S/g\ adsorbent$. However the amount of adsorbed H$_2$S molecules using the equation (5-13), which is 80.45 $mg\ H_2S/g\ adsorbent$. In order to monitor the desorbed H$_2$S molecules more precisely desorption heating rate was decreased from 10 to $2°C/min$. The amount of adsorbed H$_2$S obtained from equation (5-15) is $27.2\ mg\ H_2S/g\ adsorbent$

119

which is still much less than the one calculated from the breakthrough curve by equation (5-13). This difference can be explained by longer desorption time required at 500°C or higher desorption temperature. However the most probable reason can be regarding the fraction that cannot be desorbed with helium because of sulfidation reaction.

5.6. Conclusions

Diluted H_2S breakthrough experiments through a packed bed of Cu-ETS-2 adsorbent were modeled applying the continuity equation to the system by taken into account the characteristics of the adsorbent material. The increase of the H_2S breakthrough times as the experiment temperature increased can be explained by the growing chemisorption interaction as temperature rose from 25 to 250°C. This was also consistent with the temperature programmed desorption experiments which showed desorption peaks of larger magnitudes at temperatures higher than 200°C. A fixed bed model with reaction was able to fit the experimental data as well and it could partially explain the breakthrough profiles behavior through the increasing reaction kinetics with temperature.

5.7. References

[1] T. Baird, K. Campbell, P. Holliman, R. Hoyle, M. Huxam, D. Stirling, B. Williams and M. Morris, "Cobalt-zinc oxide absorbents for low temperature gas desulfurisation," *J. Mater. Chem.,* vol. 9, pp. 599-605, 1999.

[2] C. Babé, M. Tayakout-Fayolle, C. Geantet, M. Vrinat, G. Bergeret, T. Huard and D. Bazer-Bachi, "Crystallite size effect in the sulfidation of ZnO by H2S: Geometric and kinetic modelling of the transformation," *Chemical Engineering Science,* vol. 82, pp. 73-83, 2012.

[3] A. Moezzi, A. M. McDonagh and M. B. Cortie, "Zinc oxide particles: Synthesis, properties and applications," *Chem. Eng. J.,* vol. 185–186, pp. 1-22, 2012.

[4] M. Xue, R. Chitrakar, K. Sakane and K. Ooi, "Screening of adsorbents for removal of H2S at room temperature," *Green Chem.,* vol. 5, pp. 529-534, 2003.

[5] C. L. Carnes and K. J. Klabunde, "Unique chemical reactivities of nanocrystalline metal oxides toward hydrogen sulfide," *Chemistry of Materials,* vol. 14, pp. 1806-1811, 2002.

[6] Westmoreland P.R. , Harrison D.P., " Evaluation of candidate solids for high-temperature desulfurization of low-Btu gases," *Environmental Science and Technology,* vol. 10, pp. 659, 1976.

[7] D. Melo, J. de Souza, M. Melo, A. Martinelli, G. Cachima and J. Cunha, "Evaluation of the zinox and zeolite materials as adsorbents to remove H2S from natural gas," *Colloid Surf. A-Physicochem. Eng. Asp.,* vol. 272, pp. 32-36, 2006.

[8] D. Crespo, G. Qi, Y. Wang, F. H. Yang and R. T. Yang, "Superior sorbent for natural gas desulfurization," *Ind Eng Chem Res,* vol. 47, pp. 1238-1244, 2008.

[9] P. Kumar, C. Sung, O. Muraza, M. Cococcioni, S. Al Hashimi, A. McCormick and M. Tsapatsis, "H2S adsorption by Ag and Cu ion exchanged faujasites," *Microporous Mesoporous Mat.,* vol. 146, pp. 127-133, 2011.

[10] D. Nguyen-Thanh and T. Bandosz, "Activated carbons with metal containing bentonite binders as adsorbents of hydrogen sulfide," *Carbon,* vol. 43, pp. 359-367, 2005.

[11] F. Li, J. Wei, Y. Yang, G. H. Yang and T. Lei, "Preparation of Sorbent Loaded with Nano-CuO for Room Temperature to Remove of Hydrogen Sulfide," *Applied Mechanics and Materials,* vol. 475, pp. 1329-1333, 2014.

[12] Q. Xue and Y. Liu, "Removal of minor concentration of H2S on MDEA-modified SBA-15 for gas purification," *J. Ind. Eng. Chem.,* vol. 18, pp. 169-173, 2012.

[13] M. Hussain, N. Abbas, D. Fino and N. Russo, "Novel mesoporous silica supported ZnO adsorbents for the desulphurization of biogas at low temperatures," *Chem. Eng. J.,* vol. 188, pp. 222-232, 2012.

[14] X. Wang, T. Sun, J. Yang, L. Zhao and J. Jia, "Low-temperature H2S removal from gas streams with SBA-15 supported ZnO nanoparticles," *Chem. Eng. J.,* vol. 142, pp. 48-55, 2008.

[15] D. Montes, E. Tocuyo, E. Gonzaĺez, D. Rodriǵuez, R. Solano, R. Atencio, M. A. Ramos and A. Moronta, "Reactive H2S chemisorption on mesoporous silica molecular sieve-supported CuO or ZnO," *Microporous and Mesoporous Materials,* vol. 168, pp. 111-120, 2013.

[16] S. Rezaei, A. Tavana, J. A. Sawada, L. Wu, A. S. M. Junaid and S. M. Kuznicki, "Novel Copper-Exchanged Titanosilicate Adsorbent for Low Temperature H2S Removal," *Ind Eng Chem Res,* vol. 51, pp. 12430-12434, 2012.

[17] S. Rezaei, M. O. D. Jarligo, L. Wu and S. M. Kuznicki, "Breakthrough performances of metal-exchanged nanotitanate ETS-2 adsorbents for room temperature desulfurization," *Chemical Engineering Science,* vol. 123, pp. 444-449, 2015.

[18] A. N. Startsev, I. I. Zakharov, O. V. Voroshina, A. V. Pashigreva and V. N. Parmon, "Low-temperature decomposition of hydrogen sulfide under the conditions of conjugate chemisorption and catalysis," *Doklady Physical Chemistry,* vol. 399, pp. 283-286, 2004.

[19] Y. M. Choi, C. Compson, M. C. Lin and M. Liu, "A mechanistic study of H2S decomposition on Ni- and Cu-based anode surfaces in a solid oxide fuel cell," *Chemical Physics Letters,* vol. 421, pp. 179-183, 2006.

[20] I. I. Zakharov, A. N. Startsev, O. V. Voroshina, A. V. Pashigreva, N. A. Chashkova and V. N. Parmon, "The molecular mechanism of low-temperature decomposition of hydrogen sulfide under conjugated chemisorption-catalysis conditions," *Russian Journal of Physical Chemistry A,* vol. 80, pp. 1403-1410, 2006.

[21] D. R. Alfonso, "First-principles studies of H2S adsorption and dissociation on metal surfaces," *Surf Sci,* vol. 602, pp. 2758-2768, 2008.

[22] Q. L. Tang, S. R. Zhang and Y. P. Liang, "Influence of Step Defects on the H2S Splitting on Copper Surfaces from First-Principles Microkinetic Modeling," *Journal of Physical Chemistry C,* vol. 116, pp. 20321-20331, 2012.

[23] S. H. Chen, S. Q. Sun, B. J. Lian, Y. F. Ma, Y. G. Yan and S. Q. Hu, "The adsorption and dissociation of H2S on Cu(100) surface: A DTF study," *Surf Sci,* vol. 620, pp. 51-58, 2014.

[24] J. A. Rodriguez, S. Chaturvedi, M. Kuhn and J. Hrbek, "Reaction of H2S and S2 with metal/oxide surfaces: band-gap size and chemical reactivity," *J Phys Chem B,* pp. 5511, 1998.

[25] A. Fahmi, J. Ahdjoudj and C. Minot, "A theoretical study of H2S and MeSH adsorption on TiO2," *Surf Sci,* vol. 352–354, pp. 529-533, 1996.

[26] J. Sun, S. Modi, K. Liu, R. Lesieur and J. Buglass, "Kinetics of zinc oxide sulfidation for packed-bed desulfurizer modeling," *Energy Fuels,* vol. 21, pp. 1863-1871, 2007.

[27] S. Guntuka, S. Farooq and A. Rajendran, "A- and B-Site substituted lanthanum cobaltite perovskite as high temperature oxygen sorbent. 2. Column dynamics study," *Ind Eng Chem Res,* vol. 47, pp. 163-170, 2008.

[28] Y. Xiao, S. Wang, D. Wu and Q. Yuan, "Experimental and simulation study of hydrogen sulfide adsorption on impregnated activated carbon under anaerobic conditions," *J. Hazard. Mater.,* vol. 153, pp. 1193-1200, 2008.

[29] S. N. Nobar and S. Farooq, "Experimental and modeling study of adsorption and diffusion of gases in Cu-BTC," *Chemical Engineering Science,* pp. 801, 2012.

[30] R. Haghpanah, A. Rajendran, S. Farooq, I. A. Karimi and M. Amanullah, "Discrete Equilibrium Data from Dynamic Column Breakthrough Experiments," *Ind Eng Chem Res,* vol. 51, pp. 14834-14844, 2012.

[31] K. B. Lee, A. Verdooren, H. S. Caram and S. Sircar, "Chemisorption of carbon dioxide on potassium-carbonate-promoted hydrotalcite," *Journal of Colloid & Interface Science,* vol. 308, pp. 30-39, 04, 2007.

[32] O. Levenspiel, *Chemical Reaction Engineering; an Introduction to the Design of Chemical Reactors.* New York, Wiley, 1962.

[33] C. H. Bartholomew, "Mechanisms of catalyst deactivation," *Applied Catalysis A: General,* vol. 212, pp. 17-60, 2001.

[34] T. Doğu, "The Importance of Pore Structure and Diffusion in the Kinetics of Gas-Solid Non-catalytic Reactions: Reaction of Calcined Limestone with SO2," *The Chemical Engineering Journal,* vol. 21, pp. 213-222, 1981.

[35] N. Yaşyerli, T. Doğu, G. Doğu and i. Ar, "Deactivation model for textural effects of kinetics of gas-solid noncatalytic reactions "char gasification with CO2"," *Chemical Engineering Science,* vol. 51, pp. 2523-2528, 6, 1996.

[36] Y. Suyadal, M. Erol and H. Oguz, "Deactivation model for the adsorption of trichloroethylene vapor on an activated carbon bed," *Ind Eng Chem Res,* vol. 39, pp. 724-730, 2000.

[37] S. Yasyerli, G. Dogu, I. Ar and T. Dogu, "Activities of copper oxide and Cu-V and Cu-Mo mixed oxides for H2S removal in the presence and absence of hydrogen and predictions of a deactivation model," *Ind Eng Chem Res,* vol. 40, pp. 5206-5214, 2001.

[38] S. Yasyerli, I. Ar, G. Dogu and T. Dogu, "Removal of hydrogen sulfide by clinoptilolite in a fixed bed adsorber," *Chem. Eng. Process,* vol. 41, pp. 785-792, 2002.

[39] S. Yasyerli, G. Dogu, I. Ar and T. Dogu, "Breakthrough Analysis of H 2 S Removal on Cu-V-Mo, Cu-V, and Cu-Mo Mixed Oxides," *Chem. Eng. Commun.,* vol. 190, pp. 1055, 05, 2003.

[40] T. Kopac and S. Kocabas, "Deactivation models for sulfur dioxide adsorption on silica gel," *Adv. Environ. Res.,* vol. 8, pp. 417-424, 2004.

[41] H. F. Garces, H. M. Galindo, L. J. Garces, J. Hunt, A. Morey and S. L. Suib, "Low temperature H2S dry-desulfurization with zinc oxide," *Microporous Mesoporous Mat.,* vol. 127, pp. 190-197, 2010.

[42] T. Ko and H. Hsueh, "Removal of Hydrogen Sulfide by Iron-Rich Soil: Application of the Deactivation Kinetic Model for Fitting Breakthrough Curve," *Aerosol Air Qual. Res.,* vol. 12, pp. 1355-1361, DEC, 2012.

[43] K. J. Leary, J. N. Michaels and A. M. Stacy, "Temperature-programmed desorption: Multisite and subsurface diffusion models," *AICHE J.,* vol. 34, pp. 263, 02, 1988.

[44] A.M. de Jong and J.W. Niemantsverdriet, "Thermal desorption analysis: Comparative test of ten commonly applied procedures," Surface Science vol. 233 pp. 355-365, 1990.

[45] R. Haghpanah, A. Majumder, R. Nilam, A. Rajendran, S. Farooq, I. A. Karimi and M. Amanullah, "Multiobjective Optimization of a Four-Step Adsorption Process for Postcombustion CO2 Capture Via Finite Volume Simulation," *Ind Eng Chem Res,* vol. 52, pp. 4249-4265, 2013.

[46] A. Startsev, O. Kruglyakova, Y. Chesalov, S. Ruzankin, E. Kravtsov, T. Larina and E. Paukshtis, "Low Temperature Catalytic Decomposition of Hydrogen Sulfide into Hydrogen and Diatomic Gaseous Sulfur," *Topics in Catalysis,* vol. 56, pp. 969-980, 08, 2013.

[47] K. J. Leary, J. N. Michaels and A. M. Stacy, "Temperature-programmed desorption: Multisite and subsurface diffusion models," *AICHE J.,* vol. 34, pp. 263, 02, 1988.

6. Adsorption Behaviour of Cu(II) onto Nano-titanate ETS-2

6.1. Summary

In this work copper (II) removal from aqueous solution by nanotitanate ETS-2 through the batch technique is investigated. The paper focused on the characterization and sorption properties of ETS-2. Structure and chemical properties of ETS-2 sorbent and aqueous solution are studied by means of different characterization tests (TGA, XRD, XPS, EDX, ICP). Copper adsorption capacity increased in the pH range of 2 to 7 and the maximum uptake of Cu^{2+} by ETS-2 occurred at a pH of 7 with an adsorption maximum of 99% copper removal.

The mechanism for removing Cu^{2+} ions from aqueous solution onto ETS-2 surfaces were also examined. It was experimentally concluded that ETS-2 possesses ion-exchange properties and copper removal happens through the cation exchange mechanism.

6.2. Introduction

The problem of discharged heavy metal pollutants to the environment with the huge increase in the industrial activities is a major concern due to their minatory hazards to the life on land as well as in water [1-3]. Water contamination by metal ions is growing environmental issues since the toxicity of metal pollution is slow but long lasting plus such ions are non-biodegradable[8] [4, 5].

Copper is one of the hazardous heavy metals, which is widely used in various industries such as power transmission, plumbing and refining [6, 7] and is frequently released to the surface water in different component forms and concentrations [1]. Human intake of excessively large doses of copper leads to severe mucosal irritation, widespread capillary damage, central nervous problems, hepatic, renal and liver damage, gastrointestinal irritation and depression [8].

Many techniques such as chemical precipitation, electrochemical treatment, solvent extraction, ion exchange, membrane technology and adsorption have been conventionally employed for the removal of heavy metal ions [6, 9]. Among them ion exchange and adsorption is one of the most popular methods has been thought a simple efficient and cost-effective feasible method [3, 10, 11]. It has been then

---

[8] remains contaminated for a long-term.

widely used in industrial wastewater treatment processes for the removal of effluents of heavy metal ions [10].

The application of adsorption technology using different adsorbents including activated carbons and graphene oxide [1, 12, 13], titanate nanotubes [12], mesoporous silica and silica gel [9, 14, 15], synthesized zeolitic materials and membranes [16-18] and different types of ion exchange resins [10] has become the most effective technologies for the removal of heavy metals. However many of the above adsorbents such as widely studied activated carbon and ion exchange resins suffer from high cost and are difficult to establish at an industrial scale [12, 16]. Thus many researchers have been encouraged to look for low cost materials for heavy metal removal in the past decay [2, 5, 12, 19, 20].

ETS-2 is a nanotitanate characterized by a high specific surface area [21, 22], which may offer a special environment for the removal of heavy metal ions. In the present study, the potential of ETS-2 as an adsorbent for the removal of copper ions form aqueous solution is examined. Different characterization tests have been carried out to investigate the sorption characteristics of ETS-2 for the removal of Cu(II) from its aqueous solution. Change in the pH of solution was also studied to study the loading of competing proton ions onto ETS-2.

6.3. Experimental

6.3.1. ETS-2 adsorbent

Na-ETS-2 (ETS-2) was synthesized using a hydrothermal process using a commercial source of titanium (Titanium (III) chloride solution 20% stabilized, Fisher Scientific, Canada) following the same procedure explained in [22].

6.3.2. Characterization tests

6.3.2.1. Thermogravimetric Analysis

TGA was also carried out using Q500 thermogravimetric analyzer (TA Instruments) from an ambient temperature to 1000 °C, with airflow and a ramp rate of 10 °C/min.

6.3.2.2. Energy Dispersive X-ray Spectroscopy

EDX measurements were conducted on a Zeiss EVO MA 15LaB6 filament scanning electron microscope. The data were acquired with a peltier-cooled 10 mm^2 Bruker Quantax 200 Silicon drift detector with 123eV resolution.

6.3.2.3. X-ray photoelectron spectroscopy measurement

The XPS measurements were performed on AXIS 165 spectrometer (Kratos Analytical). The base pressure in the analytical chamber was lower than 3e-8 Pa. Monochromatic Al Kα source (hν = 1486.6 eV) was used at a power of 210 W. The analysis spot was 400 by 700 um. The resolution of the instrument is 0.55 eV for Ag 3d and 0.70 eV for Au 4f peaks.

6.3.2.4. Inductively coupled plasma measurement

ICP tests have been done using Perkin Elmer's Elan 6000 with ICP RF power of 1300 W; Dual Detector mode. Subtract blank was done after internal standard correction. Measurement units were cps (counts per second); Auto lens on; 4 points calibration curves (0, 0.25, 0.50, 1.00 ppm for Na, Ca, Mg, Fe, K & P; 0, 0.005, 0.010, 0.020 ppm for rest elements). Typical count rates for 10 ppb Pb is obtained between 150000 cps to 200000 cps. Bi, Sc and In are used as internal standards.

6.3.3. Batch adsorption experiments

In order to study the heavy metal removal characteristics of ETS-2 sample, Cu^{2+} solution was prepared from copper nitrate ($Cu(NO_3)_2.2.5.H_2O$, MW: 232.59, Anachemia, Chemicals) . Copper removal experiment was done by immersing 0.1 g as-synthesized ETS-2 in the 100mL of Cu(II) ions aqueous solutions with the desired concentrations (54 mg/L) at room temperature. The initial pH value of the solution was adjusted with NaOH (0.1N) or HCl (0.1N) solution to the desired value. The pH measurements were performed with an AB 15+ pH meter (Fisher Scientific accumet). After 1 hour contact time the solid phase was filtered and the Cu^{2+} concentration for the filtrated solution was determined by ICP/OES spectroscopy.

The copper adsorption capacity (metal uptake) of ETS-2 was easily calculated according to the mass balance and from the following equation:

$$q = (c^o - c)V/w \qquad\qquad (6-1)$$

where q is the adsorption capacity per unit mass of ETS-2 [mg/g], c^o and c are the initial and the final equilibrium concentration of adsorbate solution [ppm: μg/ml] respectively. w is the mass of ETS-2 adsorbent [g] and V is the sample volume [L].

The copper removal percentage was also calculated using the following equation:

$$\% \text{ Cu ion removal} = (c^o - c)/c^o * 100 \qquad\qquad (6-2)$$

6.4. Results and Discussion

6.4.1. Characterization of ETS-2 adsorbent and spent sample[9]

6.4.1.1. TGA analysis for ETS-2

The TGA curve of ETS-2 sample given in Figure 6-1 shows a rapid mass loss of about 15 wt.%, which is due to the loss in water content of the sample or any adsorbed contamination from the air (such as CO_2). The minor mass loss around 600°C is likely assigned to a phase change and a bulk conversion where the amorphous phase in ETS-2 gradually changes.

---

[9] After Cu adsorption
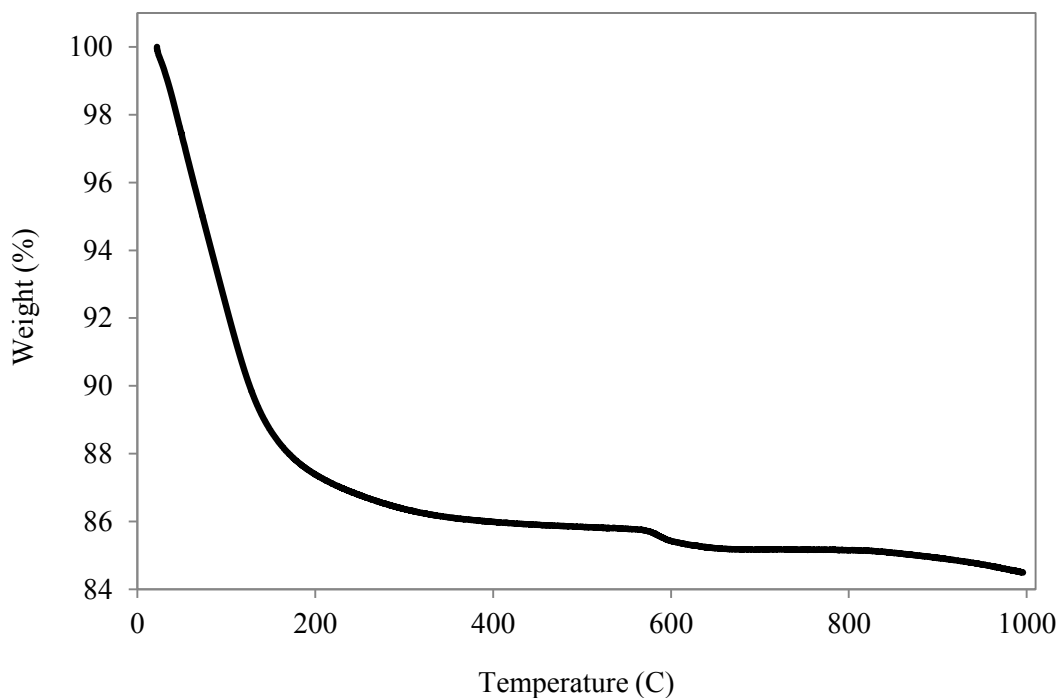
Figure 6- 1 TGA Curve of ETS-2 (ramp 10 °C/min under air).

6.4.1.2. EDX analysis for ETS-2

EDX spectra were performed by point specific elemental analysis of a compressed ETS-2 disc and results are summarized in Table 6-1. Na:Ti atomic ratio (1:3) was then calculated by averaging a set of these numbers.

6.4.1.3. Binding energy data for ETS-2

The X-ray photoelectron spectroscopy lines of ETS-2 sample have been shifted to higher energies because of surface charging effects. Therefore all binding energies obtained from high-resolution XPS spectra, were calibrated using the assigned value of C 1s peak (284.6eV) as the internal standard. Figure 6-2 shows

Ti 2p photoemission signal of ETS-2 sample. The two main peaks, at 458.3eV and 464.0eV binding energies are good match with the Ti 2p3/2 and Ti 2p1/2 of Ti^{+4}, respectively [23].

Table 6- 1 Elemental composition of ETS-2 obtained by EDX.

Element	Atomic conc. at %	Mass conc. %
Na	8.45	7.92
O	66.19	43.19
Ti	24.53	47.90
Si	0.78	0.90
Ca	0.05	0.09

Figure 6-3 shows O (1s) spectra of ETS-2 sample. The peaks at 529.79eV corresponded to that of the Ti–O in which the valence of Ti is +4 [23]. The binding energy at 531.79eV is about 0.2eV different than the attributed to OH^- groups. The splitting of the O (1s) line at this binding energy is not due to residual sodium hydroxide, but due to the existence of Na^+-O-Ti bonds [24].

The surface composition is about Na:Ti = 1:1 by measuring the area of the Na (1s) and Ti (2p) peaks (Table 6-2), which is more than the ratio value (1:3) from Table 6-1. This is because ETS-2 like other sodium titanates [23, 24] has numerous Na+–

O–Ti bonds on its surface and the Na:Ti atomic ratio of surface (by XPS) is more than the ratio value obtained from EDX. According to the fact that XPS analysis is a surface technique (depth of information is order of nm) but EDX is a relatively surface technique (penetration depth is order of micron) and it penetrates more than one molecule thickness as XPS does.
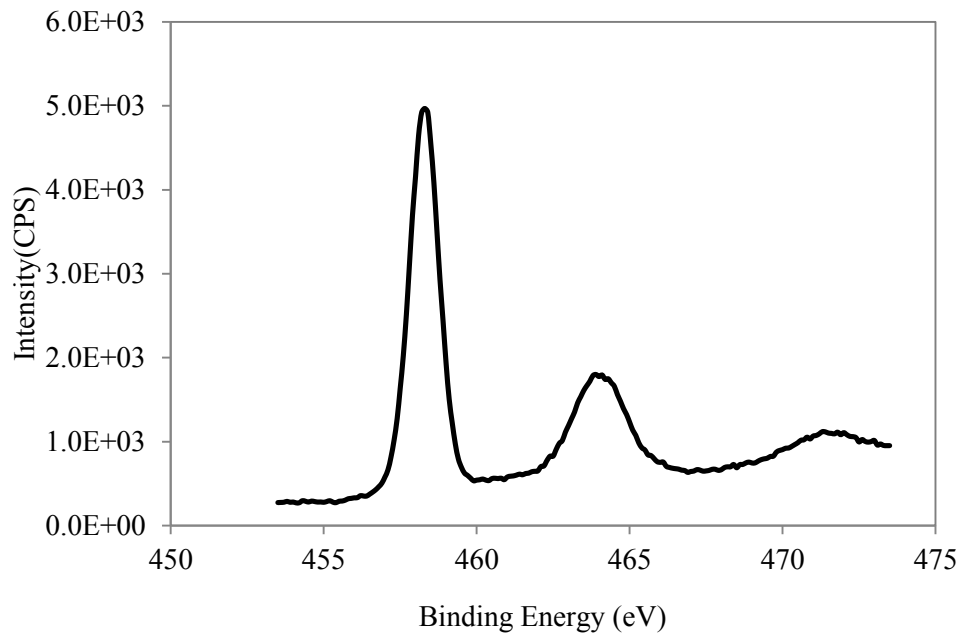
Figure 6- 2 Ti 2p photoemission signal of ETS-2.
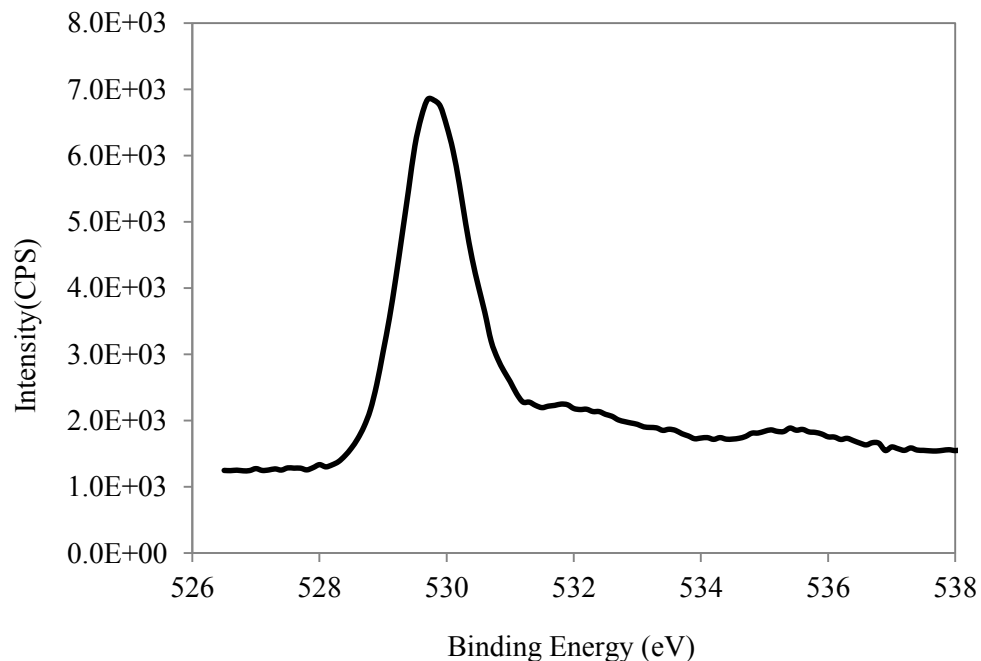
Figure 6- 3 O 1s photoemission signal of ETS-2.

Results from XPS and EDX are in good agreement with what is reported earlier based on the XRD results that surface of ETS-2 have been converted to sodium titanate and the bulk is TiO_2 [25].

6.4.1.4. Chemical property changes for spent ETS-2

Inductively coupled plasma mass spectrometry (ICP-MS) was performed to determine the chemical composition of the aqueous solution before and after copper removal. Results are given in Table 6-3.

Table 6- 2 Quantification results by XPS on ETS-2.

Peak	Position BE (ev)	Atomic conc. %	Mass conc. %
Na 1s	1071.40	13.84	16.04
O 1s	529.70	33.83	27.28
Ti 2p	458.30	13.82	33.35
C 1s	284.70	38.51	23.32

From Table 6-3 it can be calculated that 0.0021 mmol sodium is released in to the final product of 1ml copper nitrate solution containing ETS-2. Also 0.0008 mmol copper is was removed from solution during this time. This is approximately half of the number of sodium (in mmol), which clearly shows that Na ions are replaced with the equivalent amount for divalent copper. Since the pH change for the solution after adding ETS-2 is small the proton change is negligible. This shows strong affinity of ETS-2 for metal exchange.

Table 6- 3 Concentration (ppm) of different ions during the copper exchange process

Sample	Ti ±0.00006	Cu ±0.00003	Na ±0.005	Si ±0.005
$Cu(NO_3)_2$	Below detection limit	54.1	3.33	Below detection limit
$Cu(NO_3)_2$ + ETS-2	2.22	1.67	50.9	8.72

Table 6- 4 The content of different elements in Cu-ETS-2 by EDX

Element	Atomic conc. at %	Mass conc. %
Na	0.12	0.10
O	67.51	40.04
Ti	26.08	46.29
Cu	5.29	12.47
Si	0.86	0.89
Ca	0.14	0.21

Point specific elemental analysis has been done for a compressed Cu-ETS-2 disc and results are given in Table 6-4. Results in Table 6-1 and 6-4 show that Na:Ti of ETS-2 sample dropped dramatically after copper removal process (0.34 to

0.0046). Besides, Cu:Ti atomic ratio of Cu-ETS-2 (0.20) is close to the half of what it is for the ratio of Na:Ti (0.34) on ETS-2.

The amount of sodium ions released to the aqueous solution during the copper removal process can be calculated through a mass balance for the solid phase, from the ICP results (Table 6-3). Results show that 0.0766 g sodium was removed from the solid phase after copper removal. Since ICP is a volumetric technique, which detects all sodium amounts, this number is the total amount of sodium ions removed from solid phase. This is also very close to the same value obtained from EDX results, 0.0792 g, showing that all displaced sodium ions could be detected by EDX analysis.

Therefore, copper removal occurs on the surface of ETS-2, the sodium titanate layer. Unlike XPS, EDX can detect the whole titanate layer and may go even deeper to the titanium dioxide core. That is another reason for why EDX detects more Ti than XPS and the Na:Ti ratio from the tests differ.

6.4.2. Effect of pH

Figure 6-4 displays the effect of pH on the adsorption of Cu^{2+} ions onto ETS-2 sample. As it can be seen the heavy metal ion removal by ETS-2 adsorbent is significantly affected by the pH value of the aqueous solution at strongly acidic medium (pH=2).

This indicates that during the process H_3O^+ ions are competing with copper ions for the sorption sites. Therefore, at very low pH when the number of H_3O^+ ions is very

high, removal of copper ions is less favorable than higher PH. However in the previous section (6.4.1.3) that number of sodium ions release to the solution was two times of the adsorbed copper ions, PH was higher than 2 (PH=5.16). And it was in good agreement with the valences of the two ions.
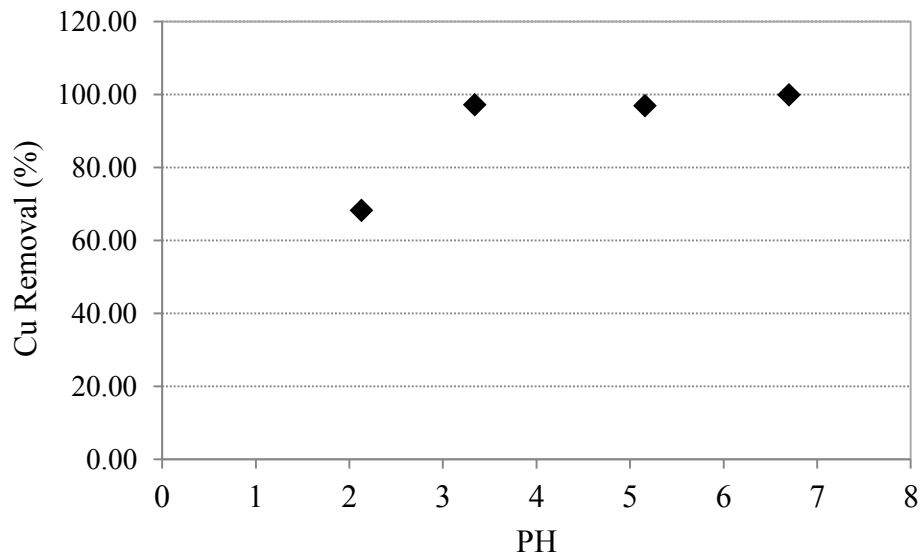
Figure 6- 4 Effect of pH on the Cu removal capacity of ETS-2 at room temperature and initial Cu^{2+} concentration 54 mg/L and 1 hour contact time.

With a further increase in pH (to 7) the copper removal capacity increased noticeably. This happens due to the fact that there is less competing ion (proton) in the system. Besides, the copper ions in the aqueous solution are the forms of Cu^{2+}, $Cu(OH)^{+}$ and $Cu_2(OH)_2^{+2}$ at pH around 5, which is favorable for the Cu^{2+} adsorption [14]. Precipitation of the metal hydroxide on the surface also appears at higher pH values [12, 14].

At PH around 5 it has been seen that after adding ETS-2 the pH of the aqueous solution increases slightly, which means that very few H_3O^+ ions adsorb on ETS-2. Thus the small pH change after adding the ETS-2 sorbent shows that in the competition between copper and H_3O^+, copper is more successful to sit in sodium place.

6.4.3. Mechanism of Cu ions adsorption

Activated carbon is often used as an adsorbent for the heavy metal ions removal from wastewater [12]. The impregnation mechanism proposed by [26] show that copper ions are deposited in the form of $Cu(OH)_2$ on activated carbon.

Unlike activated carbon, data presented in this work clearly show that ion exchange is the dominant removal mechanism for Cu^{2+} removal by ETS-2. Hence, dissolved copper ions are displaced with sodium ions from ETS-2 structure and are not impregnated onto the external-surface of ETS-2 substrate in the form of $Cu(OH)_2$ and become part of the ETS-2; known as Cu-ETS-2.

$Cu(OH)_2$ has a very high solubility in ammonium hydroxide (NH_4OH). Thus adding NH_4OH to the solution during the copper removal process is a good indicator if any impregnated $Cu(OH)_2$ forms on ETS-2 surface. Results from EDX analysis implies that the amount of copper on Cu-ETS-2 sample is not decreased after NH_4OH, which is another evidence for the ion exchange mechanism and there is more affinity for copper than proton to seat in Na place in ETS-2 structure.

6.5. Conclusions

The potential of ETS-2 as an adsorbent for the removal of copper ions from aqueous solutions is investigated. ETS-2 showed high copper capacity (over 98% removal) showing the high affinity of ion exchange ETS-2 for copper removal. With an adjustment for the pH of the solution, uptake of Cu ions improves sharply up to 99% removal at pH=6.7. The results indicate the potential application of ETS-2 for effluent heavy metal treatment in industries and also provide strong experimental evidences to support the ion exchange mechanism proposed.

6.6. References

[1] S. Rengaraj, Y. Kim, C. K. Joo, K. H. Choi and J. H. Yi, "Batch adsorptive removal of copper ions in aqueous solutions by ion exchange resins: 1200H and IRN97H," Korean Journal of Chemical Engineering, vol. 21, pp. 187-194, 2004.

[2] S. R. Shukla and R. S. Pai, "Adsorption of Cu(II), Ni(II) and Zn(II) on dye loaded groundnut shells and sawdust," *Separation & Purification Technology,* vol. 43, pp. 1-8, 2005.

[3] A. K. Meena, K. Kadirvelu, G. K. Mishra, C. Rajagopal and P. N. Nagar, "Adsorptive removal of heavy metals from aqueous solution by treated sawdust (Acacia arabica)," *J. Hazard. Mater.,* vol. 150, pp. 604-611, 2008.

[4] S. R. Shukla and R. S. Pai, "Adsorption of Cu(II), Ni(II) and Zn(II) on modified jute fibres," *Bioresour. Technol.,* vol. 96, pp. 1430-1438, 2005.

[5] K. G. Bhattacharyya and S. S. Gupta, "Adsorptive Accumulation of Cd(II), Co(II), Cu(II), Pb(II) and Ni(II) Ions from Water onto Kaolinite: Influence of Acid Activation," *Adsorption Science & Technology,* vol. 27, pp. 47-68, 02, 2009.

[6] X. Sun, X. Huang, X. Liao and B. Shi, "Adsorptive removal of Cu(II) from aqueous solutions using collagen-tannin resin," *J. Hazard. Mater.,* vol. 186, pp. 1058-1063, 2011.

[7] B. Singha and S. K. Das, "Adsorptive removal of Cu(II) from aqueous solution and industrial effluent using natural/agricultural wastes," *Colloids and Surfaces B: Biointerfaces,* pp. 97, 2013.

[8] T. S. Anirudhan and P. G. Radhakrishnan, "Adsorptive Removal and Recovery of U(VI), Cu(II), Zn(II), and Co(II) from Water and Industry Effluents," *Bioremediation J.,* vol. 15, pp. 39-56, 2011.

[9] H. Dumrul, A. N. Kursunlu, O. Kocyigit, E. Guler and S. Ertul, "Adsorptive removal of Cu(II) and Ni(II) ions from aqueous media by chemical immobilization of three different aldehydes," *Desalination,* vol. 271, pp. 92-99, 2011.

[10] S. Kocaoba, "Comparison of Amberlite IR 120 and dolomite's performances for removal of heavy metals," *J. Hazard. Mater.,* vol. 147, pp. 488-496, 2007.

[11] S. R. Popuri, Y. Vijaya, V. M. Boddu and K. Abburi, "Adsorptive removal of copper and nickel ions from water using chitosan coated PVC beads," *Bioresour. Technol.,* vol. 100, pp. 194-199, 2009.

[12] S. Liu, C. Lee, H. Chen, C. Wang and L. Juang, "Application of titanate nanotubes for Cu(II) ions adsorptive removal from aqueous solution," *Chem. Eng. J.,* vol. 147, pp. 188-193, 2009.

[13] R. Sitko, E. Turek, B. Zawisza, E. Malicka, E. Talik, J. Heimann, A. Gagor, B. Feist and R. Wrzalik, "Adsorption of divalent metal ions from aqueous solutions using graphene oxide," *Dalton Transactions,* vol. 42, pp. 5682-5689, 2013.

[14] X. Xue and F. Li, "Removal of Cu(II) from aqueous solution by adsorption onto functionalized SBA-16 mesoporous silica," *Microporous and Mesoporous Materials,* vol. 116, pp. 116-122, 2008.

[15] A. Shahbazi, H. Younesi and A. Badiei, "Functionalized SBA-15 mesoporous silica by melamine-based dendrimer amines for adsorptive characteristics of Pb(II), Cu(II) and Cd(II) heavy metal ions in batch and fixed bed column," *Chem. Eng. J.,* vol. 168, pp. 505-518, 2011.

[16] B. A. Shah, C. B. Mistry and A. V. Shah, "Sequestration of Cu(II) and Ni(II) from wastewater by synthesized zeolitic materials: Equilibrium, kinetics and column dynamics," *Chem. Eng. J.,* vol. 220, pp. 172-184, 2013.

[17] W. Jiang, X. Chen, B. Pan, Q. Zhang, L. Teng, Y. Chen and L. Liu, "Spherical polystyrene-supported chitosan thin film of fast kinetics and high capacity for copper removal," *J. Hazard. Mater.,* vol. 276, pp. 295-301, 2014.

[18] S. Zarghami, T. Mohammadi and M. Kazemimoghadam, "Adsorption Behavior of Cu(II) Ions on Crosslinked Chitosan/Polyvinyl Alcohol Ion Imprinted Membrane," *Journal of Dispersion Science & Technology,* vol. 36, pp. 190-195, 02, 2015.

[19] A. Çimen, A. Bilgiç, A. N. Kursunlu, I. H. Gübbük and H. I. Uçan, "Adsorptive removal of Co(II), Ni(II), and Cu(II) ions from aqueous media using chemically modified sporopollenin of Lycopodium clavatum as novel biosorbent," *Desalination & Water Treatment,* vol. 52, pp. 4837, 07, 2014.

[20] N. S. Randhawa, N. N. Das and R. K. Jana, "Adsorptive remediation of Cu(II) and Cd(II) contaminated wate using manganese nodule leaching residue," *Desalination & Water Treatment,* vol. 52, pp. 4197-4211, 06, 2014.

[21] S. Rezaei, A. Tavana, J. A. Sawada, L. Wu, A. S. M. Junaid and S. M. Kuznicki, "Novel Copper-Exchanged Titanosilicate Adsorbent for Low Temperature H2S Removal," *Ind Eng Chem Res,* vol. 51, pp. 12430-12434, 2012.

[22] S. Rezaei, M. O. D. Jarligo, L. Wu and S. M. Kuznicki, "Breakthrough performances of metal-exchanged nanotitanate ETS-2 adsorbents for room temperature desulfurization," *Chemical Engineering Science,* vol. 123, pp. 444-449, 2015.

[23] X. Meng, D. Wang, J. Liu and S. Zhang, "Preparation and characterization of sodium titanate nanowires from brookite nanocrystallites," *Mater. Res. Bull.,* vol. 39, pp. 2163-2170, 2004.

[24] R. A. Zárate, S. Fuentes, J. P. Wiff, V. M. Fuenzalida and A. L. Cabrera, "Chemical composition and phase identification of sodium titanate nanostructures grown from titania by hydrothermal processing," *Journal of Physics and Chemistry of Solids,* vol. 68, pp. 628-637, 2007.

[25] F. Yazdanbakhsh, M. Blasing, J. A. Sawada, S. Rezaei, M. Muller, S. Baumann and S. M. Kuznicki, "Copper Exchanged Nanotitanate for High Temperature H2S Adsorption," Industrial and Engineering Chemistry Research, vol. 53, pp. 11734-11739, 2014.

[26] C. Huang, C. Chen and S. Chu, "Effect of moisture on H2S adsorption by copper impregnated activated carbon," *J. Hazard. Mater.,* vol. 136, pp. 866-873, 2006.

7. Low Temperature Regenerable ETS-10 Titanosilicate Desiccants for Carbon Dioxide Drying

7.1. Summary

Moisture removal from CO_2 is an interesting alternative to liquid absorbers for post-combustion capture (PCC) systems. The purified CO_2 stream from a PCC system has high moisture content and, due to equipment corrosion issues and the risk of hydrate formation, the CO_2 stream must be thoroughly dried prior to being compressed. This chapter reports the first study on solid adsorbent selection for CO_2 using low-grade heat and ambient air as a regeneration gas. Water adsorption performances for different adsorbents have been investigated for the desiccation of a pure CO_2 stream. Considering the little value of the CO_2 product gas for sequestration, the drying process should require no supporting process operations and should consume little additional energy. In addition, due to the costs and complexity of separating and purifying CO_2 from a flue gas stream, the drying process should keep as much CO_2 as possible for the compression stage. A desired desiccant for CO_2 drying should have a high moisture capacity and selectivity as well as being regenerable with waste heat and humid air.

The CO_2 drying performance of different forms of ETS-10 were compared to that of commercial silica and 4A zeolite. Results show that Ca-ETS-10 have the highest moisture capacity for a temperature swing of 30-70 °C and a CO_2 feed stream of 50–100% relative humidity. All desiccants tested had a CO_2 recovery greater than 95% because of their intrinsic selectivity for water over CO_2.

7.2. Introduction

There has been increased attention on the high levels of CO_2 emissions and their direct effect on global warming and climate change in the last decade. Since the global production of CO_2 is projected to increase from 30 billion tons in 2008 to 43.2 billion tons by 2035 [1], various methods have been proposed to mitigate the environmental effect of rising CO_2 emissions. An appealing design is post combustion capture (PCC), which uses an adsorptive separation process to selectively remove and concentrate CO_2 from the combustion gas stream. The concentrated CO_2 is then compressed and permanently separated preventing significant volumes of CO_2 from releasing to the atmosphere. The combustion process may be modified to run on pure oxygen and/or through a turbine in an integrated gasification combined (IGC) cycle [2-4] to improve the efficiency of the separation. Through IGC systems a combustion stream with a high concentration of CO_2 is generated however such advantages come at increased cost and added process complexity.

146

Different types of adsorbents with a high selectivity for CO_2 over other atmospheric gases including zeolites [5-9], metal oxides [10-15], and solid-supported amines [16-20] have been investigated for recovering CO_2. Despite different characteristics of these materials, they all co-adsorb water to some extent which will be desorbed with the CO_2. But the moisture content needs to be reduced to trace levels prior to compression of the carbon dioxide streams to meet the requirements for underground carbon sequestration [21], and to prevent the formation of CO_2 hydrates [22].

A desired desiccant would noticeably have a high water capacity at low partial pressure and would demonstrate a large difference in moisture capacity over a narrow temperature swing. Besides for the CO_2 streams the adsorbents' selectivity toward water over CO_2 is also important to lend the main stream gas losses and cause a high CO_2 recovery. The extra cost and complexity related to improving CO_2 capture have to be met with process efficiency at the drying stage, since losses at the drying stage will affect the overall efficiency of the PCC system.

Liquid absorption drying systems are known as a mature technology, however they are unsuitable for PCC/CO_2 sequestration since the thermal input required in the reboiler and the poor selectivity of the liquid. A famous example is triethyleneglycol (TEG) drying system which need a regeneration temperature of 200°C to remove the adsorbed moisture [23] and is limited to generating gas streams having a dew point of about -40 °C which may not outfit all compression and sequestration requirements. Besides, TEG has a significant absorption capacity for CO_2 [24], which reduces the CO_2 recovery.

Temperature swing adsorption (TSA) drying systems, with zeolites as desiccants, have been used for drying of natural gas. They are capable of generating gas streams having very low dew points, but zeolites require a regeneration step at temperatures more than 200°C [25]. The moisture selectivity and capacity of zeolite molecular sieves are extremely high, then it would be expected that the CO_2 losses from a conventional TSA system would be minimal. But generating high-grade heat to regenerate the zeolite desiccant through the combustion of fossil fuels is not economically and environmentally reasonable for PCC because the product gas has limited or no value.

Silica gel desiccants on the other hand can be regenerated at temperatures as low as 100°C, which allows the use of low-grade waste heat streams as a regeneration source. However its water adsorption capacity decreases linearly with concentration [7] which causes little adsorption capacity at trace levels of moisture. Engelhard Titanosilicate 10 (ETS-10) is a large-pored, titanium silicate molecular sieve composed of a mixture of tetrahedral silicon oxide and octahedral titanium oxide [26, 27]. The porous structure of ETS-10 is composed of a network of connected 7.6 Å by 4.9 Å channels formed by 12 membered rings [26] which are composed entirely of silica tetrahedral that give the molecular sieve a chemical stability. This is typically reserved for highly dealuminated zeolites. The orthogonal titania chains maintain a net negative charge which is balanced by cationic counter ions. Therefore ETS-10 combines the ion exchange capability of zeolite molecular sieves with the chemically passive characteristics of silica gel. The combination of these unique properties, made ETS-10 as a template for

148

precious metal nanodots [28, 29], quantum wires [30, 31], hydrocarbon separations [32, 33], an additive to improve the conductivity of PEM fuel cell membranes [34, 35], and a continuous membrane itself [36-39].

Although ETS-10 has previously been identified as a desiccant material for air [40], its use for drying CO_2 streams has not been investigated. Even as an air desiccant, no breakthrough test was conducted and its ability as a regenerable desiccant was explored through isotherm study. It was shown that the adsorption behavior of ETS-10 is unique due to the high moisture capacity at low partial pressures at ambient temperatures, but rapid loses in moisture capacity at elevated temperatures [40].

This chapter describes the CO_2 drying performance of different ion exchanged forms of ETS-10 (Na-, Ca- and Ca/H-ETS-10) and compares them to commercial silica and zeolite 4A adsorbents. The drying capacity of each adsorbent was compared at 50%-100% relative humidity (RH) under specific bed regeneration time and temperature, air flow, and adsorption temperature.

7.3. Materials and Methods

7.3.1. Adsorbent Preparation

The ETS-10 (or Na-ETS-10) sample was synthesized hydrothermally using a previously published technique [27]. Synthesis gels were prepared by mixing 50 g sodium silicate solution (28.7% SiO_2, 8.9% Na_2O, Fisher), 3.2 g of sodium hydroxide beads (Fisher), 3.8 g of KF (anhydrous, Fisher), and 16.3 g of $TiCl_3$

solution (20%, Fisher). The pH of the mixture was changed from about pH 12 to 10.1 by adding hydrochloric acid (1M, Fisher). The mixture was then stirred for one hour and then reacted in a sealed, Teflon lined 125 mL autoclave (PARR Instruments) at 200°C for 72 hours. The post-reaction material was then washed with de-ionized water and filtered, then dried in an 80°C oven.

The Ca^{2+} exchanged ETS-10 was carried out by mixing the synthesized powder with a $CaCl_2$ solution. The ion exchange mixture was prepared by adding 30 g $CaCl_2 \cdot 2H_2O$ (Fisher) to 150 g of de-ionized water, stirring to dissolve the calcium chloride, then adding 15 g of Na-ETS-10 powder. The mixture was then agitated and placed in a sealed vessel in an oven at 80°C under static conditions for 4 hrs. After this the powder was again washed with de-ionized water and filtered, then dried at 80°C.

The mixed calcium/hydrogen exchange ETS-10 was carried out by dissolving 4 g of $CaCl_2 \cdot 2H_2O$ in 150 g of de-ionized water and then adding 15 g of Na-ETS-10. The mixture was placed in an oven under static conditions at 80°C overnight in a sealed container. The sample was then filtered and dried at 80°C for two hours. The sample was then dispersed in 150 g of de-ionized water. The pH of the sample was lowered to 2 by adding HCl (1M, Fisher). The sample was stirred overnight at room temperature. It was then washed with deionized water, filtered, and dried in an oven at 80°C.

Zeolite 4A (Dessican Inc.) sample consisted of 4 to 2 mm beads. Grace Davison Grade 40 (lot #908) silica gel with a particle size range from 3.36 to 1.68 mm (No.6 to No.12 mesh) was used in this study

ETS-10 sample powders were pressed into binderless dense pellets. These pellets, along with the zeolite 4A and silica beads were crushed and sieved with the 1.19 mm to 0.595 mm fraction for use in the CO_2 drying experiments.

7.3.2. Characterization tests

X-ray diffraction (XRD) was used to verify the identities of and to gain qualitative information on the crystal structures of the adsorbents used in this study. A Rigaku Ultima IV with Co tube (38kV, 38mA) with an average Kα wavelength of 1.7902 Å equipped with a D/Tex detector with a Fe filter was used for all XRD characterization. XRD patterns obtained were compared to data from the International Center for Diffraction Data-Powder Diffraction File (ICDD-PDF) using JADE 9.1, along with visual comparisons to existing standards and literature to verify sample identity and purity.

Gas adsorption isotherms, surface area, and pore volume measurements were carried out using a Micrometrics ASAP 2020C volumetric physisorption system. Nitrogen at -196°C was used as the probe molecule. Samples were outgassed at 200 °C overnight at a pressure of 0.4 Pa.

7.3.3. Experimental Apparatus

Figure 7-1 and 7-2 display the picture of the drying set up and the process flow diagram for the experimental setup respectively. To control the input stream humidity, the inlet stream coming from the CO_2 cylinder (Praxair) was split and pasted through two mass flow controllers (MFC) (Alicat Scientific scaled for 0 to 500 cc/min gas flows at 25°C and 101.325 kPa mass reference conditions). The flow from the first MFC bubbled through a 300 mL liquid contactor partially filled with de-ionized water (to prevent liquid water from being carried over) to saturate with moisture. The second stream from the second MFC run directly to a 50 mL accumulator mixed in the accumulator with the moisture saturated gas streams. Different gas moisture contents from 0 to 100% RH was achieved by adjusting the flowrate of the two MFCs. Moisture blending were calibrated using the outlet humidity from the accumulator being recorded at various blending levels using a Traceable Humidity Meter (Fisher Scientific).

The exit CO_2 stream from the accumulator entered at the top of the adsorbent bed and flowed vertically downward through it. The adsorbent bed was made of a borosilicate glass tube with an inner diameter of 10.7 mm. The pressure at the inlet and outlet of the bed was monitored by a pair of 0-15 psia pressure transducers (PX209- Omega Environmental). The temperatures at the both ends of the bed were also measured using two K-type thermocouples (HGKMQSS -Omega Environmental). In order to maintain a stable temperature for humidification and to

152

prevent condensation all equipment in contact with moist CO_2 was kept inside an oven (Fisher Isotemp) at 30°C.
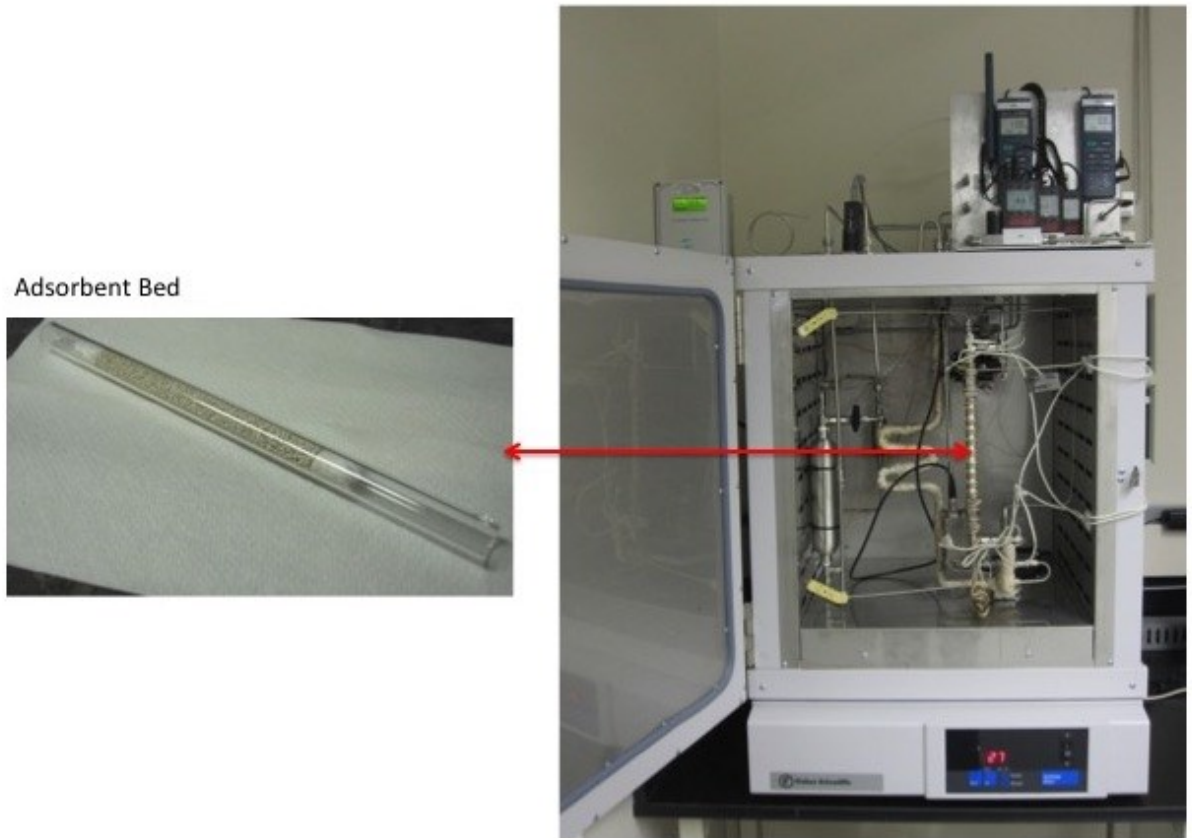
Figure 7- 1 Picture of the experimental apparatus.
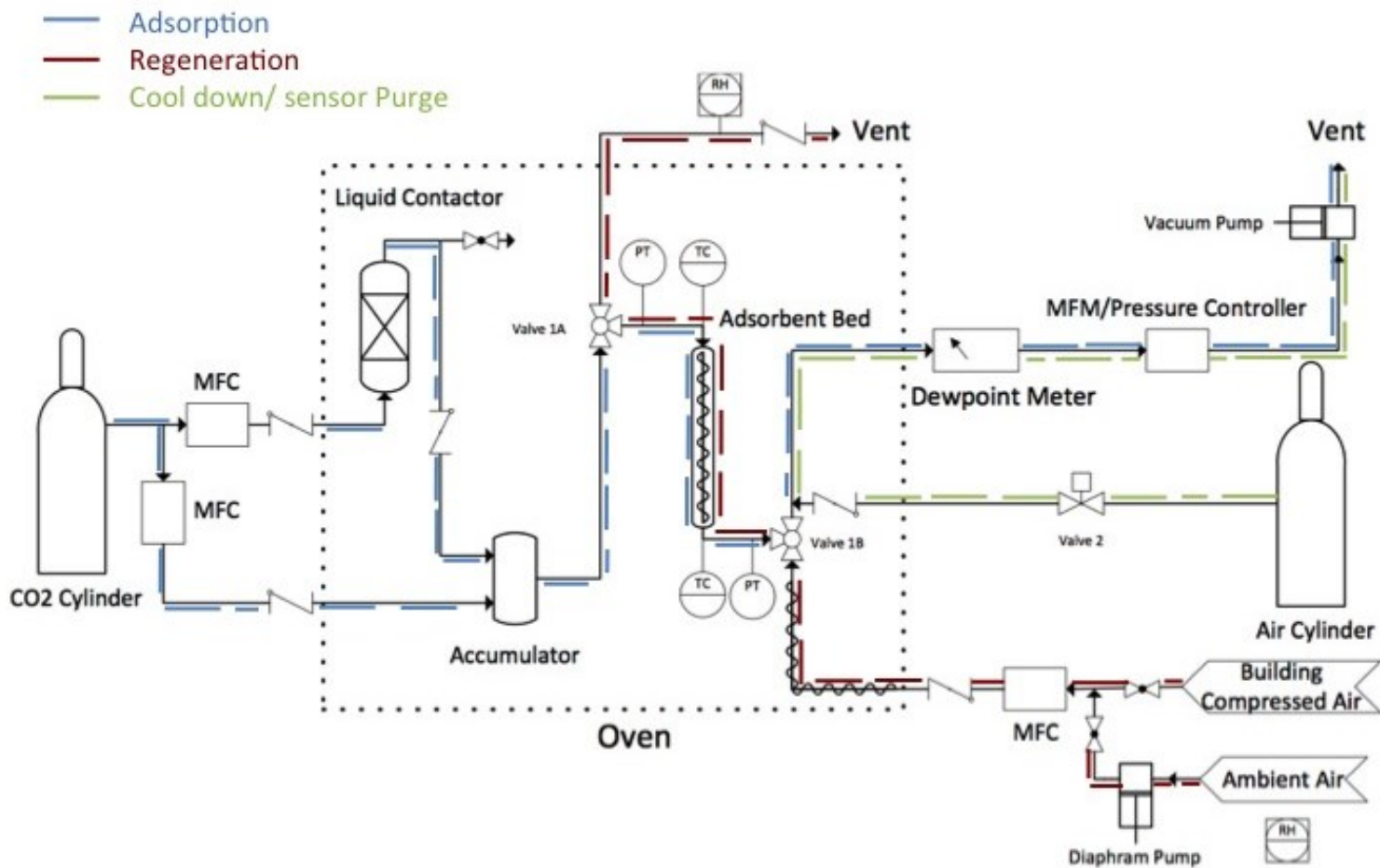
Figure 7- 2 Schematics of process flow diagram of experimental setup.

The outlet of the desiccant bed was plumbed to a dew point meter, which assessed the amount of moisture remaining in the gas stream. The sensor used was a XDT transmitter (COSA Xentaur) with a high capacitance Al_2O_3 XTR-100 sensor element capable of measuring dew points from -100°C to 20°C (0.013 ppmv to 23080 ppmv). To keep the column working at atmospheric pressure and also recording the product flow rate, the product flow rate was measured by a MC mass

flow/backpressure controller (Alicat Scientific). A vacuum pump downstream could be used to create a pressure differential for smoother operation of the backpressure controller, however this was not typically required.

The three-way valves around the bed were actuated, shifting the system from adsorption to desorption mode to regenerate the bed. A third MFC (Alicat Scientific) was used to control the flow of regeneration air. The regeneration air source was either building-supplied compressed air or ambient air (compressed and delivered via a diaphragm pump KNF Neuberger) using a three-way valve. The ambient air humidity was measured by a portable temperature/humidity meter (HH-314A - Omega Environmental). The regeneration air flowed from the third MFC and then was heated to 70°C by a heating cord (HTC-120- Omega Environmental) wrapped around the tubing before sweeping through the adsorbent bed. It pasted the adsorbent bed upward to make a counter current with the wet gas stream in the adsorption phase. During this time the adsorbent bed was wrapped with a heating cord (HTC-030 - Omega Environmental) and was heated up to 70°C. Then the regeneration air was run through another portable temperature/humidity meter (HH-314A - Omega Environmental) humidity of the and finally was vented to the room.

After the regeneration step the bed was cooled down and at the same time the dew point sensor was blown down with dry nitrogen stream (Praxair) to remove the adsorbed moisture. After the bed had cooled and the dew point sensor level had been reduced to below -65°C, another adsorption cycle would be begun. Each cycle started with a desorption step, followed by cool down step, ending with an

adsorption step. Adsorption, regeneration /desorption, and cool-down/ sensor purge stages of the cycle operation are depicted in different colors in Figure 7-2.

The entire experiment was controlled and data collected through a Labview program (Les Dean, Instrument shop, Department of Chemical and Materials Engineering, University of Alberta).

7.3.4. Breakthrough experiments

CO_2 drying performances for five different adsorbents including silica gel, zeolite 4A, Na-ETS-10, Ca-ETS-10, and Ca/H-ETS-10 were studied at moisture contents of 50, 75, and 100 % RH. The moisture adsorption conditions were adjusted at 30°C (near-ambient condition) and a CO_2 flow rate of 500 sccm. For the bed regeneration conditions were set at a bed temperature of 70°C, with ambient room air used at a flow rate of 500 sccm and one hour for the regeneration time. The low regeneration temperature was selected to compare the performance of the adsorbents using low-grade heat for regeneration, such as the waste heat available from the low-pressure steam of a power plant. Reproducibility of the data was checked through replicate runs for each set of experimental conditions.

7.4. Results and Discussion

7.4.1. Characterization of the adsorbent samples

Figure 7-3 displays the XRD patterns for Na-, Ca-, and Ca/H-ETS-10. All patterns are very similar, which shows the ion exchange procedures do not change the ETS-10 crystal structure significantly. As it can be seen all major peaks are characteristic of ETS-10, except for the peak at $2\theta = 35°$ which is likely identified as being characteristic of ETS-4, a typical by-product of ETS-10 synthesis.

EDX point analysis has been conducted on the ion-exchanged ETS-10 desiccant samples and data are shown in Table 7-1.

The amount of Na+K decreased significantly after Ca and Ca/H exchanges, indicating that the Na^+ and K^+ ions are being displaced by the Ca^{2+} and H^+ ions. However the K^+ ions are exchanged proportionally less than the Na^+, which can be explained by the stronger affinity of K+ ions for their sites in the lattice, compared to Na^+. Anderson et al. proposed that some of the K^+ ions are locked within the cages of the structure and therefore unavailable for exchange, while the Na^+ ions are more exposed and can be displaced more easily [41].

The cation to titanium (Na:Ti, Ca:Ti) can be used to determine the degree of the ion exchange procedure. As expected Na:Ti ratio in the Ca-ETS-10 decreases significantly. However, in order to balance the net negative charge of the TiO_6^{2-} octahedral in the framework, a net 2+ charge is required. This might be done by the presence of H^+ in addition to K^+ and Na^+ in the as-synthesized Na-ETS-10.

However the protons would have exchanged in during the washing of Na-ETS-10, the H:Ti ratio for the washed, as-synthesized Na/K-ETS-10 should be ~0.34.
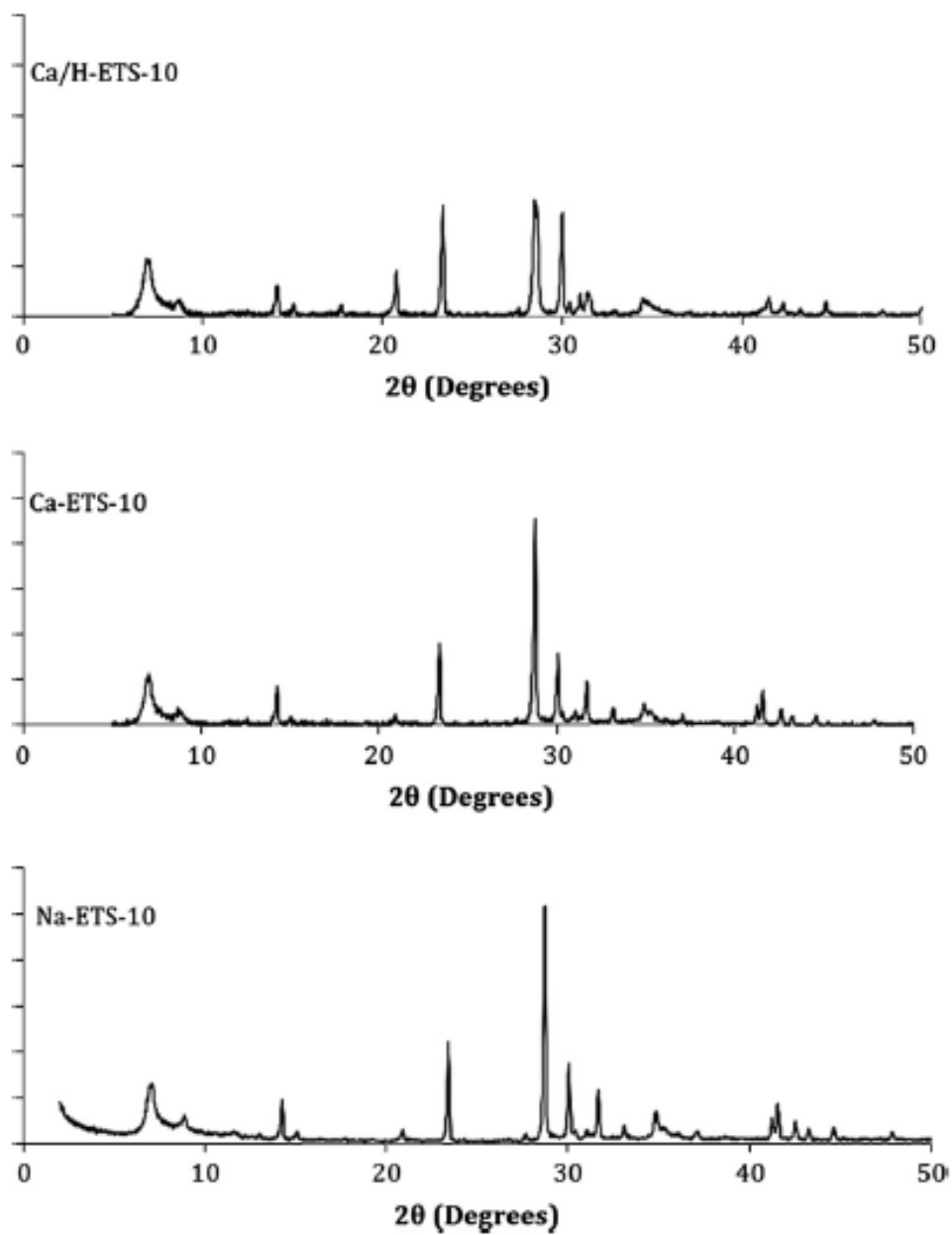
Figure 7- 3 shows the XRD patterns for Na-, Ca-, and Ca/H-ETS-10

For Ca-ETS-10, as expected, the H:Ti ratio drops (to ~0.15) because protons like other monovalent cations are exchanged for Ca^{2+}. Ca/H-ETS-10 shows the H:Ti ratio of ~0.87, which suggest that the ion affinity of ETS-10 follows the trend of $Ca^{2+} > H^+ > Na^+ / K^+$. This is also shown by literature reports that ETS-10 has a strong affinity for divalent cations and for protons [30, 42, 43].

Table 7- 1 Atomic ratios of various ETS-10 samples calculated from EDX results

Adsorbent	Atomic Ratios with 95% Confidence Intervals				Total Charge:Ti
	Si:Ti	Na:Ti	Ca:Ti	K:Ti	
Na-ETS-10 A	3.73±0.32	1.30±0.15	-	0.38±0.03	1.68±0.15
Na-ETS-10 B	3.75±0.32	1.22±0.15	-	0.42±0.03	1.64±0.15
Na-ETS-10 C	3.79±0.32	1.25±0.15	-	0.40±0.03	1.65±0.15
Ca-ETS-10 A	3.26±0.28	0.49±0.07	0.55±0.04	0.24±0.02	1.83±0.11
Ca-ETS-10 B	3.02±0.28	0.26±0.02	0.61±0.05	0.37±0.06	1.85±0.12
Ca-ETS-10 C	3.85±0.37	0.50±0.07	0.58±0.05	0.22±0.02	1.88±0.12
Ca/H-ETS-10 A	3.96±0.37	0.23±0.02	0.35±0.03	0.18±0.03	1.11±0.07
Ca/H-ETS-10 B	3.12±0.28	0.27±0.02	0.35±0.03	0.17±0.03	1.14±0.07
Ca/H-ETS-10 C	3.85±0.36	0.26±0.02	0.37±0.03	0.13±0.03	1.13±0.07

Nitrogen adsorption isotherms were used for the pore volume and surface areas determination of the tested adsorbents. Results are given in Table 7-2 except for zeolite 4A since it will not adsorb nitrogen at -196°C. BET and Langmuir methods have been used for surface area calculation of the silica gel sample and ETS-10 samples respectively. And the deBoer t-plots method was used to determine the pore volume, micropore and external surface areas. The surface areas and pore volumes of the ETS-10 samples are very close since ion exchange is not expected to affect these properties.

Table 7- 2 Surface areas and pore volumes of the adsorbent samples

Adsorbent	Total Surface Area (m^2/g)	Micropore Volume (cc/g)	Micropore Area (m^2/g)	External Surface Area (m^2/g)
Silica Gel	677.9±9.8	0.0854	171.5	506.4
Na-ETS-10	389.8±0.5	0.1327	341.6	48.85
Ca-ETS-10	380.1±0.1	0.1214	336.4	43.7
Ca/H-ETS-10	392.7±0.2	0.1249	348.2	44.4

7.4.2. Moisture Breakthrough Capacities

Moisture breakthrough capacities for silica gel, zeolite 4A, Na-ETS-10, Ca-ETS-10, and Ca/H-ETS-10 are reported in Table 7-3.

Table 7- 3 Moisture breakthrough capacities of the tested adsorbents at different CO_2 feed stream humidities

Adsorbent[a]	Capacity (wt% H_2O)		
	50% RH	75% RH	100 % RH
Ca-ETS-10	7.9 ± 1.6	7.6 ± 1.4	9.0 ± 1.0
Ca/H-ETS-10	4.7 ± 0.4	7.2 ± 0.6	9.7 ± 1.3
Na-ETS-10	4.5 ± 1.6	4.5[b]	6.2 ± 0.2
Zeolite 4A	3.8 ± 0.2	4.8 ± 0.6	6.7 ± 0.8
Silica	2.5 ± 0.7	3.4 ± 0.3	2.3 ± 0.1

[a] Adsorbents sorted by average capacity from highest to lowest

[b] Multiple data points were not collected

The breakthrough capacity of zeolite 4A and the ETS-10 materials remain constant as the feed stream moisture content increased since the water adsorption isotherms

for these adsorbents show an essentially constant equilibrium water capacity at the humidity range investigated.

At 30°C the 50%-100% RH range the feed stream moisture level is not low enough to have moved out of the rectangular region of the adsorption isotherm. And, thus, this moisture level corresponds to the rectangular region of these isotherms. This can be also attributed to the fact that for zeolite 4A, Na-ETS-10, and Ca/H-ETS-10, the bed length is not long enough for the mass transfer front to fully develop, leading to the breakthrough before any portion of the bed is fully saturated.

The variability in the data presented in Table 7-3 is likely due to the change in the humidity of the ambient air used for the regeneration. Since the data sets with a larger variability in moisture capacity measurements had a higher degree of variability in the recorded ambient air humidity.

Increasing moisture in the regeneration gas associates with a decrease in bed moisture capacity, as shown for Ca-ETS-10 at 75% RH in Figure 7-4. The presence of moisture in the regenerating air stream limits the amount of water desorbed from the water-saturated bed by maintaining an elevated partial pressure of moisture. Figure 8-5 shows the effect of regeneration air stream humidity on bed moisture capacity for silica gel, zeolite 4A and Ca-ETS-10 using a feed stream humidity of 100% RH CO_2 and one hour regeneration time. The building compressed air had a measured humidity of 46 ppmv while the ambient air humidity was from 3100 ppmv to 4100 ppmv. For all adsorbent beds, the moisture capacity was lower when using ambient air for regeneration. Results show the regeneration stream humidity

significantly affects Silica gel. The difference in the 4A bed loses is almost 50% of its capacity, which is well outside of the test-to-test variability for this sample, while the results for the Ca-ETS-10 may be considered within the error.
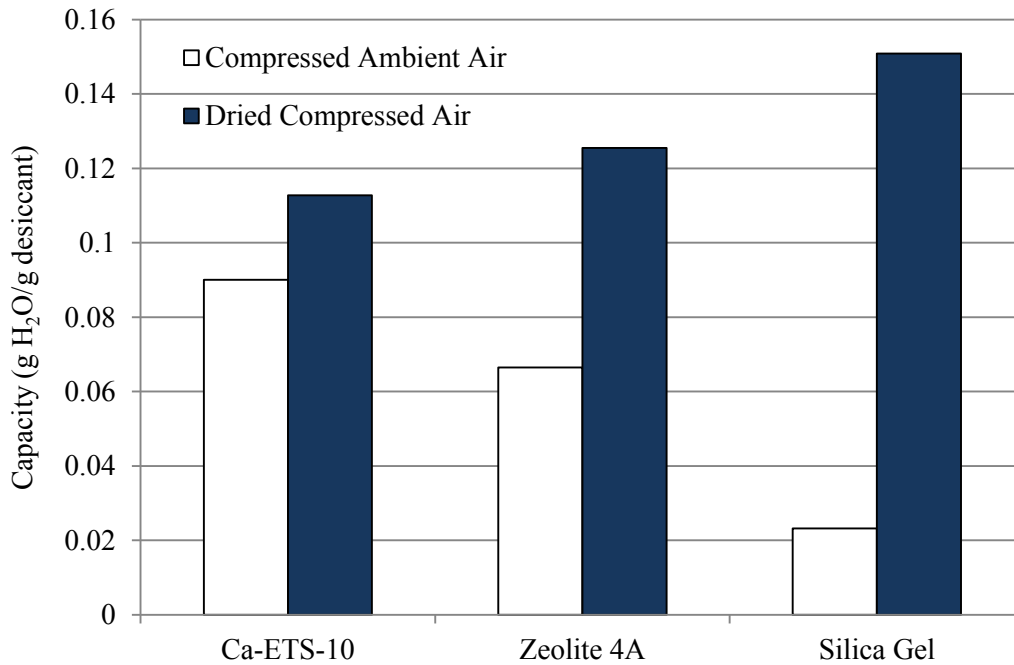
Figure 7- 4 Moisture breakthrough capacity for different adsorbents at 30° C using different regeneration air sources with a 100% RH CO_2 feed stream.

The difference in bed capacity under humid and dry regeneration air can be understood by comparing the isotherms for the various materials. The water adsorption isotherms for silica gel, 4A, and Ca-ETS-10 are shown in Figure 7-5. It can be seen that silica gel has a linear response to moisture concentration across a range of temperatures and it has little water capacity at low partial pressure. Adsorption capacity at low moisture partial pressure is limited by the presence of humidity in the regeneration gas stream. This residual moisture loading as well as

low moisture capacity at low partial pressures will significantly drop the adsorption capacity of the silica gel and explains the difference seen in the silica gel experiments (Figure 7-5 (a)). Zeolite 4A shows a rectangular adsorption isotherm which is typical of aluminosilicate zeolites. 4A is saturated at relatively low levels of humidity and the adsorption capacity results in a much smaller swing capacity over the range of temperatures selected (Figure 7-5 (b)). Figure 7-5 (c) shows the water adsorption isotherms for Ca-ETS-10, which is fundamentally different than the one for silica gel and 4A. The rectangularity of the isotherm at ambient temperature confirms a high moisture capacity at low partial pressure however this rectangularity collapses at elevated temperatures. Since the adsorption profile for Ca-ETS-10 falls as a function of temperature, a larger swing capacity over a narrow temperature window is acceptable even when humid air is used as the regeneration gas.
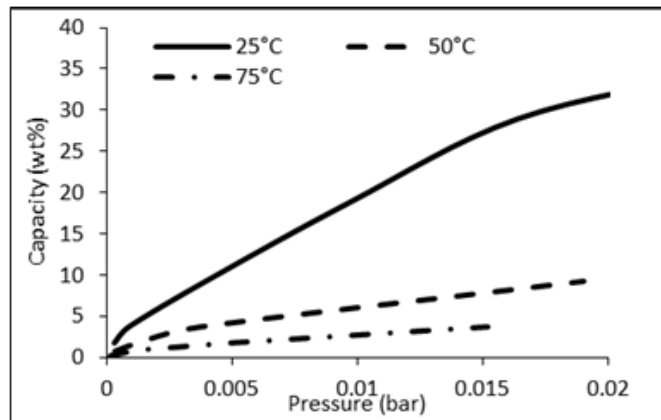
(a)
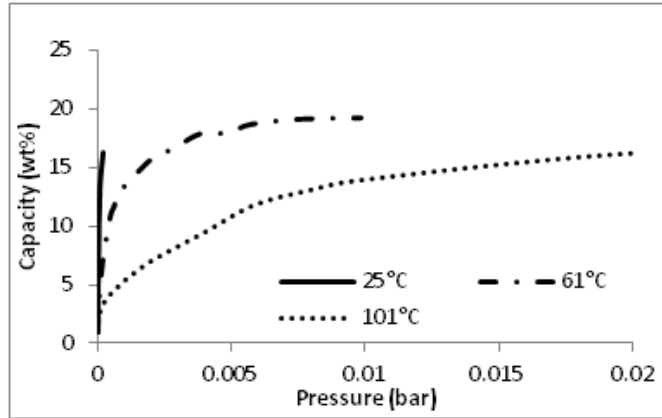
(b)
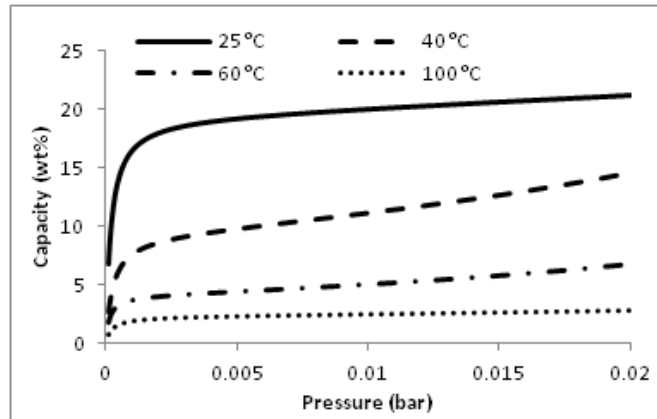
(c)

Figure 7- 5 Water adsorption isotherms for (a) Silica gel-Grade Davidson GD 40 [7], (b) Zeolite 4A Bayer [44], and (c) Ca-ETS-10 [40].

Comparing the breakthrough capacities per unit volume of adsorbent basis (g H_2O adsorbed per cc adsorbent) is relevant because the adsorbent bed volume is a major factor in determining the capital cost of an adsorptive gas separation unit. In this manner Ca-ETS-10 has the highest capacity for both 50% RH (0.0582 g/cc) and

75% RH (0.0564 g/cc) CO_2 feed streams. For the 50% RH CO_2 feed this is noticeably higher than Na-ETS-10 (0.0335 g/cc), the second highest capacity adsorbent, and higher than the capacity of zeolite 4A (0.0311 g/cc). For the 75% RH CO_2 feed Ca/H-ETS-10 breakthrough capacity (0.0493 g/cc) is close to that of Ca-ETS-10. The capacity of zeolite 4A (0.0390 g/cc) is still noticeably lower than the one for Ca-ETS-10 and Ca/H-ETS-10. At 100% RH CO_2 feed stream, Ca/H-ETS-10 (0.0671 g/cc) and Ca-ETS-10 (0.0666 g/cc) have approximately the same breakthrough capacity, higher than that of the other adsorbents.

The consistently low breakthrough capacity of silica gel can be explained by its relatively low affinity for moisture compared to the other adsorbents. This gives it a low equilibrium capacity at low inlet moisture levels, allowing ppm levels of moisture to easily breakthrough.

The breakthrough capacity of zeolite 4A has a similar trend to that of Na-ETS-10 and Ca/H-ETS-10. The breakthrough capacity of Ca/H-ETS-10 increased the most with the increasing feed stream humidity, followed by zeolite 4A. The increasing moisture content less affects na-ETS-10.

7.4.3. CO_2 Recovery

The recovery of the product (the amount of produced target gas / the amount of target gas fed to the system) is an important performance parameter in separations processes. In these breakthrough experiments the dry CO_2 exiting the

166

system can be considered the product stream. The CO_2 percent recoveries for the various breakthrough experiments are shown in Table 8-4. It can be seen that for all adsorbents, the recovery was greater than 95%. This was expected due to the high selectivity these materials have for water over most other gases and vapour. The high selectivity of the adsorbents for water over CO_2 leads to the high recovery for the process.

Table 8-4. CO_2 percent recovery at moisture breakthrough for various adsorbents at 50, 75 and 100 % RH CO_2 feed streams

Adsorbent	Percent Recovery at CO_2 Feed Stream Humidities		
	50% RH	75% RH	100 % RH
Ca-ETS-10	99.1±0.6	98.1±0.9	97.4±0.4
Ca/H-ETS-10	97.9±0.1	98.1±0.2	97.5±0.6
Na-ETS-10	98.2±1.3	96.9±1.2	96.1±0.5
Zeolite 4A	97.4±0.2	98.5±2.5	96.6±0.6
Silica	95.8±1.1	95.4±0.1	95.5±0.9

Ca-ETS-10 was then presented as a potential air desiccant to Parker Hannifin Corporation (NJ, US). Moisture breakthrough tests for Ca-ETS-2 compared to that of commercial Activated alumina (Parker Hannifin Corpora as the reference desiccant) show higher moisture breakthrough time. Four adsorption-desorption cyclic tests show less capacity loss for Ca-ETS-10 compare to the one for Activated Alumina. Results are given in Appendix section.

7.5. Conclusions

This work has focused on drying a humid CO_2 stream, which would be generated from a PCC system. It has been shown that ETS-10 is a promising desiccant for drying CO_2 to trace levels of moisture. Ca-ETS-10 had the highest breakthrough capacity of the desiccants examined under the specified test conditions and a swing regeneration temperature as low as 70°C using humid, ambient air. The relative insensitivity of ETS-10 towards humidity in the regeneration stream eliminates the need for a separate regeneration air drying step which further diminishes the energy requirements of the system. The ability to regenerate with humid, ambient air and low grade waste heat, as well as high CO_2 recovery, makes ETS-10-based adsorptive drying an attractive alternative to solvent-based absorptive drying.

7.6. References

[1] *International Energy Outlook 2011*.

 Available: http://large.stanford.edu/courses/2011/ph240/nagasawa2/docs/0484-2011.pdf. (Accessed on Dec. 20th, 2015).

[2] C. Cormos, A. Padurean and P. S. Agachi, "GHGT-10: Technical evaluations of carbon capture options for power generation from coal and biomass based on integrated gasification combined cycle scheme," *Energy Procedia,* vol. 4, pp. 1861-1868, 2011.

[3] Y. Hu, H. Li and J. Yan, "Integration of Evaporative Gas Turbine with Oxy-Fuel Combustion for Carbon Dioxide Capture," *International Journal of Green Energy,* vol. 7, pp. 615-631, 2010.

[4] A. Kather and S. Kownatzki, "Assessment of the different parameters affecting the CO2 purity from coal fired oxyfuel process," *International Journal of Greenhouse Gas Control,* vol. 5, pp. S204-S209, 2011.

[5] C. O. Areán and M. R. Delgado, "Variable-temperature FT-IR studies on the thermodynamics of carbon dioxide adsorption on a faujasite-type H-Y zeolite," *Appl. Surf. Sci.,* vol. 256, pp. 5259-5262, 2010.

[6] Z. Liu, C. A. Grande, P. Li, J. Yu and A. E. Rodrigues, "Adsorption and Desorption of Carbon Dioxide and Nitrogen on Zeolite 5A," *Separation Science & Technology,* vol. 46, pp. 434-451, 02, 2011.

[7] Y. Wang and M. D. Levan, "Adsorption Equilibrium of Carbon Dioxide and Water Vapor on Zeolites 5A and 13X and Silica Gel: Pure Components," *J. Chem. Eng. Data,* vol. 54, pp. 2839-2844, 2009.

[8] Z. Zhao, X. Cui, J. Ma and R. Li, "Adsorption of carbon dioxide on alkali-modified zeolite 13X adsorbents," *International Journal of Greenhouse Gas Control,* vol. 1, pp. 355-359, 2007.

[9] A. Zukal, J. Mayerová and M. Kubu, "Adsorption of Carbon Dioxide on High-Silica Zeolites with Different Framework Topology," *Topics in Catalysis,* vol. 53, pp. 1361-1366, 11, 2010.

[10] J. Baltrusaitis, J. Schuttlefield, E. Zeitler and V. H. Grassian, "Carbon dioxide adsorption on oxide nanoparticle surfaces," *Chem. Eng. J.,* vol. 170, pp. 471-481, 2011.

[11] P. H. Chang, Y. P. Chang, S. Y. Chen, C. T. Yu and Y. P. Chyou, "Ca-Rich Ca-Al-Oxide, High-Temperature-Stable Sorbents Prepared from Hydrotalcite Precursors: Synthesis, Characterization, and CO2 Capture Capacity," *Chemsuschem,* vol. 4, pp. 1844-1851, 2011.

[12] G. S. Grasa and J. C. Abanades, "CO2 capture capacity of CaO in long series of carbonation/calcination cycles," *Ind Eng Chem Res,* vol. 45, pp. 8846-8851, 2006.

[13] H. Lu, P. G. Smirniotis, F. O. Ernst and S. E. Pratsinis, "Nanostructured Ca-based sorbents with high CO2 uptake efficiency," *Chemical Engineering Science,* vol. 64, pp. 1936-1943, 2009.

[14] G. Ramis, G. Busca and V. Lorenzelli, "Low-Temperature CO2 Adsorption on Metal-Oxides - Spectroscopic Characterization of some Weakly Adsorbed Species," *Mater. Chem. Phys.,* vol. 29, pp. 425-435, 1991.

[15] S. P. Wang, S. L. Yan, X. B. Ma and J. L. Gong, "Recent advances in capture of carbon dioxide using alkali-metal-based oxides," *Energy & Environmental Science,* vol. 4, pp. 3805-3819, 2011.

169

[16] B. Arstad, H. Fjellvag, K. O. Kongshaug, O. Swang and R. Blom, "Amine functionalised metal organic frameworks (MOFs) as adsorbents for carbon dioxide," *Adsorption,* pp. 755, 2008.

[17] F. Chang, K. Chao, H. Cheng and C. Tan, "Adsorption of CO2 onto amine-grafted mesoporous silicas," *Separation and Purification Technology,* vol. 70, pp. 87-95, 2009.

[18] R. Chatti, A. K. Bansiwal, J. A. Thote, V. Kumar, P. Jadhav, S. K. Lokhande, R. B. Biniwale, N. K. Labhsetwar and S. S. Rayalu, "Amine loaded zeolites for carbon dioxide capture: Amine loading and adsorption studies," *Microporous and Mesoporous Materials,* vol. 121, pp. 84-89, 2009.

[19] C. Knöfel, J. Descarpentries, A. Benzaouia, V. Zeleňák, S. Mornet, P. L. Llewellyn and V. Hornebecq, "Functionalised micro-/mesoporous silica for the adsorption of carbon dioxide," *Microporous and Mesoporous Materials,* vol. 99, pp. 79-85, 2007.

[20] O. G. Nik, B. Nohair and S. Kaliaguine, "Aminosilanes grafting on FAU/EMT zeolite: Effect on CO2 adsorptive properties," *Microporous and Mesoporous Materials,* vol. 143, pp. 221-229, 2011.

[21] L. Marini, *Geological Sequestration of Carbon Dioxide. [Electronic Resource] : Thermodynamics, Kinetics, and Reaction Path Modeling.* Amsterdam ; Oxford : Elsevier, 2007.

[22] A. Y. Manakov, Y. A. Dyadin, A. G. Ogienko, A. V. Kurnosov, E. Y. Aladko, E. G. Larionov, F. V. Zhurko, V. I. Voronin, I. F. Berger, S. V. Goryainov, A. Y. Lihacheva and A. I. Ancharov, "Phase Diagram and High-Pressure Boundary of Hydrate Formation in the Carbon Dioxide-Water System," *J Phys Chem B,* vol. 113, pp. 7257-7262, 2009.

[23] V. Hernandez-Valencia, M. W. Hlavinka, J. A. Bullin and I. N. C. Bryan, "Design glycol units for maximum efficiency," Research & Eng., pp. 310-317, 1992.

[24] O. Aschenbrenner and P. Styring, "Comparative study of solvent properties for carbon dioxide absorption," *Energy & Environmental Science,* vol. 3, pp. 1106-1113, 2010.

[25] D. W. Breck, *Zeolite Molecular Sieves: Structure, Chemistry, and Use.* New York, Wiley, 1974.

[26] M. W. Anderson, O. Terasaki, T. Ohsuna, A. Philippou, S. P. MacKay, A. Ferreira, J. Rocha and S. Lidin, "Structure of the microporous titanosilicate ETS-10," *Nature,* pp. 347, 1994.

[27] S. M. Kuznicki, "Large-pored crystalline titanium molecular sieve zeolites," US 5011591, 1991.

[28] C. Lin, M. Danaie, D. Mitlin and S. M. Kuznicki, "Palladium Nanoparticles Formed on Titanium Silicate ETS-10,"Journal of Nanoscience and Nanotechnology*, vol. 11, pp. 2537-2539, 2011.

[29] M. Shi, C. Lin, L. Wu, C. Holt, D. Mitlin and S. M. Kuznicki, "Nanosilver Particle Formation on a High Surface Area Titanate," Journal of Nanoscience and Nanotechnology, vol. 10, pp. 8448-8451, 2010.

[30] N. C. Jeong, Y. J. Lee, J. H. Park, H. Lim, C. H. Shin, H. Cheong and K. B. Yoon, "New Insights into ETS-10 and Titanate Quantum Wire: A Comprehensive Characterization," *J. Am. Chem. Soc.,* vol. 131, pp. 13080-13092, 2009.

[31] B. Yilmaz, J. Warzywoda and A. Sacco, "Spectroscopic characterization of the quantum wires in titanosilicates ETS-4 and ETS-10," *Nanotechnology,* vol. 17, pp. 4092-4099, 2006.

[32] A. Anson, Y. Wang, C. C. H. Lin, T. M. Kuznicki and S. M. Kuznicki, "Adsorption of ethane and ethylene on modified ETS-10," *Chemical Engineering Science,* vol. 63, pp. 4171-4175, 2008.

[33] M. Shi, C. C. H. Lin, T. M. Kuznicki, Z. Hashisho and S. M. Kuznicki, "Separation of a binary mixture of ethylene and ethane by adsorption on Na-ETS-10," *Chemical Engineering Science,* vol. 65, pp. 3494-3498, 2010.

[34] A. Eguizábal, J. Lemus, M. Urbiztondo, O. Garrido, J. Soler, J. A. Blazquez and M. P. Pina, "Novel hybrid membranes based on polybenzimidazole and ETS-10 titanosilicate type material for high temperature proton exchange membrane fuel cells: A comprehensive study on dense and porous systems," *J. Power Sources,* vol. 196, pp. 8994-9007, 2011.

[35] T. Sancho, J. Soler and M. P. Pina, "Conductivity in zeolite-polymer composite membranes for PEMFCs," *J. Power Sources,* pp. 92, 2007.

[36] Z. Lin, J. Rocha, A. Navajas, C. Téllez, J. Coronas and J. Santamari´a, "Synthesis and characterisation of titanosilicate ETS-10 membranes," *Microporous and Mesoporous Materials,* vol. 67, pp. 79-86, 2004.

[37] H. Jeong, J. Krohn, K. Sujaoti and M. Tsapatsis, "Oriented molecular sieve membrane by heteroepitaxial growth," *J. Am. Chem. Soc.,* 2002.

[38] I. Tiscornia, I. Kumakiri, R. Bredesen, C. Téllez and J. Coronas, "Microporous titanosilicate ETS-10 membrane for high pressure CO2 separation," *Separation and Purification Technology,* vol. 73, pp. 8-12, 2010.

[39] A. Nalaparaju, Z. Q. Hu, X. S. Zhao and J. W. Jiang, "Exchange of heavy metal ions in titanosilicate Na-ETS-10 membrane from molecular dynamics simulations," *J. Membr. Sci.,* vol. 335, pp. 89-95, 2009.

[40] S. M. Kuznicki, K. A. Thrush and H. M. Garfinkel, "Use of crystalline molecular sieves containing charged octahedral sites in cyclic desiccating processes" WO1993000152 A1, 1993.

[41] M. Anderson W., J. Agger R., D. Luigi, A. Baggaley K. and J. Rocha, "Cation sites in ETS-10: 23Na 3Q MAS NMR and lattice energy minimisation calculations," *Physical Chemistry Chemical Physics (PCCP),* vol. 1, pp. 2287, 1999.

[42] E. D. Camarinha, P. F. Lito, B. M. Antunes, M. Otero, Z. Lin, J. Rocha, E. Pereira, A. C. Duarte and C. M. Silva, "Cadmium(II) removal from aqueous solution using microporous titanosilicate ETS-10," *Chem. Eng. J.,* vol. 155, pp. 108-114, 2009.

[43] L. Lv, G. Tsoi and X. S. Zhao, "Uptake equilibria and mechanisms of heavy metal ions on microporous titanosilicate ETS-10," *Ind Eng Chem Res,* vol. 43, pp. 7900-7906, 2004.

[44] A. Gorbach, M. Stegmaier and G. Eigenberger, "Measurement and modeling of water vapor adsorption on zeolite 4A-equilibria and kinetics," *Adsorption-Journal of the International Adsorption Society,* vol. 10, pp. 29-46, 2004.

8. Conclusions and Recommendations

8.1. General Conclusions

This dissertation was focused on low temperature (up to 250°C) removal of hydrogen sulfide to sub-ppm levels of H_2S. The data collected during this research demonstrate that, at room temperature, copper supported on Engelhard Titanosilicate-2 (Cu-ETS-2) is an H_2S adsorbent with a high gravimetric adsorption capacity. Cu-ETS-2 adsorbent maintains its capacity over a wide range of activation temperatures. The copper utilization in Cu-ETS-2 is higher than that of highly developed commercial samples due to high surface area and the degree of copper dispersion in ETS-2.

Room temperature H_2S breakthrough experimental results showed that Cu-ETS-2 has the best performance among Ag, Ca, and Zn -ETS-2 and that of a fully developed commercial H_2S adsorbent (BASF). Several characterization tests (i.e. XRD, EDX, SEM and Surface area measurements) have been conducted to explain the difference in adsorption capacities. Lower H_2S removal capacities for silver,

zinc and calcium samples can be attributed to the presence of inactive sites such as metallic silver dots and the rigidity of physical structure of the material.

Diluted H_2S breakthrough experiments through a Cu-ETS-2 packed bed were modeled applying the continuity equation to the system. The improvement of the H_2S breakthrough times as the experiment temperature increased can be explained by the growing chemisorption interaction as temperature rose from 25 to 250°C. This was also in good agreement with the temperature programmed desorption experiments which showed desorption peaks of larger magnitudes at temperatures higher than 200°C. A fixed bed model with reaction was able to fit the experimental data as well and it could explain the breakthrough profiles behaviour through the increasing reaction kinetics with temperature.

Copper ions removal from aqueous solutions by ETS-2 was also studied. ETS-2 showed high copper capacity, which is associated with high affinity of ion exchange ETS-2. By adjusting the PH of the solution, uptake of Cu ions improved sharply up to 89% removal at PH=4.5. It is therefore concluded that ETS-2 is a promising adsorbent for the efficient removal of copper from water and wastewater through ion exchange mechanism.

Finally, low energy input regenerable drying a humid CO_2 stream was studied. The purified CO_2 stream from a post-combustion capture (PCC) system has high moisture content, which causes equipment corrosion and increases the risk of hydrate formation. Therefore, the CO_2 stream must be thoroughly dried prior to being compressed. It has been shown that ETS-10 has a high selectivity of moisture

174

over CO_2 and is a promising desiccant for drying CO_2 to trace levels of moisture. Ca exchanged ETS-10 had the highest breakthrough capacity of the desiccants examined under the specified test conditions using a swing regeneration temperature as low as 70°C with humid, ambient air.

8.2. Recommendations for future work

Nanotitanate ETS-2 has been identified as the best support for active metal loading due to its great characteristics such as high external surface area and cation exchange affinity. For the first part of this work (low temperature H_2S removal) ETS-2 has been loaded with different active metals such as Cu, Zn, Ag and Ca. Among them Cu-ETS-2 showed the best uptake capacity. All the tests have been done for dry H_2S stream, however it has been hypothesized that ETS-2 samples are a potential H_2S removal adsorbent for wet streams. This postulated because ETS-2 structure is mainly nonporous which is ideal for pore mouth blockage by moisture. The next step will then be to investigate how to apply Cu-ETS-2 to practical H_2S separation systems where moisture exists.

In chapter 5 the proposed model includes the kinetic parameter, which predicts the breakthrough curve well. Running H_2S sorption isotherms on Cu-ETS-2 is worth to calculate the henry constant and compare with what is estimated from the proposed

model. Also desorption tests at different heating rates are suggested to be able to calculate the desorption energy through Redhead's peak maximum method [1].

H2S adsorption-regeneration cycles through oxidation of the sulfidated adsorbent are recommended as well.

ETS-2 showed potential copper removal capacity in chapter 6. It is recommended to conduct the experiments at different concentration of copper solution to produce the sorption isotherms. Experimental data can be fitted by different isotherm models such as Langmuir and Freundlich. Kinetic study is also recommended for copper removal tests at different temperatures.

Since copper removal capacity of ETS-2 improved with PH increase, higher H2S removal capacity is expected using Cu-ETS-2 prepared at PH=4.5.

ETS-10 desiccants introduced and employed as low energy input regenerable moisture removal adsorbents for CO_2 streams in chapter 7. Preliminary tests have been conducted for air-drying applications when through drying are required. It is highly recommended to pursue air-drying studies using ETS-10 adsorbent.

8.3. References

[1] A.M. de Jong and J.W. Niemantsverdriet, "Thermal desorption analysis: Comparative test of ten commonly applied procedures," Surface Science vol. 233 pp. 355-365, 1990.

Bibliography

A. Anson, Y. Wang, C. C. H. Lin, T. M. Kuznicki and S. M. Kuznicki, "Adsorption of ethane and ethylene on modified ETS-10," Chemical Engineering Science, vol. 63, pp. 4171-4175, 2008.

A. Çimen, A. Bilgiç, A. N. Kursunlu, I. H. Gübbük and H. I. Uçan, "Adsorptive removal of Co(II), Ni(II), and Cu(II) ions from aqueous media using chemically modified sporopollenin of Lycopodium clavatum as novel biosorbent," Desalination & Water Treatment, vol. 52, pp. 4837, 2014.

A. Eguizábal, J. Lemus, M. Urbiztondo, O. Garrido, J. Soler, J. A. Blazquez and M. P. Pina, "Novel hybrid membranes based on polybenzimidazole and ETS-10 titanosilicate type material for high temperature proton exchange membrane fuel cells: A comprehensive study on dense and porous systems," J. Power Sources, vol. 196, pp. 8994-9007, 2011.

A. Fahmi, J. Ahdjoudj and C. Minot, "A theoretical study of H2S and MeSH adsorption on TiO2," Surf Sci, vol. 352–354, pp. 529-533, 1996.

A. Gervasini, C. Picciau and A. Auroux, "Characterization of copper-exchanged ZSM-5 and ETS-10 catalysts with low and high degrees of exchange," Microporous and Mesoporous Materials, vol. 35, pp. 457-469, 2000.

A. Gorbach, M. Stegmaier and G. Eigenberger, "Measurement and modeling of water vapor adsorption on zeolite 4A-equilibria and kinetics," Adsorption-Journal of the International Adsorption Society, vol. 10, pp. 29-46, 2004.

A. K. Meena, K. Kadirvelu, G. K. Mishra, C. Rajagopal and P. N. Nagar, "Adsorptive removal of heavy metals from aqueous solution by treated sawdust (Acacia arabica)," J. Hazard. Mater., vol. 150, pp. 604-611, 2008.

A. Kather and S. Kownatzki, "Assessment of the different parameters affecting the CO2 purity from coal fired oxyfuel process," International Journal of Greenhouse Gas Control, vol. 5, pp. S204-S209, 2011.

A. L. Myers, "Thermodynamics of adsorption in porous materials," AICHE J., vol. 48, pp. 145-160, 2002.

A. Moezzi, A. M. McDonagh and M. B. Cortie, "Zinc oxide particles: Synthesis, properties and applications," Chem. Eng. J., vol. 185–186, pp. 1-22, 2012.

A. N. Startsev, I. I. Zakharov, O. V. Voroshina, A. V. Pashigreva and V. N. Parmon, "Low-temperature decomposition of hydrogen sulfide under the conditions of conjugate chemisorption and catalysis," Doklady Physical Chemistry, vol. 399, pp. 283-286, 2004.

A. Nalaparaju, Z. Q. Hu, X. S. Zhao and J. W. Jiang, "Exchange of heavy metal ions in titanosilicate Na-ETS-10 membrane from molecular dynamics simulations," J. Membr. Sci., vol. 335, pp. 89-95, 2009.

178

A. Startsev, O. Kruglyakova, Y. Chesalov, S. Ruzankin, E. Kravtsov, T. Larina and E. Paukshtis, "Low Temperature Catalytic Decomposition of Hydrogen Sulfide into Hydrogen and Diatomic Gaseous Sulfur," Topics in Catalysis, vol. 56, pp. 969-980, 2013.

A. Shahbazi, H. Younesi and A. Badiei, "Functionalized SBA-15 mesoporous silica by melamine-based dendrimer amines for adsorptive characteristics of Pb(II), Cu(II) and Cd(II) heavy metal ions in batch and fixed bed column," Chem. Eng. J., vol. 168, pp. 505-518, 2011.

A. Y. Manakov, Y. A. Dyadin, A. G. Ogienko, A. V. Kurnosov, E. Y. Aladko, E. G. Larionov, F. V. Zhurko, V. I. Voronin, I. F. Berger, S. V. Goryainov, A. Y. Lihacheva and A. I. Ancharov, "Phase Diagram and High-Pressure Boundary of Hydrate Formation in the Carbon Dioxide-Water System," J Phys Chem B, vol. 113, pp. 7257-7262, 2009.

A. Zukal, J. Mayerová and M. Kubu, "Adsorption of Carbon Dioxide on High-Silica Zeolites with Different Framework Topology," Topics in Catalysis, vol. 53, pp. 1361-1366, 2010.

"Adsorption, Gas Separation," Kirk-Othmer Encyclopedia of Chemical Technology, pp. 617, 2007.

"Adsorption," Kirk-Othmer Encyclopedia of Chemical Technology, pp. 582, 2007.

A.B.M. Heesink, W. Prins, and W.P.M. van Swaaij, "A grain size distribution model for non-catalytic gas-solid reactions," The Chemical Engineering Journal and the Biochemical Engineering Journal, vol. 53, pp. 25-37, 1993.

An Introduction to Surface Chemistry.

Available: http://www.chem.qmul.ac.uk/surfaces/scc/. (Accessed on Jan. 20th, 2015).

B. Arstad, H. Fjellvag, K. O. Kongshaug, O. Swang and R. Blom, "Amine functionalised metal organic frameworks (MOFs) as adsorbents for carbon dioxide," Adsorption, pp. 755, 2008.

B. A. Shah, C. B. Mistry and A. V. Shah, "Sequestration of Cu(II) and Ni(II) from wastewater by synthesized zeolitic materials: Equilibrium, kinetics and column dynamics," Chem. Eng. J., vol. 220, pp. 172-184, 2013.

B. D. Bhide, A. Voskericyan and S. A. Stern, "Hybrid processes for the removal of acid gases from natural gas," J. Membr. Sci., vol. 140, pp. 27-49, 1998.

B. Singha and S. K. Das, "Adsorptive removal of Cu(II) from aqueous solution and industrial effluent using natural/agricultural wastes," Colloids and Surfaces B: Biointerfaces, pp. 97, 2013.

B. Tanchuk, J. A. Sawada, S. Rezaei and S. M. Kuznicki, "Adsorptive drying of CO2 using low grade heat and humid, ambient air," Separation and Purification Technology, vol. 120, pp. 354-361, 2013.

B. Yilmaz, J. Warzywoda and A. Sacco, "Spectroscopic characterization of the quantum wires in titanosilicates ETS-4 and ETS-10," Nanotechnology, vol. 17, pp. 4092-4099, 2006.

C. Babé, M. Tayakout-Fayolle, C. Geantet, M. Vrinat, G. Bergeret, T. Huard and D. Bazer-Bachi, "Crystallite size effect in the sulfidation of ZnO by H2S: Geometric and kinetic modelling of the transformation," Chemical Engineering Science, vol. 82, pp. 73-83, 2012.

C. Cormos, A. Padurean and P. S. Agachi, "GHGT-10: Technical evaluations of carbon capture options for power generation from coal and biomass based on integrated gasification combined cycle scheme," Energy Procedia, vol. 4, pp. 1861-1868, 2011.

C. H. Bartholomew, "Mechanisms of catalyst deactivation," Applied Catalysis A: General, vol. 212, pp. 17-60, 2001.

C. Huang, C. Chen and S. Chu, "Effect of moisture on H2S adsorption by copper impregnated activated carbon," J. Hazard. Mater., vol. 136, pp. 866-873, 2006.

C. Knöfel, J. Descarpentries, A. Benzaouia, V. Zeleňák, S. Mornet, P. L. Llewellyn and V. Hornebecq, "Functionalised micro-/mesoporous silica for the adsorption of carbon dioxide," Microporous and Mesoporous Materials, vol. 99, pp. 79-85, 2007.

C. L. Carnes and K. J. Klabunde, "Unique chemical reactivities of nanocrystalline metal oxides toward hydrogen sulfide," Chemistry of Materials, vol. 14, pp. 1806-1811, 2002.

C. Lin, M. Danaie, D. Mitlin and S. M. Kuznicki, "Palladium Nanoparticles Formed on Titanium Silicate ETS-10," Journal of Nanoscience and Nanotechnology, vol. 11, pp. 2537-2539, 2011.

C. N. Satterfield, Mass Transfer in Heterogeneous Catalysis. Malabar, Fla. : R. E. Krieger Pub. Co., 1981.

C. O. Areán and M. R. Delgado, "Variable-temperature FT-IR studies on the thermodynamics of carbon dioxide adsorption on a faujasite-type H-Y zeolite," Appl. Surf. Sci., vol. 256, pp. 5259-5262, 2010.

C. T. Rettner, D. J. Auerbach, J. C. Tully and A. W. Kleyn, "Chemical dynamics at the gas-surface interface," J. Phys. Chem., vol. 100, pp. 13021-13033, 1996.

Canada's Oilsands and Heavy Oil Deposits.

Available: www.energy.gov.ab.ca/oilsands/pdfs/rpt_chops_app1.pdf. (Accessed on Jan. 20th, 2015).

Chemical Solvent-Based Processes for Acid Gas Removal in Gasification Application.

Available:

http://msdssearch.dow.com/PublishedLiteratureDOWCOM/dh_003a/0901b803800

3a89e.pdf?filepath=gastreating/pdfs/noreg/170-01406.pdf&fromPage=GetDoc.

(Accessed on Jan. 17th, 2015).

Chemisorption.

Available:http://www.micromeritics.com/Repository/Files/Chemisorption_Poster.p

df. (Accessed on Jan. 20th, 2015).

D. A. Berry, D. Shekhawat and J. J. Spivey, Fuel Cells. [Electronic Resource] :

Technologies for Fuel Processing. Amsterdam ; Boston : Elsevier, 2011.

D. A. Bhandari, N. Bessho and W. J. Koros, "Dual layer hollow fiber sorbents for

trace H2S removal from gas streams," Chemical Engineering Science, vol. 94, pp.

256-264, 2013.

D. Crespo, G. Qi, Y. Wang, F. H. Yang and R. T. Yang, "Superior sorbent for

natural gas desulfurization," Ind Eng Chem Res, vol. 47, pp. 1238-1244, 2008.

D. Jiang, L. Su, L. Ma, N. Yao, X. Xu, H. Tang and X. Li, "Cu-Zn-Al mixed metal

oxides derived from hydroxycarbonate precursors for H2S removal at low

temperature," Appl. Surf. Sci., vol. 256, pp. 3216-3223, 2010.

D. Melo, J. de Souza, M. Melo, A. Martinelli, G. Cachima and J. Cunha,

"Evaluation of the zinox and zeolite materials as adsorbents to remove H2S from

natural gas," Colloid Surf. A-Physicochem. Eng. Asp., vol. 272, pp. 32-36, 2006.

183

D. Montes, E. Tocuyo, E. Gonza̓lez, D. Rodri̓guez, R. Solano, R. Atencio, M. A. Ramos and A. Moronta, "Reactive H2S chemisorption on mesoporous silica molecular sieve-supported CuO or ZnO," Microporous and Mesoporous Materials, vol. 168, pp. 111-120, 2013.

D. Nguyen-Thanh and T. Bandosz, "Activated carbons with metal containing bentonite binders as adsorbents of hydrogen sulfide," Carbon, vol. 43, pp. 359-367, 2005.

D. R. Alfonso, "First-principles studies of H2S adsorption and dissociation on metal surfaces," Surf Sci, vol. 602, pp. 2758-2768, 2008.

D. Stirling, The Sulfur Problem [Electronic Resource] : Cleaning Up Industrial Feedstocks / Diane Stirling. Cambridge, UK : Royal Society of Chemistry, 2000.

D. W. Breck, Zeolite Molecular Sieves: Structure, Chemistry, and Use. New York, Wiley, 1974.

E. D. Camarinha, P. F. Lito, B. M. Antunes, M. Otero, Z. Lin, J. Rocha, E. Pereira, A. C. Duarte and C. M. Silva, "Cadmium(II) removal from aqueous solution using microporous titanosilicate ETS-10," Chem. Eng. J., vol. 155, pp. 108-114, 2009.

F. Chang, K. Chao, H. Cheng and C. Tan, "Adsorption of CO2 onto amine-grafted mesoporous silicas," Separation and Purification Technology, vol. 70, pp. 87-95, 2009.

F. Gholampour and S. Yeganegi, "Molecular simulation study on the adsorption and separation of acidic gases in a model nanoporous carbon," Chemical Engineering Science, vol. 117, pp. 426-435, 2014.

F. Li, J. Wei, Y. Yang, G. H. Yang and T. Lei, "Preparation of Sorbent Loaded with Nano-CuO for Room Temperature to Remove of Hydrogen Sulfide," Applied Mechanics and Materials, vol. 475, pp. 1329-1333, 2014.

F. Ullmann, Ullmann's Encyclopedia of Industrial Chemistry. [Electronic Resource]. New York] : Wiley, 7th ed., 2010.

F. Yazdanbakhsh, M. Blasing, J. A. Sawada, S. Rezaei, M. Muller, S. Baumann and S. M. Kuznicki, "Copper Exchanged Nanotitanate for High Temperature H2S Adsorption," Industrial and Engineering Chemistry Research, vol. 53, pp. 11734-11739, 2014.

Fundamentals of Stack Gas Dispersion.

Available: http://www.air-dispersion.com/default.htm. (Accessed on Jan. 10th, 2015).

G. Monteleone, M. De Francesco, S. Galli, M. Marchetti and V. Naticchioni, "Deep H2S removal from biogas for molten carbonate fuel cell (MCFC) systems," Chem. Eng. J., vol. 173, pp. 407-414, 2011.

G. Ramis, G. Busca and V. Lorenzelli, "Low-Temperature Co2 Adsorption on Metal-Oxides - Spectroscopic Characterization of some Weakly Adsorbed Species," Mater. Chem. Phys., vol. 29, pp. 425-435, 1991.

G. S. Grasa and J. C. Abanades, "CO2 capture capacity of CaO in long series of carbonation/calcination cycles," Ind Eng Chem Res, vol. 45, pp. 8846-8851, 2006.

L. D. Gasper-Galvin, A. T. Atimtay, R. P. Gupta, " Zeolite-Supported Metal Oxide Sorbents for Hot-Gas Desulfurization," Ind. Eng. Chem. Res., vol. 37, pp. 4157, 1998.

Gas Sweetening, Available:
http://msdssearch.dow.com/PublishedLiteratureDOWCOM/dh_0039/0901b803800 391f8.pdf?filepath=gastreating/pdfs/noreg/170 01395.pdf&fromPage=GetDoc. (Accessed on Jan. 20th, 2015).

H. A. Jakobsen, "Fixed Bed Reactors," Department of Chemical Engineering Norwegian University of Science and Technology, 2011.

H. Dumrul, A. N. Kursunlu, O. Kocyigit, E. Guler and S. Ertul, "Adsorptive removal of Cu(II) and Ni(II) ions from aqueous media by chemical immobilization of three different aldehydes," Desalination, vol. 271, pp. 92-99, 2011.

H. F. Garces, H. M. Galindo, L. J. Garces, J. Hunt, A. Morey and S. L. Suib, "Low temperature H2S dry-desulfurization with zinc oxide," Microporous Mesoporous Mat., vol. 127, pp. 190-197, 2010.

H. Jeong, J. Krohn, K. Sujaoti and M. Tsapatsis, "Oriented molecular sieve membrane by heteroepitaxial growth," J. Am. Chem. Soc., 2002.

H. Lu, P. G. Smirniotis, F. O. Ernst and S. E. Pratsinis, "Nanostructured Ca-based sorbents with high CO2 uptake efficiency," Chemical Engineering Science, vol. 64, pp. 1936-1943, 2009.

H. S. Fogler, Elements of Chemical Reaction Engineering. Upper Saddle River, NJ: Prentice Hall PTR, 4th ed., 2006.

H. Yang and B. Tatarchuk, "Novel-doped zinc oxide sorbents for low temperature regenerable desulfurization applications," AICHE J., 2010.

I. I. Zakharov, A. N. Startsev, O. V. Voroshina, A. V. Pashigreva, N. A. Chashkova and V. N. Parmon, "The molecular mechanism of low-temperature decomposition of hydrogen sulfide under conjugated chemisorption-catalysis conditions," Russian Journal of Physical Chemistry A, vol. 80, pp. 1403-1410, 2006.

I. Langmuir, "The Adsorption of Gases on Plane Surfaces of Glass, Mica and Platinum," J. Am. Chem. Soc., vol. 40, pp. 1361-1403, 1918.

I. Tiscornia, I. Kumakiri, R. Bredesen, C. Téllez and J. Coronas, "Microporous titanosilicate ETS-10 membrane for high pressure CO2 separation," Separation and Purification Technology, vol. 73, pp. 8-12, 2010.

International Energy Outlook 2011.

Available: http://large.stanford.edu/courses/2011/ph240/nagasawa2/docs/0484-2011.pdf. (Accessed on Jan. 20th, 2015).

Introduction to Chemical Adsorption Analytical Techniques and their Applications to Catalysis.

Available: http://www.micromeritics.com/repository/files/intro_to_chemical_adsorption.pdf. (Accessed on Jan. 20th, 2015).

J. A. Rodriguez, S. Chaturvedi, M. Kuhn and J. Hrbek, "Reaction of H2S and S2 with metal/oxide surfaces: band-gap size and chemical reactivity," J Phys Chem B, pp. 5511, 1998.

J. Abbasian, A. H. Hill, J. R. Wangerow, M. Flytzani-Stephanopoulos, L. Bo and C. Patel, "Development of novel copper-based sorbents for hot-gas cleanup," [Quarterly] technical report, 1992.

J. Baltrusaitis, J. Schuttlefield, E. Zeitler and V. H. Grassian, "Carbon dioxide adsorption on oxide nanoparticle surfaces," Chem. Eng. J., vol. 170, pp. 471-481, 2011.

J. M. Smith and H. C. Van Ness, Introduction to Chemical Engineering Thermodynamics. New York, McGraw-Hill, 1959; 2d ed., 1959.

J. R. Schrieffer and R. Gomer, "Induced covalent bond mechanism of chemisorption," Surf Sci, vol. 25, pp. 315-320, 1971.

J. Sun, S. Modi, K. Liu, R. Lesieur and J. Buglass, "Kinetics of zinc oxide sulfidation for packed-bed desulfurizer modeling," Energy Fuels, vol. 21, pp. 1863-1871, 2007.

K. B. Lee, A. Verdooren, H. S. Caram and S. Sircar, "Chemisorption of carbon dioxide on potassium-carbonate-promoted hydrotalcite," Journal of Colloid & Interface Science, vol. 308, pp. 30-39, 2007.

K. G. Bhattacharyya and S. S. Gupta, "Adsorptive Accumulation of Cd(II), Co(II), Cu(II), Pb(II) and Ni(II) Ions from Water onto Kaolinite: Influence of Acid Activation," Adsorption Science & Technology, vol. 27, pp. 47-68, 2009.

K. J. Leary, J. N. Michaels and A. M. Stacy, "Temperature-programmed desorption: Multisite and subsurface diffusion models," AICHE J., vol. 34, pp. 263, 1988.

K. Y. Foo and B. H. Hameed, "Insights into the modeling of adsorption isotherm systems," Chem. Eng. J., pp. 2, 2010.

L. Lv, G. Tsoi and X. S. Zhao, "Uptake equilibria and mechanisms of heavy metal ions on microporous titanosilicate ETS-10," Ind Eng Chem Res, vol. 43, pp. 7900-7906, 2004.

L. Marini, Geological Sequestration of Carbon Dioxide. [Electronic Resource] : Thermodynamics, Kinetics, and Reaction Path Modeling. Amsterdam; Oxford: Elsevier, 2007.

L. Zhou, M. Yu, L. Zhong and Y. Zhou, "Feasibility study on pressure swing sorption for removing H2S from natural gas," Chemical Engineering Science, vol. 59, pp. 2401-2406, 2004.

M. Anderson W., J. Agger R., D. Luigi, A. Baggaley K. and J. Rocha, "Cation sites in ETS-10: 23Na 3Q MAS NMR and lattice energy minimisation calculations," Physical Chemistry Chemical Physics (PCCP), vol. 1, pp. 2287, 1999.

M. E. Davis and R. J. Davis, Fundamentals of Chemical Reaction Engineering. [Electronic Resource]. Boston: McGraw-Hill, International ed., 2003.

M. Hussain, N. Abbas, D. Fino and N. Russo, "Novel mesoporous silica supported ZnO adsorbents for the desulphurization of biogas at low temperatures," Chem. Eng. J., vol. 188, pp. 222-232, 2012.

M. Naderi and M. W. Anderson, "Phase transformation of microporous titanosilicate ETS-4 into narsarsukite," Zeolites, vol. 17, pp. 437-443, 1996.

M. Shi, C. C. H. Lin, T. M. Kuznicki, Z. Hashisho and S. M. Kuznicki, "Separation of a binary mixture of ethylene and ethane by adsorption on Na-ETS-10," Chemical Engineering Science, vol. 65, pp. 3494-3498, 2010.

M. Shi, C. Lin, L. Wu, C. Holt, D. Mitlin and S. M. Kuznicki, "Nanosilver Particle Formation on a High Surface Area Titanate," Journal of Nanoscience and Nanotechnology, vol. 10, pp. 8448-8451, 2010.

M. W. Anderson, O. Terasaki, T. Ohsuna, P. Malley, A. Philippou, S. P. Mackay, A. Ferreira, J. Rocha and S. Lidin, "Microporous Titanosilicate Ets-10 - a Structural Survey," Philosophical Magazine B-Physic of Condensed Matter

Statistical Mechanics Electronic Optical and Magnetic Properties, vol. 71, pp. 813-841, 1995.

M. W. Anderson, O. Terasaki, T. Ohsuna, A. Philippou, S. P. MacKay, A. Ferreira, J. Rocha and S. Lidin, "Structure of the microporous titanosilicate ETS-10," Nature, pp. 347, 1994.

M. Xue, R. Chitrakar, K. Sakane and K. Ooi, "Screening of adsorbents for removal of H2S at room temperature," Green Chem., vol. 5, pp. 529-534, 2003.

Modern Methods in Heterogeneous Catalysis Research .

Available:http://www.fhi-berlin.mpg.de/acnew/department/pages/teaching/pages/teaching__wintersemester__2010_2011/klaus_christmann__adsorption__101105.pdf. (Accessed on Jan. 8th, 2015).

N. C. Jeong, Y. J. Lee, J. H. Park, H. Lim, C. H. Shin, H. Cheong and K. B. Yoon, "New Insights into ETS-10 and Titanate Quantum Wire: A Comprehensive Characterization," J. Am. Chem. Soc., vol. 131, pp. 13080-13092, 2009.

N. S. Randhawa, N. N. Das and R. K. Jana, "Adsorptive remediation of Cu(II) and Cd(II) contaminated wate using manganese nodule leaching residue," Desalination & Water Treatment, vol. 52, pp. 4197-4211, 2014.

N. Wakao and T. Funazkri, "Effect of fluid dispersion coefficients on particle-to-fluid mass transfer coefficients in packed beds: Correlation of sherwood numbers," Chemical Engineering Science, vol. 33, pp. 1375-1384, 1978.

N. Yaşyerli, T. Doğu, G. Doğu and i. Ar, "Deactivation model for textural effects of kinetics of gas-solid noncatalytic reactions "char gasification with CO2"," Chemical Engineering Science, vol. 51, pp. 2523-2528, 1996.

NaturalGas. Available: http://naturalgas.org. (Accessed on Jan. 16th, 2015).

O. Aschenbrenner and P. Styring, "Comparative study of solvent properties for carbon dioxide absorption," Energy & Environmental Science, vol. 3, pp. 1106-1113, 2010.

O. G. Nik, B. Nohair and S. Kaliaguine, "Aminosilanes grafting on FAU/EMT zeolite: Effect on CO2 adsorptive properties," Microporous and Mesoporous Materials, vol. 143, pp. 221-229, 2011.

O. Levenspiel, Chemical Reaction Engineering; an Introduction to the Design of Chemical Reactors. New York, Wiley, 1962.

P. Dhage, A. Samokhvalov, D. Repala, E. C. Duin, M. Bowman and B. J. Tatarchuk, "Copper-Promoted ZnO/SiO2 Regenerable Sorbents for the Room Temperature Removal of H2S from Reformate Gas Streams," Ind Eng Chem Res, vol. 49, pp. 8388-8396, 2010.

P. H. Chang, Y. P. Chang, S. Y. Chen, C. T. Yu and Y. P. Chyou, "Ca-Rich Ca-Al-Oxide, High-Temperature-Stable Sorbents Prepared from Hydrotalcite Precursors: Synthesis, Characterization, and CO2 Capture Capacity," Chemsuschem, vol. 4, pp. 1844-1851, 2011.

P. Kumar, C. Sung, O. Muraza, M. Cococcioni, S. Al Hashimi, A. McCormick and M. Tsapatsis, "H2S adsorption by Ag and Cu ion exchanged faujasites," Microporous Mesoporous Mat., vol. 146, pp. 127-133, 2011.

Q. L. Tang, S. R. Zhang and Y. P. Liang, "Influence of Step Defects on the H2S Splitting on Copper Surfaces from First-Principles Microkinetic Modeling," Journal of Physical Chemistry C, vol. 116, pp. 20321-20331, 2012.

Q. Xue and Y. Liu, "Removal of minor concentration of H2S on MDEA-modified SBA-15 for gas purification," J. Ind. Eng. Chem., vol. 18, pp. 169-173, 2012.

R. A. Zárate, S. Fuentes, J. P. Wiff, V. M. Fuenzalida and A. L. Cabrera, "Chemical composition and phase identification of sodium titanate nanostructures grown from titania by hydrothermal processing," Journal of Physics and Chemistry of Solids, vol. 68, pp. 628-637, 2007.

R. Chatti, A. K. Bansiwal, J. A. Thote, V. Kumar, P. Jadhav, S. K. Lokhande, R. B. Biniwale, N. K. Labhsetwar and S. S. Rayalu, "Amine loaded zeolites for carbon dioxide capture: Amine loading and adsorption studies," Microporous and Mesoporous Materials, vol. 121, pp. 84-89, 2009.

R. E. Ayala and D. W. Marsh, "Characterization and Long-Range Reactivity of Zinc Ferrite in High-Temperature Desulfurization Processes," Ind Eng Chem Res, vol. 30, pp. 55-60, 1991.

R. Haghpanah, A. Majumder, R. Nilam, A. Rajendran, S. Farooq, I. A. Karimi and M. Amanullah, "Multiobjective Optimization of a Four-Step Adsorption Process for Postcombustion CO2 Capture Via Finite Volume Simulation," Ind Eng Chem Res, vol. 52, pp. 4249-4265, 2013.

R. Haghpanah, A. Rajendran, S. Farooq, I. A. Karimi and M. Amanullah, "Discrete Equilibrium Data from Dynamic Column Breakthrough Experiments," Ind Eng Chem Res, vol. 51, pp. 14834-14844, 2012.

R. I. Masel, Principles of Adsorption and Reaction on Solid Surfaces. New York : Wiley, 1996.

R. Sitko, E. Turek, B. Zawisza, E. Malicka, E. Talik, J. Heimann, A. Gagor, B. Feist and R. Wrzalik, "Adsorption of divalent metal ions from aqueous solutions using graphene oxide," Dalton Transactions, vol. 42, pp. 5682-5689, 2013.

R. T. Yang, Adsorbents : Fundamentals and Applications. Hoboken, N.J. : Wiley-Interscience, 2003.

R. T. Yang, Gas Separation by Adsorption Processes. Boston: Butterworths, 1987.

S. Brunauer, P. H. Emmett and E. Teller, "Adsorption of Gases in Multimolecular Layers," J. Am. Chem. Soc., vol. 60, pp. 309-319, 1938.

S. Guntuka, S. Farooq and A. Rajendran, "A- and B-Site substituted lanthanum cobaltite perovskite as high temperature oxygen sorbent. 2. Column dynamics study," Ind Eng Chem Res, vol. 47, pp. 163-170, 2008.

S. H. Chen, S. Q. Sun, B. J. Lian, Y. F. Ma, Y. G. Yan and S. Q. Hu, "The adsorption and dissociation of H2S on Cu(100) surface: A DTF study," Surf Sci, vol. 620, pp. 51-58, 2014.

S. K. Gangwal, "Chapter 11: Desulfurization for Fuel Cells," Fuel Cells: Technologies for Fuel Processing, pp. 317-360, 2011.

S. Kocaoba, "Comparison of Amberlite IR 120 and dolomite's performances for removal of heavy metals," J. Hazard. Mater., vol. 147, pp. 488-496, 2007.

S. Liu, C. Lee, H. Chen, C. Wang and L. Juang, "Application of titanate nanotubes for Cu(II) ions adsorptive removal from aqueous solution," Chem. Eng. J., vol. 147, pp. 188-193, 2009.

S. M. Kuznicki, K. A. Thrush and H. M. Garfinkel, "Use of crystalline molecular sieves containing charged octahedral sites in cyclic desiccating processes," WO1993000152 A1, 1993.

S. M. Kuznicki, "Large-pored crystalline titanium molecular sieve zeolites", 19910430, 1991.

S. N. Nobar and S. Farooq, "Experimental and modeling study of adsorption and diffusion of gases in Cu-BTC," Chemical Engineering Science, pp. 801, 2012.

S. P. Hernández, M. Chiappero, N. Russo and D. Fino, "A novel ZnO-based adsorbent for biogas purification in H2 production systems," Chem. Eng. J., vol. 176–177, pp. 272-279, 2011.

S. P. Wang, S. L. Yan, X. B. Ma and J. L. Gong, "Recent advances in capture of carbon dioxide using alkali-metal-based oxides," Energy & Environmental Science, vol. 4, pp. 3805-3819, 2011.

S. R. Popuri, Y. Vijaya, V. M. Boddu and K. Abburi, "Adsorptive removal of copper and nickel ions from water using chitosan coated PVC beads," Bioresour. Technol., vol. 100, pp. 194-199, 2009.

S. R. Shukla and R. S. Pai, "Adsorption of Cu(II), Ni(II) and Zn(II) on dye loaded groundnut shells and sawdust," Separation & Purification Technology, vol. 43, pp. 1-8, 2005.

S. R. Shukla and R. S. Pai, "Adsorption of Cu(II), Ni(II) and Zn(II) on modified jute fibres," Bioresour. Technol., vol. 96, pp. 1430-1438, 2005.

S. Rezaei, A. Tavana, J. A. Sawada, L. Wu, A. S. M. Junaid and S. M. Kuznicki, "Novel Copper-Exchanged Titanosilicate Adsorbent for Low Temperature H2S Removal," Ind Eng Chem Res, vol. 51, pp. 12430-12434, 2012.

S. Rezaei, M. O. D. Jarligo, L. Wu and S. M. Kuznicki, "Breakthrough performances of metal-exchanged nanotitanate ETS-2 adsorbents for room temperature desulfurization," Chemical Engineering Science, vol. 123, pp. 444-449, 2015.

S. Rengaraj, Y. Kim, C. K. Joo, K. H. Choi and J. H. Yi, "Batch adsorptive removal of copper ions in aqueous solutions by ion exchange resins: 1200H and IRN97H," Korean Journal of Chemical Engineering, vol. 21, pp. 187-194, 2004.

S. Velu, X. Ma and C. Song, "Zeolite-based adsorbents for desulfurization of jet fuel by selective adsorption," in ACS Division of Fuel Chemistry, Preprints, pp. 447-448, 2002.

S. Yasyerli, G. Dogu, I. Ar and T. Dogu, "Activities of copper oxide and Cu-V and Cu-Mo mixed oxides for H2S removal in the presence and absence of hydrogen and predictions of a deactivation model," Ind Eng Chem Res, vol. 40, pp. 5206-5214, 2001.

S. Yasyerli, G. Dogu, I. Ar and T. Dogu, "Breakthrough Analysis of H2S Removal on Cu-V-Mo, Cu-V, and Cu-Mo Mixed Oxides," Chem. Eng. Commun., vol. 190, pp. 1055, 2003.

S. Yasyerli, G. Dogu, I. Ar and T. Dogu, "Dynamic analysis of removal and selective oxidation of H2S to elemental sulfur over Cu-V and Cu-V-Mo mixed oxides in a fixed bed reactor," Chemical Engineering Science, vol. 59, pp. 4001-4009, 2004.

S. Yasyerli, I. Ar, G. Dogu and T. Dogu, "Removal of hydrogen sulfide by clinoptilolite in a fixed bed adsorber," Chem. Eng. Process, vol. 41, pp. 785-792, 2002.

S. Zarghami, T. Mohammadi and M. Kazemimoghadam, "Adsorption Behavior of Cu(II) Ions on Crosslinked Chitosan/Polyvinyl Alcohol Ion Imprinted Membrane," Journal of Dispersion Science & Technology, vol. 36, pp. 190-195, 2015.

Short-Term Energy Outlook, Available: http://www.eia.gov/forecasts/steo/report/global_oil.cfm. (Accessed on Jan. 20th, 2015).

T. Baird, K. Campbell, P. Holliman, R. Hoyle, M. Huxam, D. Stirling, B. Williams and M. Morris, "Cobalt-zinc oxide absorbents for low temperature gas desulfurisation," J. Mater. Chem., vol. 9, pp. 599-605, 1999.

T. Baird, P. J. Denny, R. Hoyle, F. Mcmonagle, D. Stirling and J. Tweedy, "Modified Zinc-Oxide Absorbents for Low-Temperature Gas Desulfurization," Journal of the Chemical Society-Faraday Transactions, vol. 88, pp. 3375-3382, 1992.

T. Doğu, "The Importance of Pore Structure and Diffusion in the Kinetics of Gas-Solid Non-catalytic Reactions: Reaction of Calcined Limestone with SO2," The Chemical Engineering Journal, vol. 21, pp. 213-222, 1981.

T. E. Whyte, C. M. Yon and E. H. Wagener, Industrial Gas Separations. Washington, D.C. : American Chemical Society, 1983.

T. Ko, H. Chu and L. Chaung, "The sorption of hydrogen sulfide from hot syngas by metal oxides over supports," Chemosphere, vol. 58, pp. 467-474, 2005.

T. Ko and H. Hsueh, "Removal of Hydrogen Sulfide by Iron-Rich Soil: Application of the Deactivation Kinetic Model for Fitting Breakthrough Curve," Aerosol Air Qual. Res., vol. 12, pp. 1355-1361, 2012.

T. Kopac and S. Kocabas, "Deactivation models for sulfur dioxide adsorption on silica gel," Adv. Environ. Res., vol. 8, pp. 417-424, 2004.

T. Kyotani, H. Kawashima, A. Tomita, A. Palmer and E. Furimsky, "Removal of H_2S from hot gas in the presence of Cu-containing sorbents," Fuel, vol. 68, pp. 74-79, 1989.

T. S. Anirudhan and P. G. Radhakrishnan, "Adsorptive Removal and Recovery of U(VI), Cu(II), Zn(II), and Co(II) from Water and Industry Effluents," Bioremediation J., vol. 15, pp. 39-56, 2011.

T. Sancho, J. Soler and M. P. Pina, "Conductivity in zeolite-polymer composite membranes for PEMFCs," J. Power Sources, pp. 92, 2007.

The Adsorption of Gases and Vapors, Volume I. Available: https://archive.org/details/adsorptionofgase031704mbp. (Accessed on Jan. 10th, 2015).

The Surface Analysis Forum. Available: http://www.uksaf.org/home.html. (Accessed on Jan. 16th, 2015).

A.M. de Jong and J.W. Niemantsverdriet, "Thermal desorption analysis: Comparative test of ten commonly applied procedures," Surface Science vol. 233 pp. 355-365, 1990.

V. Hernandez-Valencia, M. W. Hlavinka, J. A. Bullin and I. N. C. Bryan, "Design glycol units for maximum efficiency," Research & Eng., pp. 310-317, 1992.

W. Jiang, X. Chen, B. Pan, Q. Zhang, L. Teng, Y. Chen and L. Liu, "Spherical polystyrene-supported chitosan thin film of fast kinetics and high capacity for copper removal," J. Hazard. Mater., vol. 276, pp. 295-301, 2014.

P.R. Westmoreland, D.P. Harrison, " Evaluation of candidate solids for high-temperature desulfurization of low-Btu gases" Environmental Science and Technology, vol. 10, pp. 659, 1976.

X. Meng, D. Wang, J. Liu and S. Zhang, "Preparation and characterization of sodium titanate nanowires from brookite nanocrystallites," Mater. Res. Bull., vol. 39, pp. 2163-2170, 2004.

X. Sun, X. Huang, X. Liao and B. Shi, "Adsorptive removal of Cu(II) from aqueous solutions using collagen-tannin resin," J. Hazard. Mater., vol. 186, pp. 1058-1063, 2011.

X. Wang, T. Sun, J. Yang, L. Zhao and J. Jia, "Low-temperature H2S removal from gas streams with SBA-15 supported ZnO nanoparticles," Chem. Eng. J., vol. 142, pp. 48-55, 2008.

X. Xue and F. Li, "Removal of Cu(II) from aqueous solution by adsorption onto functionalized SBA-16 mesoporous silica," Microporous and Mesoporous Materials, vol. 116, pp. 116-122, 2008.

Y. Elsayed, M. Seredych, A. Dallas and T. J. Bandosz, "Desulfurization of air at high and low H2S concentrations," Chem. Eng. J., vol. 155, pp. 594-602, 2009.

Y. Hu, H. Li and J. Yan, "Integration of Evaporative Gas Turbine with Oxy-Fuel Combustion for Carbon Dioxide Capture," International Journal of Green Energy, vol. 7, pp. 615-631, 2010.

Y. M. Choi, C. Compson, M. C. Lin and M. Liu, "A mechanistic study of H2S decomposition on Ni- and Cu-based anode surfaces in a solid oxide fuel cell," Chemical Physics Letters, vol. 421, pp. 179-183, 2006.

Y. Suyadal, M. Erol and H. Oguz, "Deactivation model for the adsorption of trichloroethylene vapor on an activated carbon bed," Ind Eng Chem Res, vol. 39, pp. 724-730, 2000.

Y. Wang and M. D. Levan, "Adsorption Equilibrium of Carbon Dioxide and Water Vapor on Zeolites 5A and 13X and Silica Gel: Pure Components," J. Chem. Eng. Data, vol. 54, pp. 2839-2844, 2009.

Y. Xiao, S. Wang, D. Wu and Q. Yuan, "Experimental and simulation study of hydrogen sulfide adsorption on impregnated activated carbon under anaerobic conditions," J. Hazard. Mater., vol. 153, pp. 1193-1200, 2008.

201

Z. Lin, J. Rocha, A. Navajas, C. Téllez, J. Coronas and J. Santamari´a, "Synthesis and characterisation of titanosilicate ETS-10 membranes," Microporous and Mesoporous Materials, vol. 67, pp. 79-86, 2004.

Z. Liu, C. A. Grande, P. Li, J. Yu and A. E. Rodrigues, "Adsorption and Desorption of Carbon Dioxide and Nitrogen on Zeolite 5A," Separation Science & Technology, vol. 46, pp. 434-451, 2011.

Z. Renju, "Desorption of gases from graphitic and porous carbon surfaces," 2004.

Z. Zhao, X. Cui, J. Ma and R. Li, "Adsorption of carbon dioxide on alkali-modified zeolite 13X adsorbents," International Journal of Greenhouse Gas Control, vol. 1, pp. 355-359, 2007.

Appendix A

A.1. Axial temperature profile within the tube furnace (section 5.2.2)

The axial temperature profile within the tube furnace was evaluated for a set point temperature of 500C. The blank column was located within the furnace zone at 500°C to find the best area align the tube for the set point temperature without significant variation.
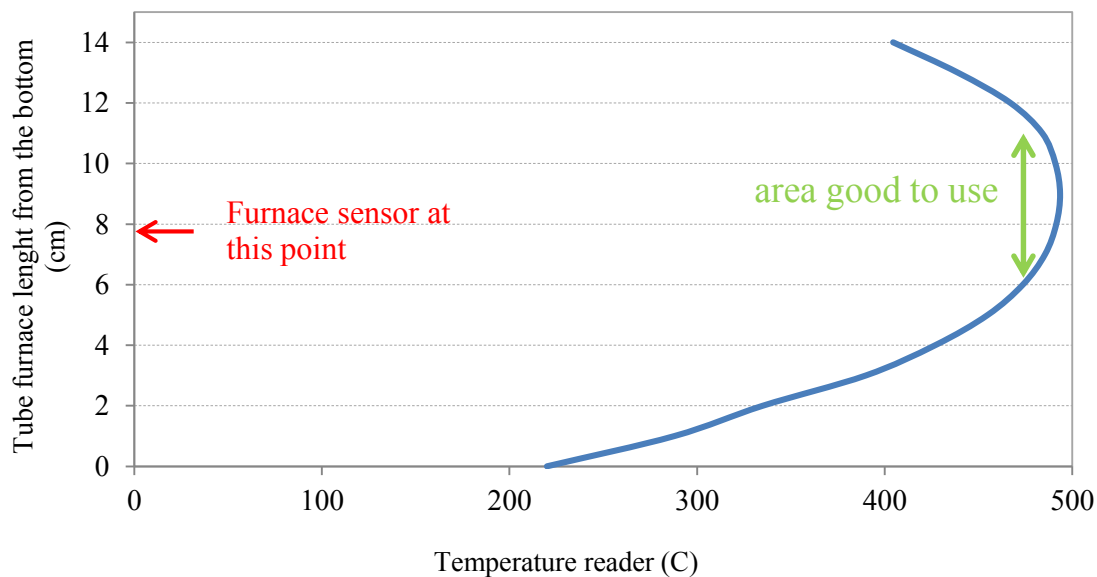

Figure A- 1 The axial temperature profile within the tube furnace at 500°C.

The green zone depicted in Figure A-1 was selected for the adsorbent bed to be installed.

A.2. Justification for assumption 6 in section 5.3.1

When there is a concentration gradient in the gas phase, for a ΔV volume of the bed, diffusive transport across a boundary layer in the vicinity of solid phase is equal to the rate of surface reaction. Thus the molar flux from the bulk gas at H_2S concentration of c_i to the surface of a spherical particle of diameter d_p at concentration c_i^S is given by:

$$Kc_i^S \Delta V = \frac{D_i}{\delta} A_p (c_i - c_i^S) \qquad (A-1)$$

Where D_i is H_2S diffusivity in the boundary layer and can be calculated using Chapman-Enskog equation [1] with *Lennard-Jones potential* parameters from [2]. The calculated diffusivity of H_2S in He (D_i) at 25°C is 0.626 cm²/s.

δ and A_p in equation $(A-1)$ are boundary layer thickness and particles surface area respectively.

With a rearrangement in equation $(A-1)$:

$$\frac{c_i - c_i^S}{c_i^S} = \frac{K}{D_i/\delta} \frac{\Delta V}{A_p} \qquad (A-2)$$

where for a spherical particle of diameter d_p

$$\frac{A_p}{\Delta V} = \frac{V_p}{\Delta V}\frac{A_p}{V_p} = (1-\varepsilon)\frac{6}{d_p} \qquad (A-3)$$

Using equation $(A-1)$ and $(A-3)$, we will have

$$\frac{c_i - c_i^s}{c_i^s} = \frac{\dfrac{\delta}{D_i}}{\dfrac{1}{Kd_p/6(1-\varepsilon)}} \qquad (A-4)$$

The last equation represents the ratio of diffusivity resistance to the kinetic resistance. It can give an idea whether the system is diffusion controlled or kinetic controlled.

There are different relations in the literature to calculate the boundary layer thickness for different conditions, an empirical relation for Re < 10 is proposed by Ranz and Marshall as follows [3]:

$$k_f = \frac{D_i}{\delta} = \left\{4.0 + 1.21\frac{(d_pU)^{2/3}}{D_i}\right\}^{1/2}\frac{D_i}{d_p} \qquad (A-5)$$

Using equation $(A-5)$, $\delta = 6.94e^{-3}$ cm at 25°C. Thus with the results of section 5.4.1 one can have an estimation of the diffusivity resistance compared to the kinetic resistance. The calculated ratio from equation $(A-4)$ at room temperature is 0.1, which confirms that the system is controlled by the kinetic rate rather than diffusion rate.

A.3. Cyclic air-drying experiments

ETS-10 has previously been patented as a desiccant material for air. However its dynamic adsorption behaviour (breakthrough study) has not been done for air stream. During this study air-drying performance of Ca exchanged forms of ETS-10 and compares them to a commercial Activated alumina adsorbents (from Parker Hannifin Corporation). A wet air stream was dried using a single packed-bed column. The moisture breakthrough time was recorded at trace moisture breakthrough for both desiccants.

The breakthrough experiments used the CO_2 drying testing stand changed and using an air flow rate of 500 sccm as a feed stream. The adsorption temperature was kept constant at 38°C to maintain a controllable, near-ambient condition. The bed regeneration conditions were set at a bed temperature of 85°C (asked by Parker Hannifin Corporation for real industrial practice), with ambient room air used at a flow rate of 500 sccm. The regeneration time was set to one hour. The regeneration temperature was selected to compare the performance of the adsorbents using low-grade heat for regeneration, such as the waste heat available from the low-pressure steam of a power plant. The performance of each adsorbent was assessed using a air inlet feed having a moisture content of 100 % RH. Data points were collected once every 5 sec throughout the experiments. Four adsorption desorption cycles have been conducted under mentioned condition. Replicate runs were performed for each set of experimental conditions.

A breakthrough profile for Ca-ETS-10 and Activated alumina are shown in Figure A-2 as an example of the typical breakthrough profile, which was seen in all experiments for all adsorbents. For both desiccants breakthrough capacity drops after first cycle, however it remains unchanged for the rest three cycles.
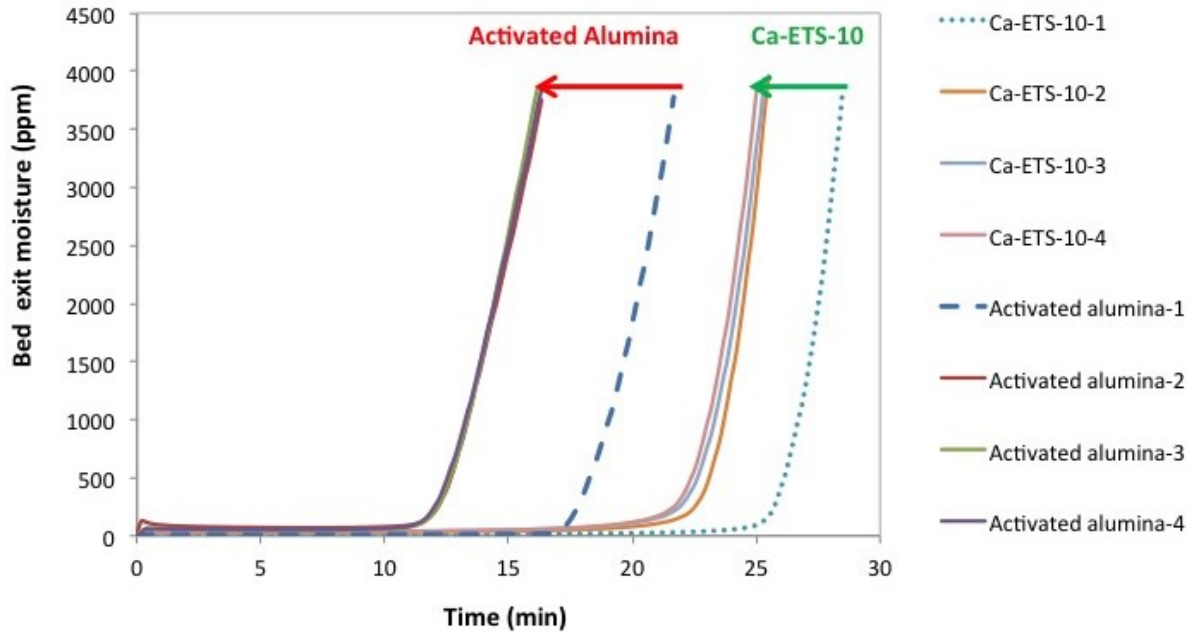

Figure A- 2 Breakthrough profile for Ca-ETS-10 and Activated alumina – four adsorption desorption cycles

The breakthrough times for 200 ppm moisture in the outlet stream of first and forth cycles are given in Table A-1. Higher moisture breakthrough capacity and less capacity loss after four adsorption desorption cycles for Ca-ETS-10 compare to Activated alumina, make Ca-ETS-10 a promising adsorbent for low energy input air drying.

Table A- 1 Breakthrough times for 200 ppm moisture in the outlet.

Desiccant	Breakthrough time (min)	
	1st cycle	4th cycle
Activated alumina	12	17.5
Ca-ETS-10	21	25

A.4. References

[1] R. B. Bird, W. E. Stewart and E. N. Lightfoot, *Transport Phenomena.* New York: J. Wiley international ed, 2002.

[2] J. S. Gulliver, *Introduction to Chemical Transport in the Environment.* Cambridge Univ Pr; Cambridge Univ Pr, 100 Brook Hill Dr, West Nyack, NY, 10994-2133, 2012.

[3] C. M. Hooijmans, S. Geraats, J. Potters and K. Luyben, "Experimental-Determination of the Mass-Transfer Boundary-Layer Around a Spherical Biocatalyst Particle," *Chemical Engineering Journal and The Biochemical Engineering Journal,* vol. 44, pp. B41-B46, 1990.